NATIONAL ADVISORY COMMITTEE FOR AERONAUTICS

TECHNICAL NOTE

No. 1276

LOW-SPEED TESTS OF FIVE NACA 66-SERIES AIRFOILS HAVING MEAN LINES DESIGNED TO GIVE HIGH CRITICAL MACH NUMBERS

By Albert E. von Doenhoff, Louis S. Stivers, Jr., and James M. O'Connor

Langley Memorial Aeronautical Laboratory
Langley Field, Va.

Washington

May 1947

NATIONAL ADVISORY COMMITTEE FOR AERONAUTICS

TECHNICAL NOTE NO. 1276

LOW-SPEED TESTS OF FIVE NACA 66-SERIES AIRFOILS HAVING MEAN LINES DESIGNED TO GIVE HIGH CRITICAL MACH NUMBERS

By Albert E. von Doenhoff, Louis S. Stivers, Jr., and James M. O'Connor

SUMMARY

The possibility of developing an airfoil to carry lift without decreasing the critical Mach number below that of the basic thickness form at zero lift has been investigated. Low-speed tests of five NACA 66-series airfoil sections having a thickness-chord ratio of 0.16 were made in the Langley two-dimensional low-turbulence pressure tunnel. By designing the mean line to carry load over the portions of the airfoil section having low induced velocities an effective design lift coefficient (the lift coefficient corresponding to the center of the range of high critical Mach numbers as obtained from the experimental pressure distribution) of approximately 0.1 was obtained for several airfoil sections without causing the maximum predicted critical Mach numbers to be appreciably less than the critical Mach number for the basic thickness form at zero lift. The maximum lift coefficients and the drag coefficients in the low-drag range were approximately the same for these airfoils as for the NACA 66-series airfoil sections having the same thickness and approximately the same effective design lift coefficient with the uniform-load mean line. The low-drag range at a Reynolds number of 9×10^6 decreased with increase in design lift coefficient above a value of 0.2. The pitching-moment coefficients were larger than those of airfoils having the same effective design lift coefficients with the uniform-load mean line but were not nearly so large as those corresponding to the design load distribution.

Recommendations concerning the use of the airfoils at high speeds cannot be made because of the lack of test data at high Mach numbers.

INTRODUCTION

A large amount of work has been done on the problem of designing airfoils that have high critical Mach numbers. The NACA 16-series airfoils, presented in reference 1, have a thickness distribution that gives unusually high critical Mach numbers for a given thickness-chord ratio. This series of airfoil sections, however, has high critical Mach numbers over only a limited range of lift coefficients. Many of the NACA 6-series airfoils, data for which are presented in reference 2, have critical Mach numbers somewhat lower than those for the corresponding airfoils of the NACA 16-series but have high critical Mach numbers over a considerably larger range of lift coefficients. The forward portion of the NACA 6-series sections are designed so that the pressure distribution forward of the point of minimum pressure becomes essentially flat at the extremities of the range of lift coefficients for low drag. For a given position of minimum pressure on the basic thickness form, this design condition gives an airfoil shape that has a minimum increase in maximum-velocity ratio throughout the range of lift coefficients for low drag.

Because the mean line corresponding to a uniform chordwise distribution of load at the design lift coefficient ($a = 1.0$) has the highest possible critical speed for a given lift coefficient, this mean line has been most frequently used as the mean line of NACA 16-series and NACA 6-series sections. Although the uniform-load mean line has the optimum critical-speed characteristics for the mean line itself, an airfoil of finite thickness having this mean line will not necessarily have the highest possible critical speed for a given thickness and design lift coefficient. The critical speed of an airfoil section is determined by the maximum velocity occurring on the airfoil surface. If the mean line for a given thickness distribution is designed so as to cause the airfoil to carry lift over the portions of the chord where the velocity is less than the maximum, the airfoil will then be able to carry some lift and not have a velocity ratio greater than the maximum for the basic thickness form. In order for the airfoil to carry the largest amount of lift without decreasing the critical Mach number below that for the

basic thickness form at zero lift, the pressures over the upper surface of the airfoil must be uniform and the pressure coefficient must equal that of the basic thickness form.

For the portion of an NACA 6-series airfoil forward of the position of minimum pressure, the load distribution associated with angle of attack is optimum at the lift coefficient corresponding to the upper extremity of the low-drag range because at this lift coefficient the pressure distribution over the upper surface becomes uniform from the leading edge back to the original position of minimum pressure. In order not to disturb the pressure distribution over the forward portion of the airfoil, the optimum mean line for high critical Mach numbers should be designed to give zero load from the leading edge to the point of minimum pressure on the basic thickness form and to give a load distribution corresponding to uniform pressure over the upper surface from this point to the trailing edge. Such a load distribution ordinarily corresponds to a large finite load at the trailing edge. Previous experience with airfoils having mean lines designed to give finite loads at the trailing edge indicates that the load distribution over most of the chord is substantially as specified but that the finite load at the trailing edge is not realized in practice.

The purposes of the present investigation are (1) to determine experimentally the extent to which the methods just described are effective in increasing the design lift coefficient of an airfoil without decreasing the critical Mach number appreciably below that of the basic thickness form and (2) to determine the effects of the corresponding unusual type of load distribution on characteristics of the airfoil section other than the critical Mach number, such as pitching moment, maximum lift, and drag. The present investigation includes low-speed tests in the Langley two-dimensional low-turbulence pressure tunnel of five airfoil sections having the NACA 66(215)-016 basic thickness form. Three of these sections have mean lines designed to carry various amounts of load back of the position of minimum pressure of the basic thickness form (0.6 chord) at the design lift coefficient. The other two airfoils have mean lines designed to carry a part of the total load uniformly over the entire chord. The tests consisted of measurements of lift, drag, and pitching moment at

Reynolds numbers of 3×10^6, 6×10^6, and 9×10^6 and at Mach numbers less than 0.17. Low-speed pressure distributions for each of the airfoils were determined at a Reynolds number of 6×10^6 through a range of angles of attack corresponding to a range of lift coefficients from large negative values to values beyond the positive stall.

Definite recommendations concerning the use of the airfoils at high speeds cannot be made because of the lack of test data at high Mach numbers. Additional data are also needed on the application of lateral-control and high-lift devices because of the unusual shape of the airfoils near the trailing edge.

SYMBOLS

a	mean-line designation, fraction of chord from leading edge over which design load is uniform
c	chord
c_d	section drag coefficient
$c_{d_{min}}$	minimum section drag coefficient
c_l	section lift coefficient
$c_{l_{max}}$	maximum section lift coefficient
c_{l_i}	design section lift coefficient
$c_{m_{a.c.}}$	moment coefficient about aerodynamic center
$c_{m_{c/4}}$	moment coefficient about quarter-chord point
H_o	free-stream total pressure
M_{cr}	critical Mach number

p	local static pressure
q_o	free-stream dynamic pressure
R	Reynolds number
S	pressure coefficient $\left(\frac{H_o - p}{q_o}\right)$
x	distance along chord line measured from leading edge
y	distance perpendicular to chord line measured from chord line
α_o	section angle of attack

DESIGN OF THE AIRFOIL SECTIONS

The basic thickness form for all the airfoils tested in this investigation was the NACA 66(215)-016 airfoil section, which has minimum pressure at 0.6c from the leading edge and a thickness-chord ratio of 0.16. As previously discussed, mean lines were desired that have zero load from $x/c = 0$ to $x/c = 0.6$ and linearly increasing load from this point to the trailing edge. Because the relations obtained from the theory of thin wing sections are linear, the theoretical mean lines and load distributions can be obtained simply by addition of the ordinates and the corresponding velocity increments of component mean lines.

The desired type of load distribution is obtained by a combination of a uniform-load mean line ($a = 1.0$) with a mean line having uniform load from the leading edge to 0.6c and linearly decreasing load from 0.6c to the trailing edge ($a = 0.6$). In order for the load to be zero over the forward portion of the airfoil, the design lift coefficient for the mean line of the type $a = 0.6$ must be -0.8 times the design lift coefficient for the mean line of the type $a = 1.0$; in order for an airfoil to have a design lift coefficient of 0.2, the sum of the design lift coefficients of the component mean lines must equal this value. These conditions

are satisfied by a mean line having the following components: (1) a mean line of the type $a = 0.6$ with a design lift coefficient of -0.8 and (2) a mean line of the type $a = 1.0$ with a design lift coefficient of 1.0. The designation of the airfoil having the chosen basic thickness form and the aforementioned mean line is as follows:

$$\text{NACA } 66(215)\text{-}216 \left\{ \begin{array}{l} a = 0.6, \quad c_{l_i} = -0.8 \\ a = 1.0, \quad c_{l_i} = 1.0 \end{array} \right\}$$

Further details of the numbering system for this type of designation are discussed in reference 2. In order to determine the effects of variation in camber, two additional airfoil sections having theoretical design lift coefficients of 0.3 and 0.4 were derived. These airfoil sections are:

$$\text{NACA } 66(215)\text{-}316 \left\{ \begin{array}{l} a = 0.6, \quad c_{l_i} = -1.2 \\ a = 1.0, \quad c_{l_i} = 1.5 \end{array} \right\}$$

$$\text{NACA } 66(215)\text{-}416 \left\{ \begin{array}{l} a = 0.6, \quad c_{l_i} = -1.6 \\ a = 1.0, \quad c_{l_i} = 2.0 \end{array} \right\}$$

For the three airfoils the theoretical pressure distributions at the design lift coefficient, presented in figure 1, indicate that even the airfoil designed for a lift coefficient of 0.2 has theoretically a slightly higher maximum value of the pressure coefficient S, and hence a lower value of the critical Mach number, than that for the basic thickness form. The experimental pressure distributions, however, were not expected to show this decrease in critical Mach number because of failure to realize fully the theoretical load distribution.

Two more airfoils were investigated for the purpose of determining the extent to which the critical Mach number characteristics of airfoils cambered with a uniform-load mean line could be improved by increasing the portion of the load carried by the rearward part of

the airfoil while holding uniform the load carried by the forward part. The two airfoils are:

$$\text{NACA } 66(215)\text{-}216 \left\{ \begin{matrix} a = 0.6, & c_{l_i} = -0.5 \\ a = 1.0, & c_{l_i} = 0.7 \end{matrix} \right\}$$

$$\text{NACA } 66(215)\text{-}216 \left\{ \begin{matrix} a = 0.6, & c_{l_i} = -0.3 \\ a = 1.0, & c_{l_i} = 0.5 \end{matrix} \right\}$$

The contours and corresponding theoretical load distributions for the five airfoil sections considered in this investigation are given in figure 2. Ordinates are given in tables I to V.

MODELS AND TESTS

Models of the five airfoil sections were built of mahogany laminated in the chordwise direction. Each model had a chord of 24 inches and a span of $35\frac{1}{2}$ inches. The models were prepared for standard tests in the Langley two-dimensional low-turbulence pressure tunnel (TDT) in the manner described in reference 2.

Lift data were obtained from measurements of the pressure reactions on the floor and ceiling of the tunnel, drag data were obtained from measurements by the wake-survey method, and pitching-moment data were measured with a torque balance. Details of the methods of obtaining the data are given in the appendix of reference 2.

Lift, drag, and pitching-moment data were obtained at Reynolds numbers of 3×10^6, 6×10^6, and 9×10^6 for models in a smooth condition. Pressure-distribution data for each model were obtained at a number of angles of attack corresponding to a range of lift coefficients from large negative values to values beyond maximum lift; these data were obtained for the smooth models at a Reynolds number of 6×10^6. With a standard roughness applied to the leading edges of the models, lift and

drag data were obtained at a Reynolds number of 6×10^6. This roughness consisted of approximately 0.011-inch grains of carborundum applied to the airfoil surface over a surface length of 0.08c measured from the leading edge on both upper and lower surfaces. The grains were thinly spread to cover 5 to 10 percent of this area.

RESULTS

The experimental pressure distributions are presented in figures 3 to 7. Lift, drag, and pitching-moment data for the five airfoil sections are presented in figures 8 to 12. The force data have been corrected for the constricting effects of the tunnel walls by equations (37) to (40) in the appendix of reference 2. For the present airfoils these equations are reduced to the following simplified forms, where the primed values represent the values measured in the tunnel:

$$c_l = 0.974 c_l'$$

$$\alpha_o = 1.015 \alpha_o'$$

$$c_{m_{c/4}} = 0.989 c_{m_{c/4}}'$$

$$c_d = 0.989 c_d'$$

Corresponding corrections have been applied to the pressure-distribution data.

DISCUSSION

Because only low-speed data were obtained, comparisons of the various airfoil sections are made on the basis of predicted critical Mach numbers. In general, critical Mach numbers (the critical Mach number is defined as that free-stream Mach number at which the local velocity of sound is first attained) predicted from low-speed experimental pressure distributions are in good agreement with high-speed-test results. This critical Mach number is somewhat lower than and is to be distinguished from the Mach number corresponding to the force breaks.

The critical Mach numbers presented in figure 13 were obtained from the theoretical and experimental low-speed pressure-distribution data by the von Kármán method by use of the curve presented on page 883 of supplement IV, reference 2. The curves of the critical Mach numbers corresponding to the theoretical and experimental low-speed pressure distributions of the present airfoil sections are compared with similar data for airfoil sections having the same basic thickness form and the same effective design lift coefficient (the lift coefficient corresponding to the center of the range of high critical Mach numbers as obtained from the experimental pressure distribution), but having a uniform-load mean line ($a = 1.0$). Although the theoretical and effective design lift coefficients may be seen to differ considerably for the newer airfoils, the data of reference 2 show that the effective and theoretical design lift coefficients are substantially equal for the airfoil sections cambered with the uniform-load mean line for moderate design lift coefficients. Numerous pressure-distribution measurements have also shown that the theoretical and experimental low-speed pressure distributions for the latter airfoils are in good agreement at low and moderate lift coefficients.

The data of figures 13(a) to (c) show that, for the airfoils having zero load from the leading edge to the position of minimum pressure, the effective design lift coefficients are less than the theoretical coefficients and this discrepancy increases with increase in camber. For these airfoils the maximum critical Mach numbers obtained from the experimental pressure distributions are equal to or greater than the maximum critical Mach numbers obtained from the theoretical pressure distributions. The critical Mach numbers obtained from the experimental pressure distributions increase with increasing lift coefficient in most of the range of high critical Mach numbers and are a maximum between lift coefficients of 0.2 and 0.3. These maximum critical Mach numbers are approximately 0.025 greater at these lift coefficients than the critical Mach numbers for the airfoils having the uniform-load mean line. The results presented in figures 13(a) to (c) indicate that the airfoils have an effective design lift coefficient of approximately 0.1 and have maximum critical Mach numbers at normal lift coefficients for high speed that approach the maximum critical Mach

number for the basic thickness form at zero lift. The difference between the critical Mach number of the basic thickness form and of the cambered airfoil sections increases with increasing camber.

For the two airfoil sections carrying a portion of the load from the leading edge to the position of minimum pressure (figs. 13(d) and (e)), the predicted critical Mach numbers obtained from the experimental and theoretical low-speed pressure distributions are much closer in agreement than for the other three airfoils. These two airfoil sections show small gains in critical Mach numbers as compared with the airfoil sections having the uniform-load mean line.

A comparison of the theoretical pressure distributions at the design lift coefficient with the experimental pressure distributions having a load distribution over the forward portion most nearly like the design load distribution is given in figure 14. Figures 14(a) to (c), which present data for the three airfoils with zero load from $x/c = 0$ to $x/c = 0.6$, show successively greater discrepancies between the experimental and the theoretical pressure distributions with increase in design lift coefficient. At the design lift coefficient, theoretically, no load should be observed over the forward portion of these airfoil sections. This condition is not fulfilled because of the failure to realize the design load over the rearward portion of the airfoil. In figures 14(a) and (b) the values of maximum pressure coefficient for the experimental pressure distributions are in good agreement with the theoretical values. The data presented in figures 14(d) and (e) indicate that the agreement between the experimental and theoretical pressure distributions becomes progressively better as the load on the rearward portion of the airfoils is decreased.

The low-speed aerodynamic data for the airfoils considered in this investigation are given in figures 8 to 12 and are summarized in table VI. A comparison of these data with those for the NACA 66-series airfoil sections (reference 2) having the same thickness and approximately the same effective design lift coefficient with the uniform-load mean line indicates no large difference in the maximum lift coefficients or in the drag coefficients in the low-drag range. At a Reynolds number of 9×10^6

the newer airfoils having theoretical design lift coefficients greater than 0.2 show a progressive decrease of the low-drag range with increase in camber and show a somewhat larger initial increase in drag coefficients at the upper end of the range of low drag coefficients than the corresponding NACA 66-series airfoils with the uniform-load mean line. The test data for the newer airfoils show a jog in the lift curves at the upper end of the low-drag range. The magnitude of the jog decreases as the Reynolds number is increased from 3×10^6 to 9×10^6. For the airfoils with a theoretical design lift coefficient of 0.2 the jog in the lift curve at a Reynolds number of 9×10^6 is very small and has approximately the same magnitude as the jogs found for the NACA 66-series airfoils (reference 2) having approximately the same effective design lift coefficient and the uniform-load mean line. The jog, however, for the newer airfoils with a theoretical design lift coefficient of 0.3 and 0.4 is greater at a Reynolds number of 9×10^6 than the jogs for the corresponding NACA 66-series airfoils (reference 2) with the uniform-load mean line or for the other airfoils of the present paper. The magnitude of the jog appears to increase with increase in theoretical design lift coefficient.

The pitching-moment coefficients of the newer airfoil sections are larger than those for the NACA 66-series airfoils (reference 2) having the same effective design lift coefficient with the uniform-load mean line but are not nearly so large as the pitching-moment coefficients corresponding to the theoretical load distribution.

CONCLUSIONS

Although recommendations concerning the use of the airfoils at high speeds cannot be made because of the lack of test data at high Mach numbers, low-speed tests of five NACA 66-series airfoil sections having mean lines designed to give high critical Mach numbers indicated the following conclusions:

1. An effective design lift coefficient (the lift coefficient corresponding to the center of the range of

high critical Mach numbers as obtained from the experimental pressure distribution) of approximately 0.1 was obtained for several airfoil sections without causing the maximum predicted critical Mach numbers to be appreciably less than the critical Mach number for the basic thickness form at zero lift.

2. The maximum lift coefficients and the drag coefficients in the low-drag range were approximately the same for these airfoils as for the NACA 66-series airfoil sections having the same thickness and approximately the same effective design lift coefficient with the uniform-load mean line.

3. The low-drag range at a Reynolds number of 9×10^6 decreased with increase in design lift coefficient above a value of 0.2.

4. The pitching-moment coefficients were larger than those of airfoils having the same effective design lift coefficients with the uniform-load mean line but were not nearly so large as those corresponding to the theoretical load distribution.

Langley Memorial Aeronautical Laboratory
National Advisory Committee for Aeronautics
Langley Field, Va., November 19, 1945

REFERENCES

1. Stack, John: Tests of Airfoils Designed to Delay the Compressibility Burble. NACA TN No. 976, Dec. 1944. (Reprint of ACR, June 1939.)

2. Abbott, Ira H., von Doenhoff, Albert E., and Stivers, Louis S., Jr.: Summary of Airfoil Data. NACA ACR No. L5C05, 1945.

TABLE I

ORDINATES OF THE

NACA 66(215)-216 $\begin{cases} a = 0.6, & c_{l_i} = -0.8 \\ a = 1.0, & c_{l_i} = 1.0 \end{cases}$

AIRFOIL SECTION

(Stations and ordinates given in percent of airfoil chord)

Upper surface		Lower surface	
Station	Ordinate	Station	Ordinate
0	0	0	0
.521	1.174	.479	-1.194
.775	1.401	.725	-1.432
1.280	1.734	1.220	-1.776
2.540	2.332	2.460	-2.424
5.054	3.208	4.946	-3.376
7.563	3.883	7.437	-4.131
10.069	4.462	9.931	-4.788
15.075	5.373	14.925	-5.835
20.074	6.066	19.926	-6.658
25.066	6.597	24.934	-7.303
30.052	6.999	29.948	-7.791
35.031	7.290	34.969	-8.134
40.002	7.476	39.998	-8.342
44.962	7.574	45.038	-8.416
49.909	7.575	50.091	-8.337
54.832	7.477	55.168	-8.079
59.677	7.269	60.323	-7.567
64.571	6.949	65.429	-6.689
69.611	6.413	70.389	-5.501
74.709	5.724	75.291	-4.182
79.832	4.877	80.168	-2.829
84.951	3.904	85.049	-1.526
90.035	2.768	89.965	-.406
95.055	1.514	94.945	.326
100.000	0	100.000	0

L.E. radius: 1.575
Slope of radius through L.E.: -0.017

TABLE II

ORDINATES OF THE

NACA 66(215)-316 $\begin{cases} a = 0.6, & c_{l_i} = -1.2 \\ a = 1.0, & c_{l_i} = 1.5 \end{cases}$

AIRFOIL SECTION

(Stations and ordinates given in percent of airfoil chord)

Upper surface		Lower surface	
Station	Ordinate	Station	Ordinate
0	0	0	0
.531	1.169	.469	-1.199
.787	1.397	.713	-1.439
1.295	1.722	1.205	-1.786
2.560	2.308	2.440	-2.416
5.080	3.165	4.920	-3.417
7.594	3.820	7.406	-4.192
10.104	4.381	9.896	-4.869
15.113	5.258	14.887	-5.950
20.112	5.917	19.888	-6.805
25.100	6.419	24.900	-7.479
30.078	6.801	29.922	-7.989
35.047	7.079	34.953	-8.345
40.003	7.259	39.997	-8.559
44.944	7.363	45.056	-8.627
49.863	7.384	50.137	-8.528
54.747	7.324	55.253	-8.228
59.516	7.185	60.484	-7.633
64.359	6.997	65.641	-6.607
69.418	6.626	70.582	-5.258
74.565	6.099	75.435	-3.787
79.749	5.385	80.251	-2.313
84.926	4.498	85.074	-.930
90.053	3.358	89.947	.186
95.082	1.971	94.918	.789
100.000	0	100.000	0

L.E. radius: 1.575
Slope of radius through L.E.: -0.026

NATIONAL ADVISORY COMMITTEE FOR AERONAUTICS

TABLE III

ORDINATES OF THE

NACA 66(215)-416 $\begin{cases} a = 0.6, & c_{l_i} = -1.6 \\ a = 1.0, & c_{l_i} = 2.0 \end{cases}$

AIRFOIL SECTION

(Stations and ordinates given in percent of airfoil chord)

Upper surface		Lower surface	
Station	Ordinate	Station	Ordinate
0	0	0	0
.541	1.163	.459	-1.203
.799	1.389	.701	-1.445
1.310	1.712	1.190	-1.796
2.580	2.285	2.420	-2.469
5.107	3.122	4.893	-3.458
7.625	3.757	7.375	-4.253
10.139	4.298	9.861	-4.950
15.151	5.141	14.849	-6.065
20.149	5.768	19.851	-6.952
25.133	6.243	24.867	-7.655
30.104	6.602	29.896	-8.186
35.062	6.868	34.938	-8.556
40.004	7.043	39.996	-8.775
44.925	7.153	45.075	-8.837
49.817	7.193	50.183	-8.717
54.663	7.171	55.337	-8.375
59.356	7.099	60.644	-7.695
64.148	7.039	65.852	-6.519
69.227	6.832	70.773	-5.008
74.421	6.470	75.579	-3.386
79.666	5.890	80.334	-1.794
84.902	5.092	85.098	-.335
90.070	3.947	89.930	.777
95.108	2.427	94.892	1.253
100.000	0	100.000	0

L.E. radius: 1.575
Slope of radius through L.E.: -0.035

TABLE IV

ORDINATES OF THE

NACA 66(215)-216 $\begin{cases} a = 0.6, & c_{l_i} = -0.5 \\ a = 1.0, & c_{l_i} = 0.7 \end{cases}$

AIRFOIL SECTION

(Stations and ordinates given in percent of airfoil chord)

Upper surface		Lower surface	
Station	Ordinate	Station	Ordinate
0	0	0	0
.475	1.197	.525	-1.171
.724	1.435	.776	-1.401
1.223	1.781	1.277	-1.729
2.473	2.419	2.527	-2.337
4.976	3.358	5.024	-3.226
7.479	4.089	7.521	-3.925
9.983	4.718	10.017	-4.534
14.989	5.713	15.011	-5.497
19.994	6.476	20.006	-6.248
24.996	7.064	25.004	-6.836
29.995	7.512	30.005	-7.278
34.991	7.835	35.009	-7.589
39.982	8.039	40.018	-7.779
44.967	8.142	45.033	-7.848
49.943	8.132	50.057	-7.782
54.904	8.001	55.096	-7.557
59.816	7.731	60.184	-7.115
64.757	7.295	65.243	-6.361
69.787	6.616	70.213	-5.316
74.851	5.777	75.149	-4.143
79.927	4.794	80.073	-2.918
84.997	3.711	85.003	-1.719
90.043	2.518	89.957	-.654
95.045	1.289	94.955	.099
100.000	0	100.000	0

L.E. radius: 1.575
Slope of radius through L.E.: 0.021

TABLE V

ORDINATES OF THE

NACA 66(215)-216 $\begin{cases} a = 0.6, & c_{l_i} = -0.3 \\ a = 1.0, & c_{l_i} = 0.5 \end{cases}$

AIRFOIL SECTION

(Stations and ordinates given in percent of airfoil chord)

Upper surface		Lower surface	
Station	Ordinate	Station	Ordinate
0	0	0	0
.445	1.210	.555	-1.156
.690	1.456	.810	-1.378
1.185	1.814	1.315	-1.694
2.428	2.476	2.572	-2.278
4.924	3.457	5.076	-3.125
7.423	4.224	7.577	-3.788
9.925	4.887	10.075	-4.363
14.932	5.939	15.068	-5.271
19.940	6.748	20.060	-5.976
24.949	7.378	25.051	-6.522
29.957	7.854	30.043	-6.936
34.964	8.197	35.036	-7.227
39.969	8.417	40.031	-7.401
44.970	8.522	45.030	-7.468
49.966	8.504	50.034	-7.410
54.952	8.352	55.048	-7.208
59.909	8.058	60.091	-6.810
64.881	7.524	65.119	-6.138
69.904	6.747	70.096	-5.191
74.945	5.811	75.055	-4.113
79.990	4.739	80.010	-2.975
85.028	3.581	84.972	-1.849
90.048	2.352	89.952	-.820
95.038	1.138	94.962	-.054
100.000	0	100.000	0

L.E. radius: 1.575
Slope of radius through L.E.: 0.046

NATIONAL ADVISORY
COMMITTEE FOR AERONAUTICS

TABLE VI

SUMMARY OF AERODYNAMIC DATA

$[R = 9 \times 10^6]$

NACA airfoil section	$c_{d_{min}}$	$c_{l_{max}}$		$c_{m_{a.c.}}$
		Smooth	Rough[1]	
66(215)-216 $\begin{cases} a = 0.6, c_{l_i} = -0.8 \\ a = 1.0, c_{l_i} = 1.0 \end{cases}$	0.0034	1.47	0.99	-0.050
66(215)-316 $\begin{cases} a = 0.6, c_{l_i} = -1.2 \\ a = 1.0, c_{l_i} = 1.5 \end{cases}$	0.0031	1.51	0.96	-0.075
66(215)-416 $\begin{cases} a = 0.6, c_{l_i} = -1.6 \\ a = 1.0, c_{l_i} = 2.0 \end{cases}$	0.0027	1.55	1.01	-0.100
66(215)-216 $\begin{cases} a = 0.6, c_{l_i} = -0.5 \\ a = 1.0, c_{l_i} = 0.7 \end{cases}$	0.0035	1.55	1.05	-0.052
66(215)-216 $\begin{cases} a = 0.6, c_{l_i} = -0.3 \\ a = 1.0, c_{l_i} = 0.5 \end{cases}$	0.0034	1.43	1.00	-0.050

[1] $R = 6 \times 10^6$.

NATIONAL ADVISORY
COMMITTEE FOR AERONAUTICS.

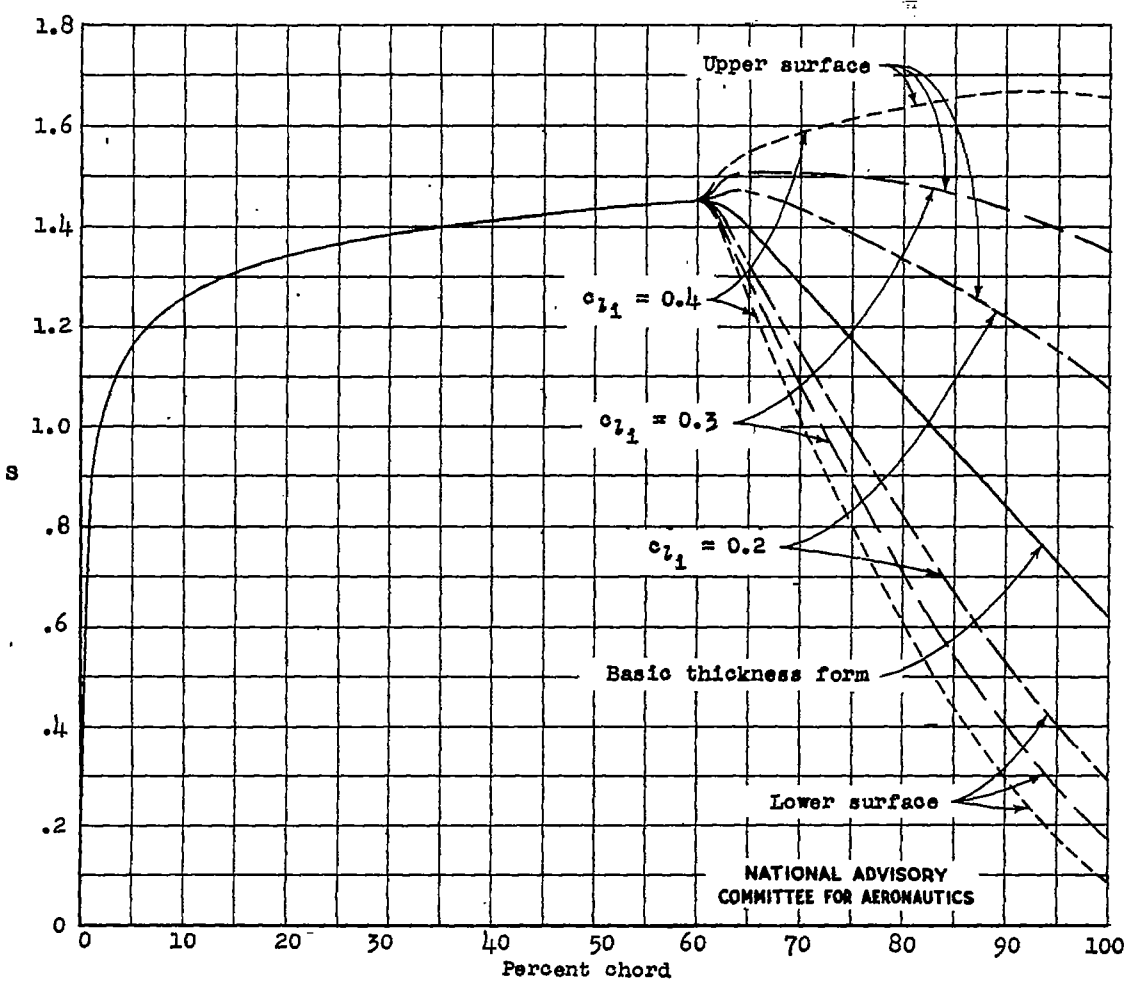

Figure 1.- Theoretical pressure distributions for the three airfoil sections having zero loading from 0 to 0.6 airfoil chord and for the NACA 66(215)-016 basic thickness form.

Theoretical chordwise loadings Airfoil contours

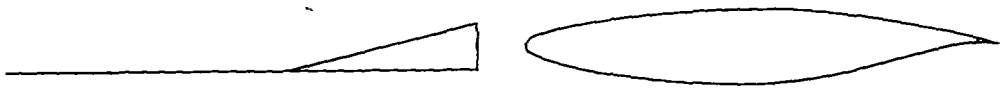

NACA 66(215)-216 $\begin{cases} a = 0.6, & c_{l_i} = -0.8 \\ a = 1.0, & c_{l_i} = 1.0 \end{cases}$

NACA 66(215)-316 $\begin{cases} a = 0.6, & c_{l_i} = -1.2 \\ a = 1.0, & c_{l_i} = 1.5 \end{cases}$

NACA 66(215)-416 $\begin{cases} a = 0.6, & c_{l_i} = -1.6 \\ a = 1.0, & c_{l_i} = 2.0 \end{cases}$

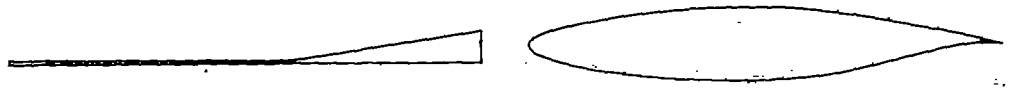

NACA 66(215)-216 $\begin{cases} a = 0.6, & c_{l_i} = -0.5 \\ a = 1.0, & c_{l_i} = 0.7 \end{cases}$

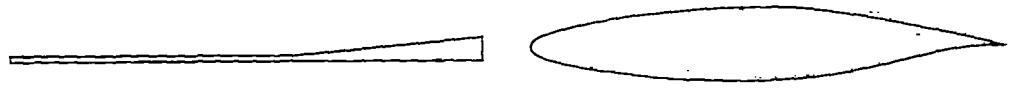

NACA 66(215)-216 $\begin{cases} a = 0.6, & c_{l_i} = -0.3 \\ a = 1.0, & c_{l_i} = 0.5 \end{cases}$

NATIONAL ADVISORY
COMMITTEE FOR AERONAUTICS

Figure 2.- Theoretical chordwise loadings and contours for the five airfoil sections.

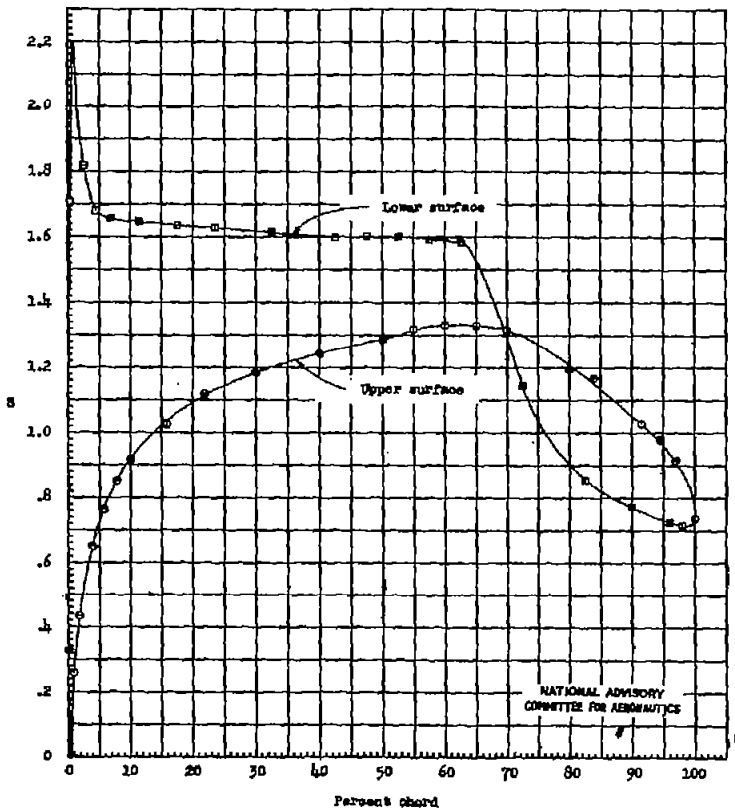

(a) $\alpha_o = -4.1°$.

Figure 3.- Experimental pressure distribution of the NACA 66(215)-216 $\begin{cases} a = 0.6, & \alpha_{l_1} = -0.8 \\ a = 1.0, & \alpha_{l_1} = 1.0 \end{cases}$ airfoil section. $R = 6 \times 10^6$; TDT test 516.

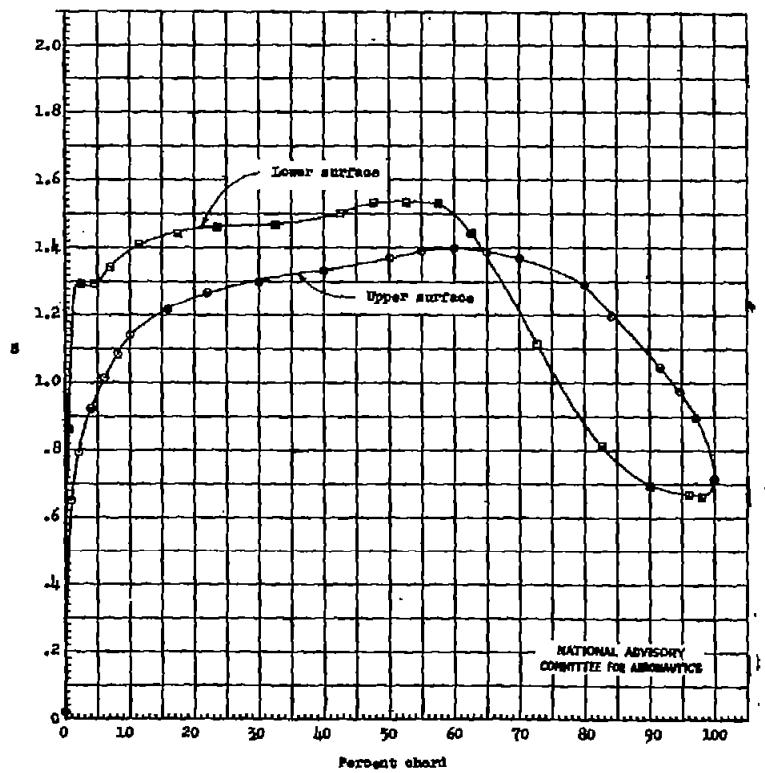

(b) $\alpha_o = -2.0°$.

Figure 3.- Continued.

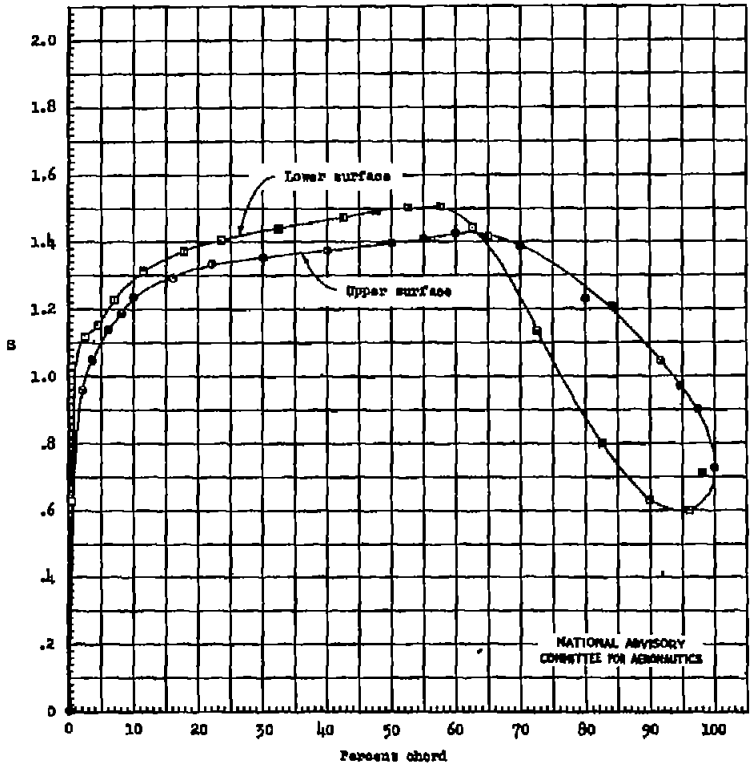

(c) $\alpha_0 = -1.3°$.

Figure 3.- Continued.

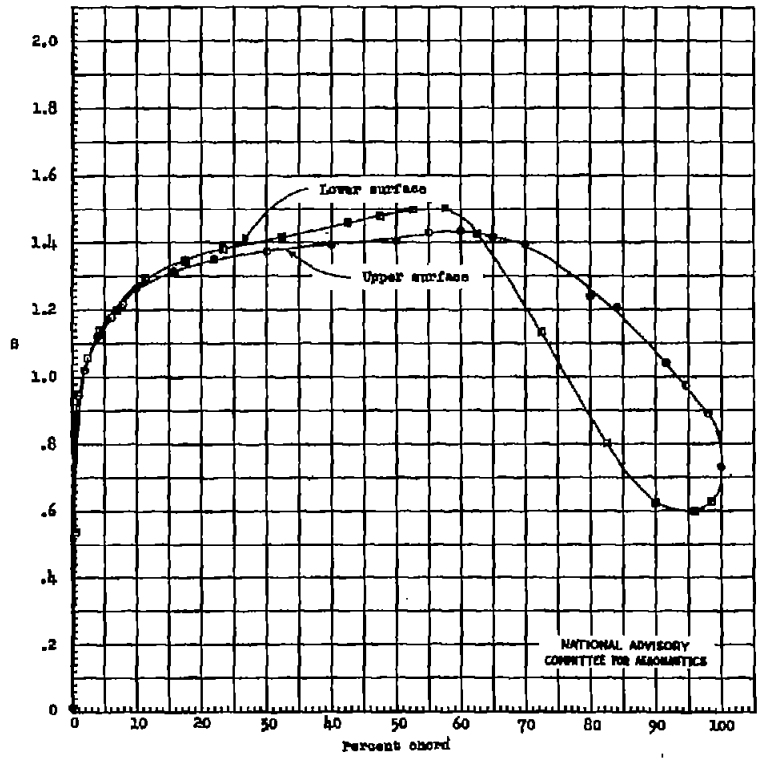

(d) $\alpha_0 = -1.0°$.

Figure 3.- Continued.

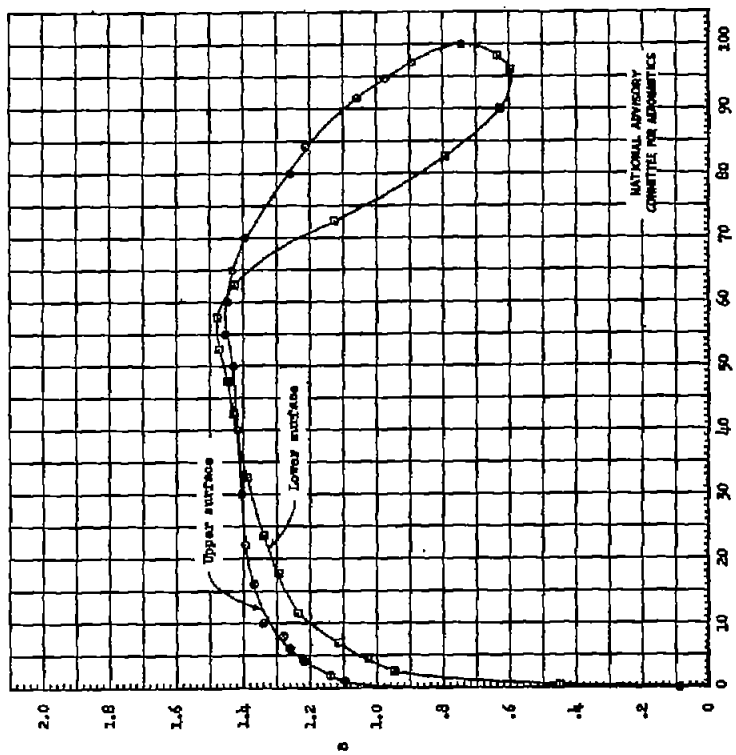

(f) $\alpha_0 = -0.5°$.

Figure 3.- Continued.

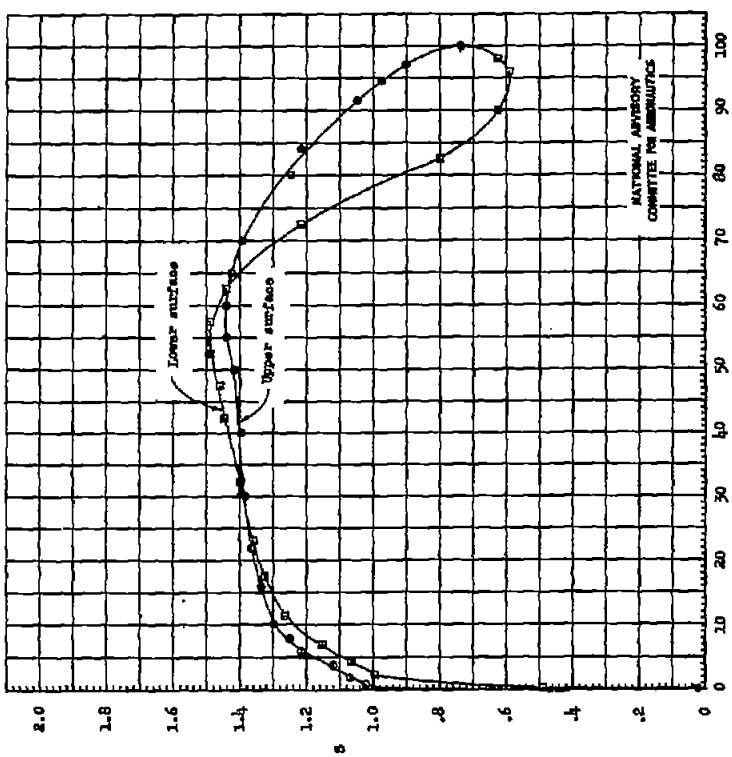

(g) $\alpha_0 = -0.8°$.

Figure 3.- Continued.

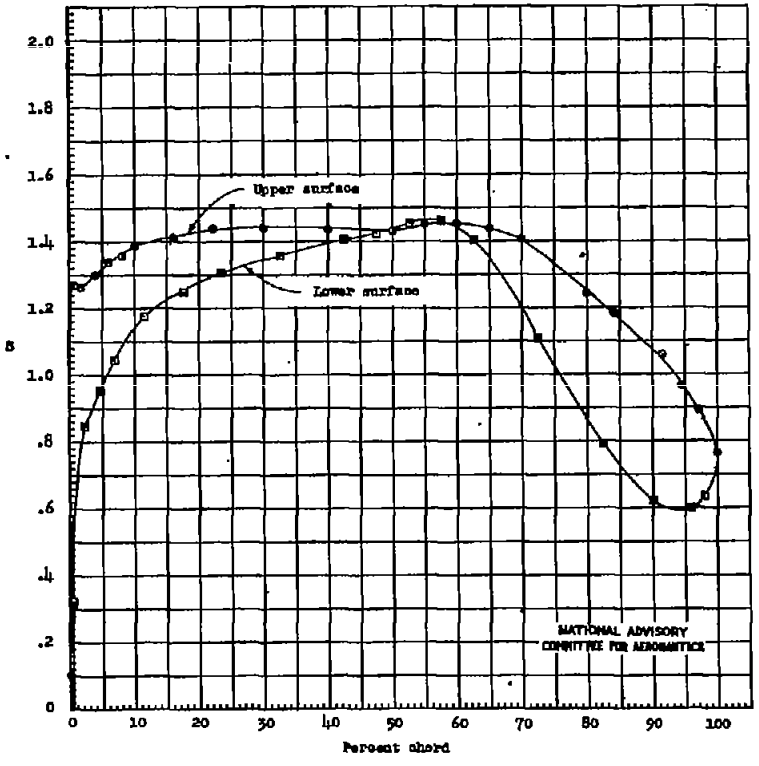

(g) $\alpha_0 = 0°$.

Figure 3.- Continued.

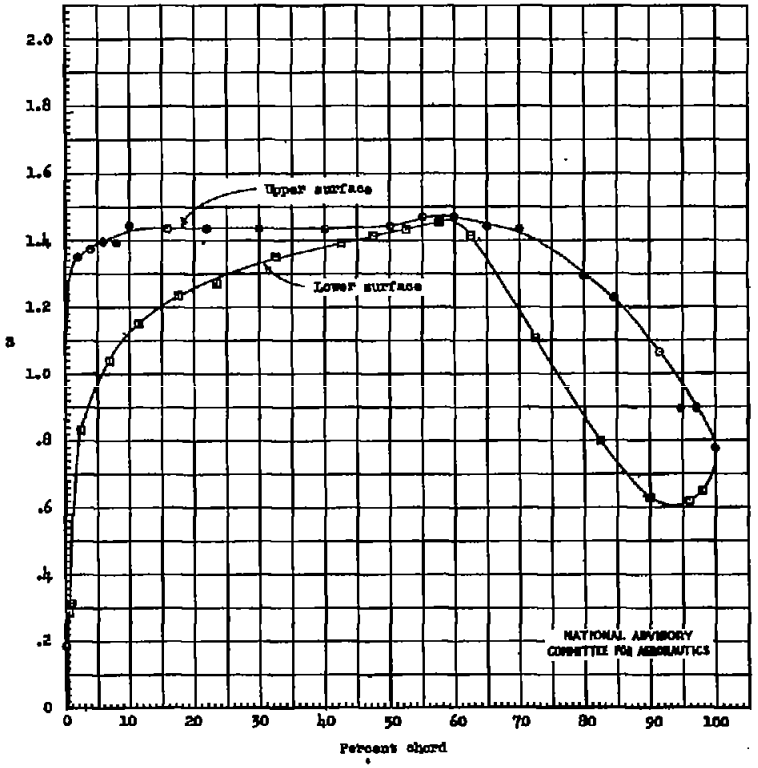

(h) $\alpha_0 = 0.5°$.

Figure 3.- Continued.

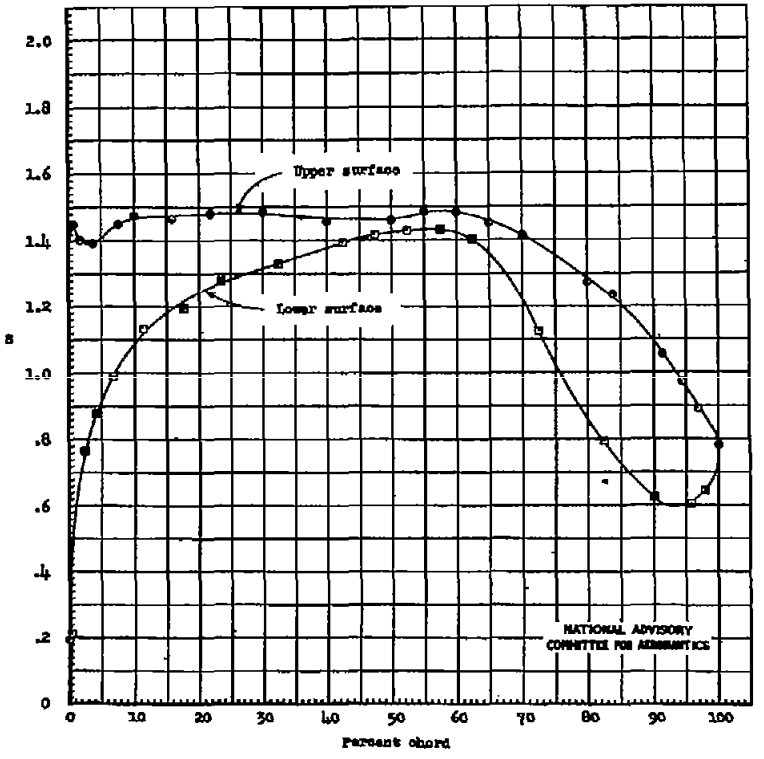

(i) $\alpha_0 = 0.5°$.

Figure 3.- Continued.

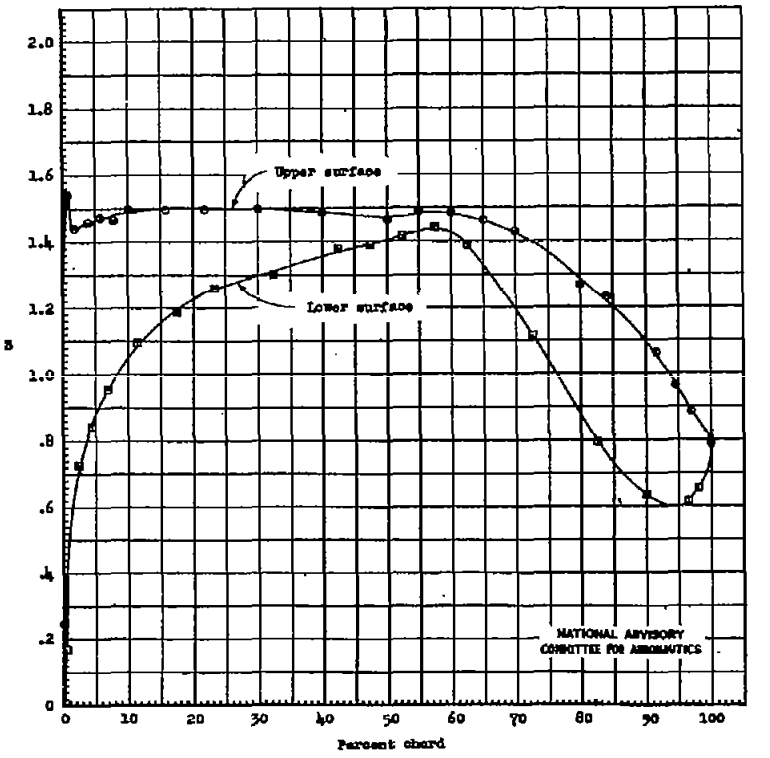

(j) $\alpha_0 = 0.8°$.

Figure 3.- Continued.

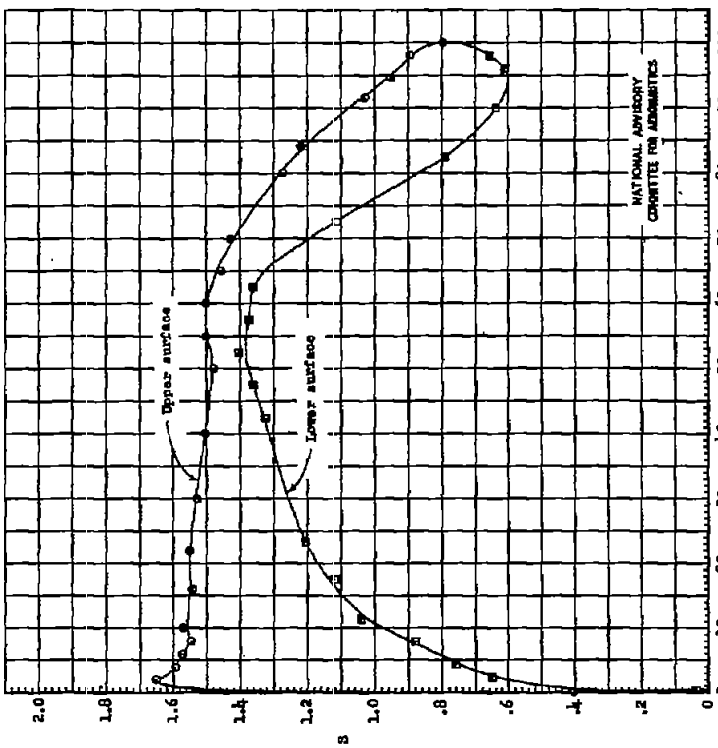

(l) $\alpha_0 = 1.5°$.

Figure 3.- Continued.

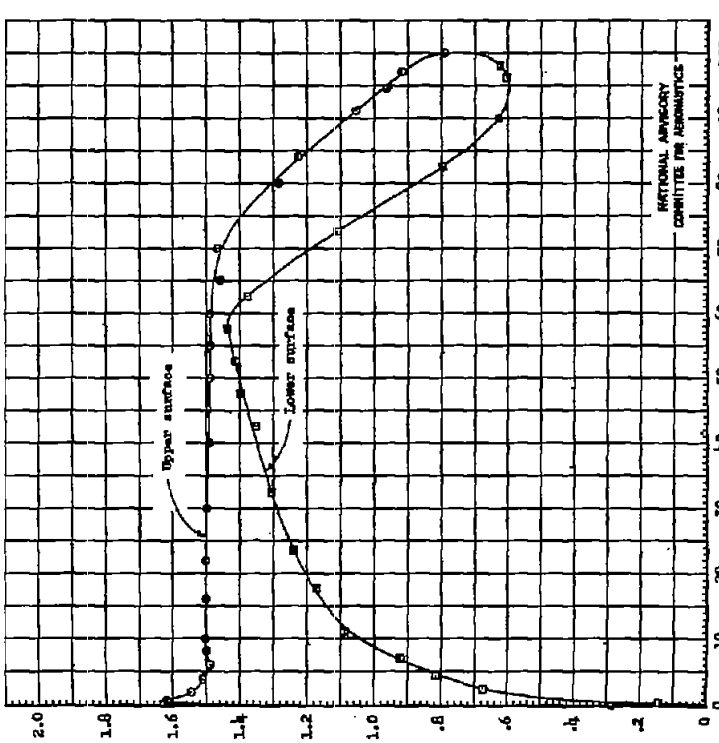

(k) $\alpha_0 = 1.0°$.

Figure 3.- Continued.

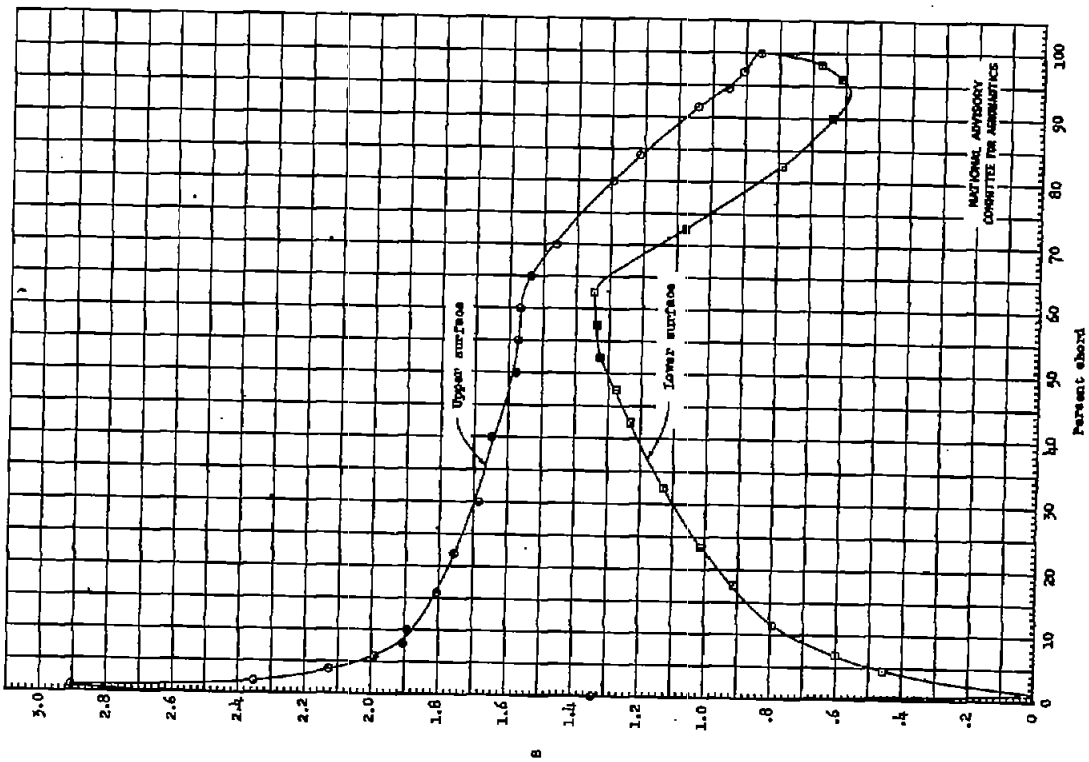

(n) $\alpha_0 = 4.1°$.

Figure 3.- Continued.

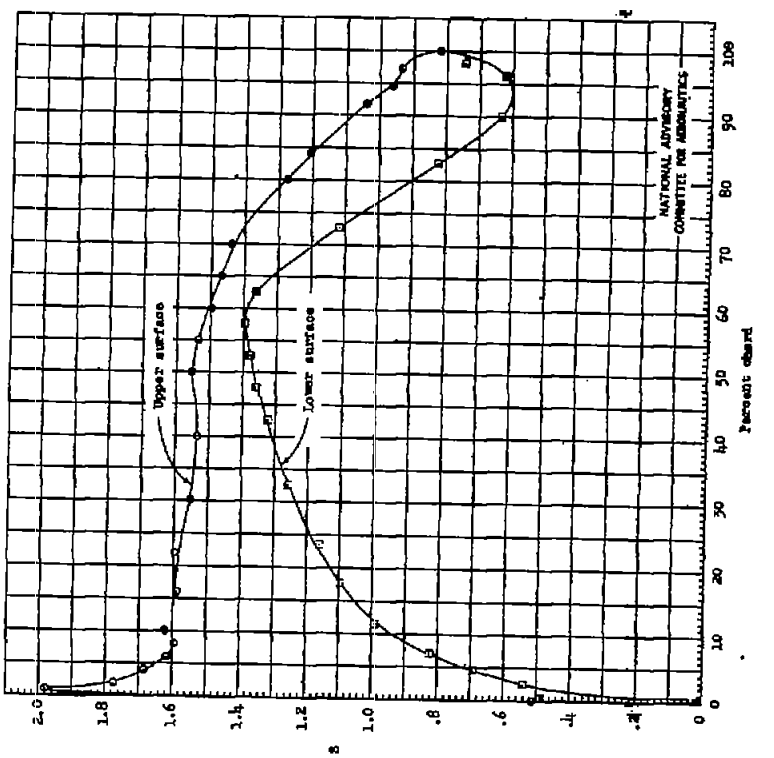

(m) $\alpha_0 = 2.0°$.

Figure 3.- Continued.

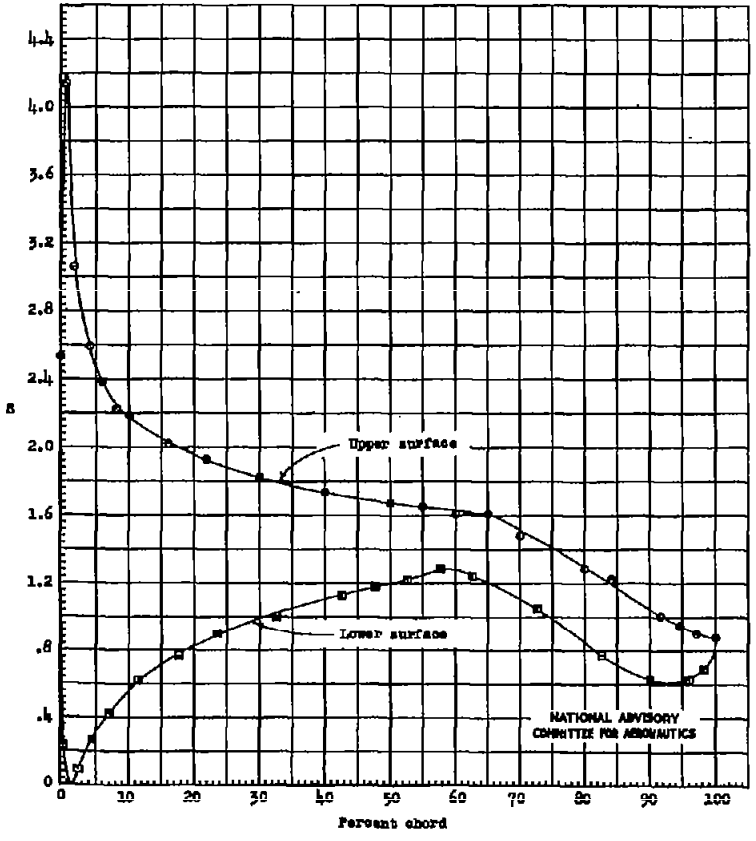

(c) $\alpha_0 = 6.1°$.

Figure 3.- Continued.

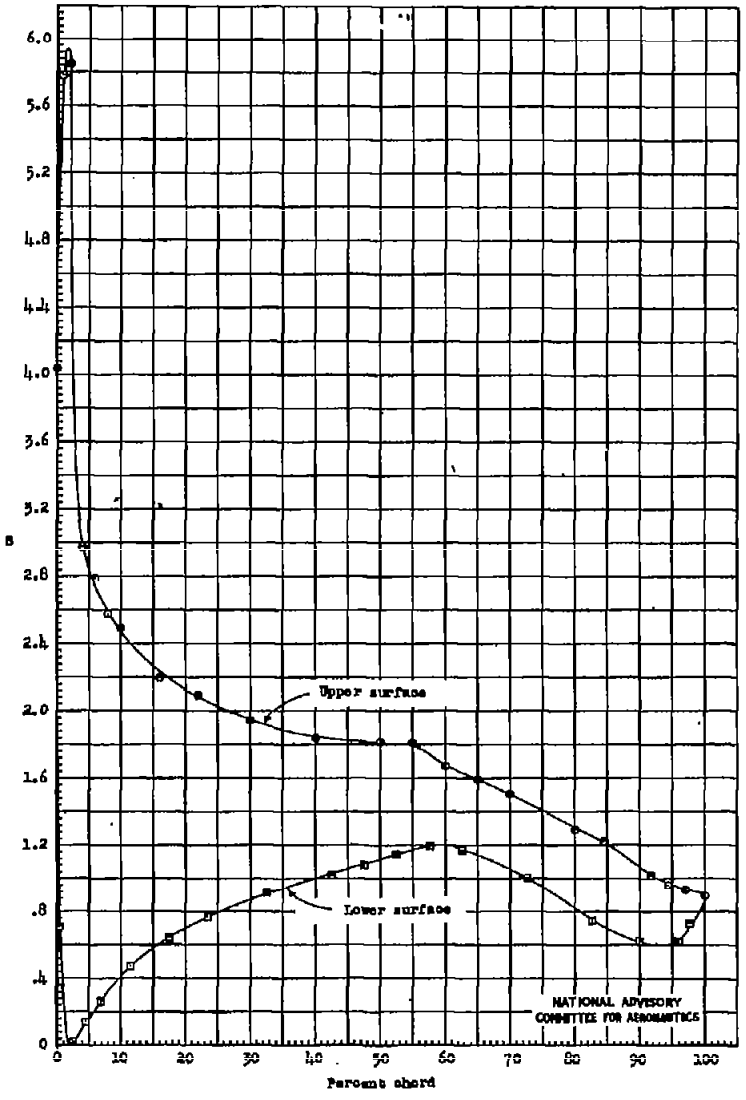

(p) $\alpha_0 = 8.1°$.

Figure 3.- Continued.

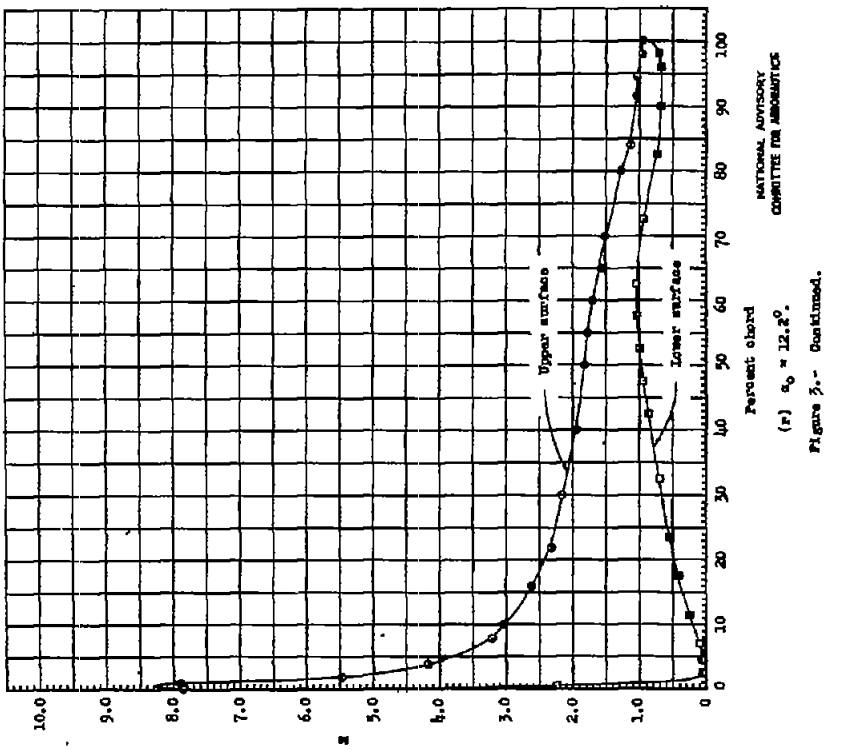

(r) $\alpha_0 = 12.2°$.

Figure 3.- Continued.

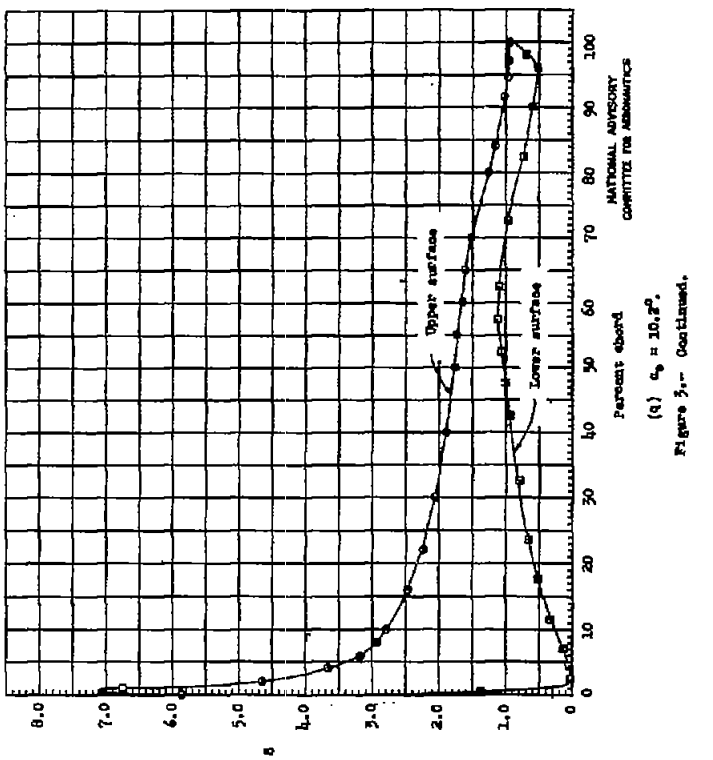

(q) $\alpha_0 = 10.2°$.

Figure 3.- Continued.

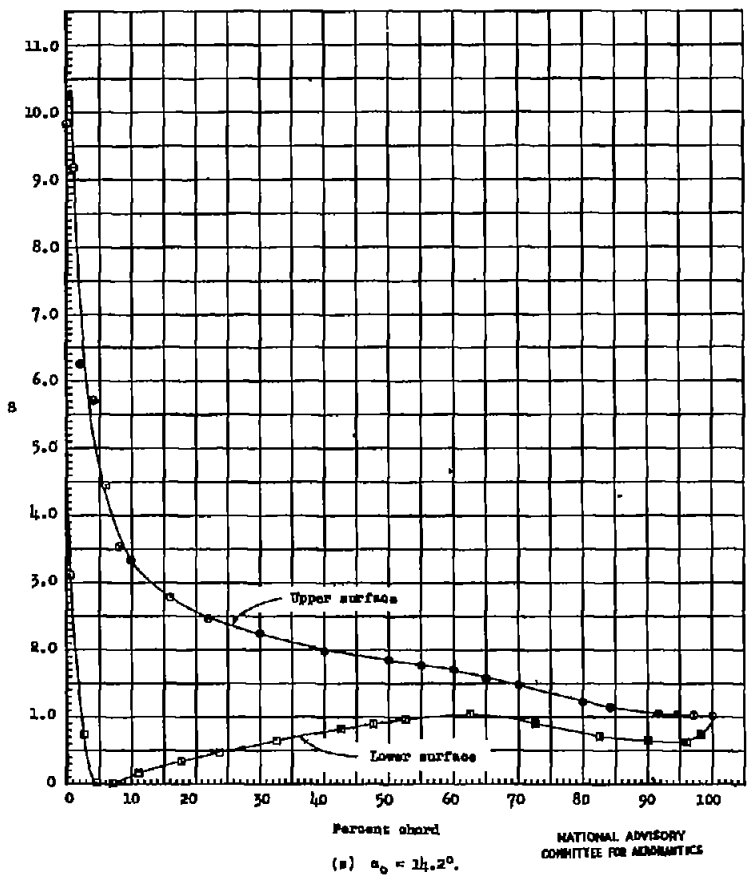

(s) $\alpha_0 = 14.2°$.

Figure 3.- Continued.

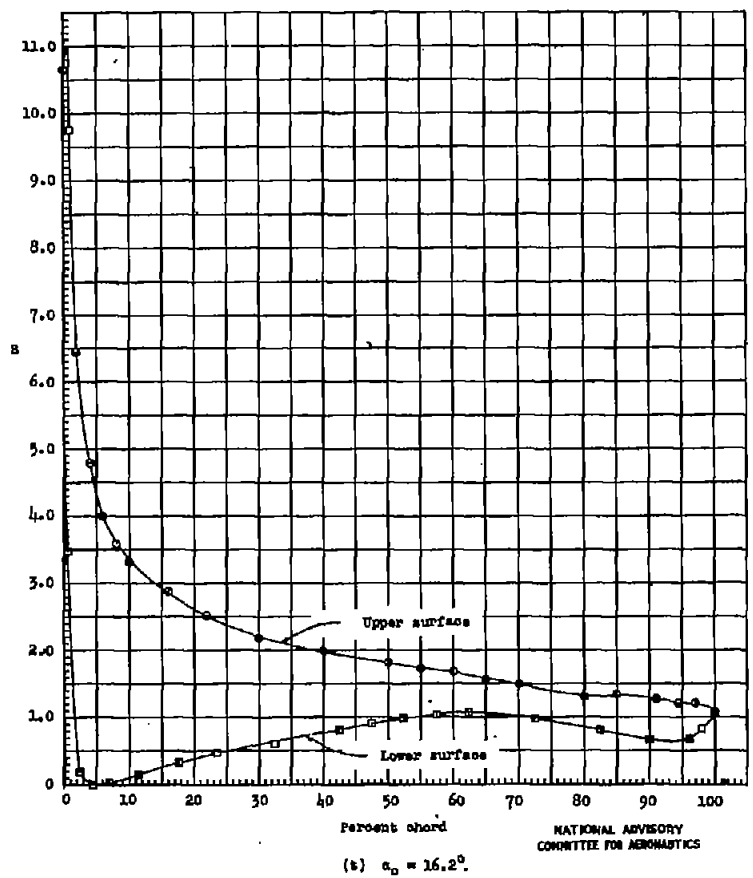

(t) $\alpha_0 = 16.2°$.

Figure 3.- Continued.

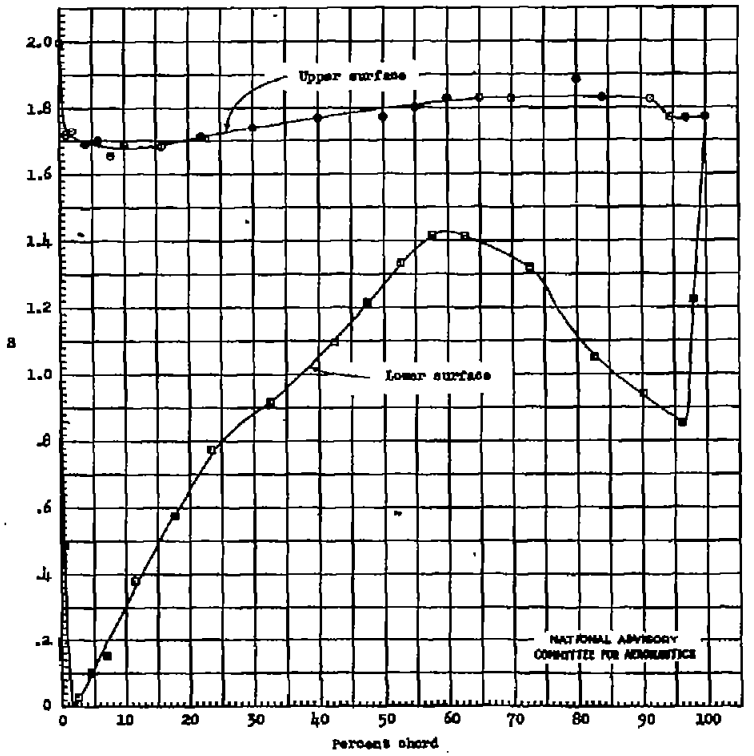

(u) $\alpha_0 = 18.3°$.

Figure 3.- Concluded.

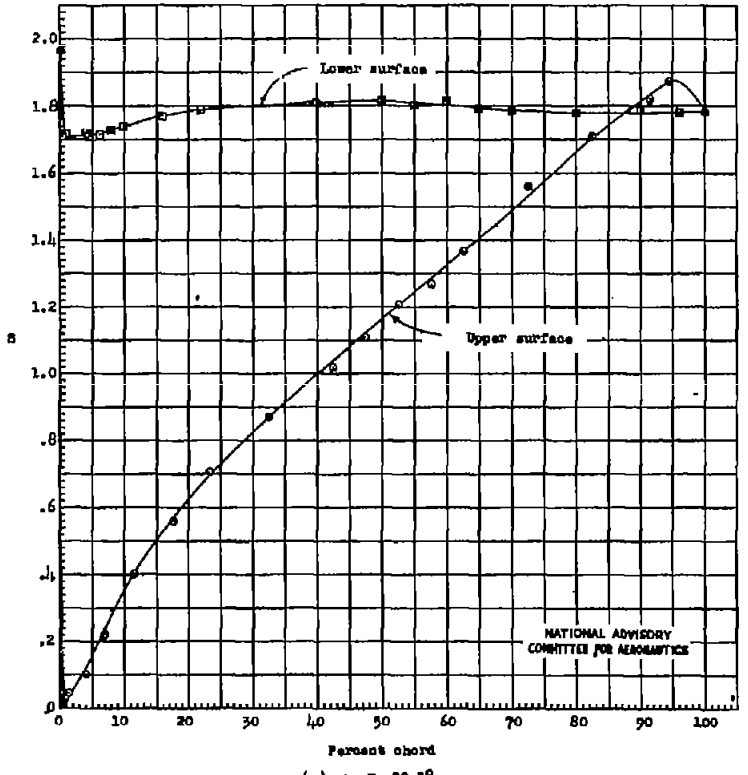

(a) $\alpha_0 = -20.3°$.

Figure 4.- Experimental pressure distribution of the NACA 66(215)-316 $\begin{cases} a = 0.6, & \alpha_{l_1} = -1.2 \\ a = 1.0, & \alpha_{l_1} = \text{...} \end{cases}$ airfoil section. $R = 6 \times 10^6$; TDT test 631.

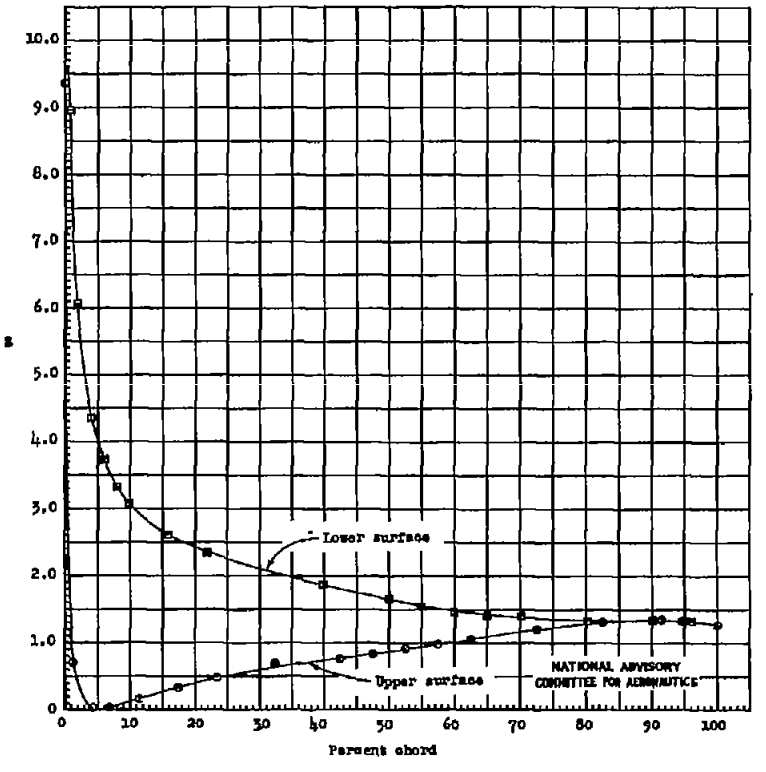

(b) $\alpha_0 = -18.5°$.

Figure 4.- Continued.

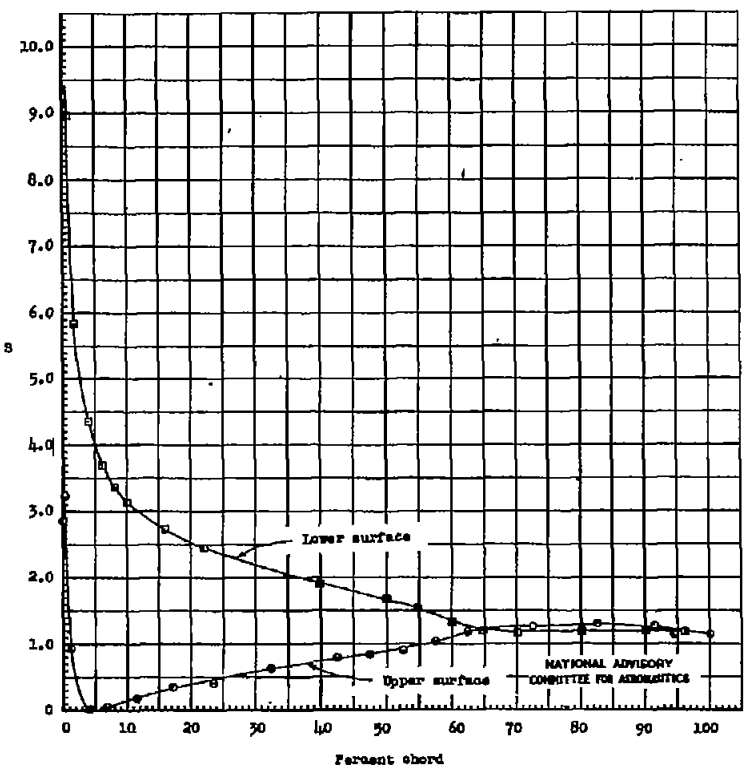

(c) $\alpha_0 = -16.2°$.

Figure 4.- Continued.

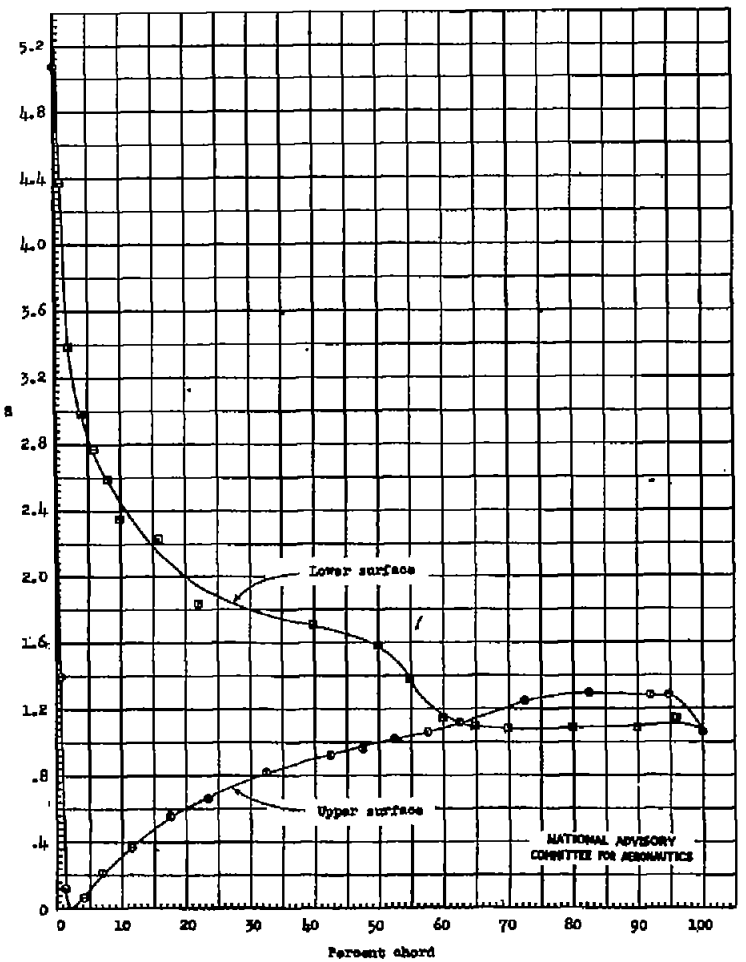

(d) $\alpha_0 = -12.2°$.

Figure 4.- Continued.

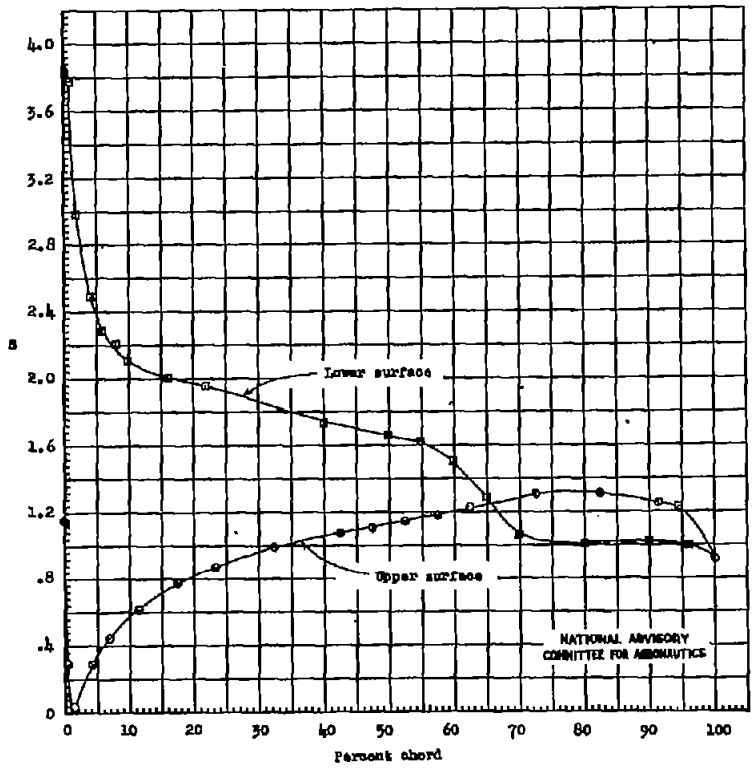

(e) $\alpha_0 = -8.1°$.

Figure 4.- Continued.

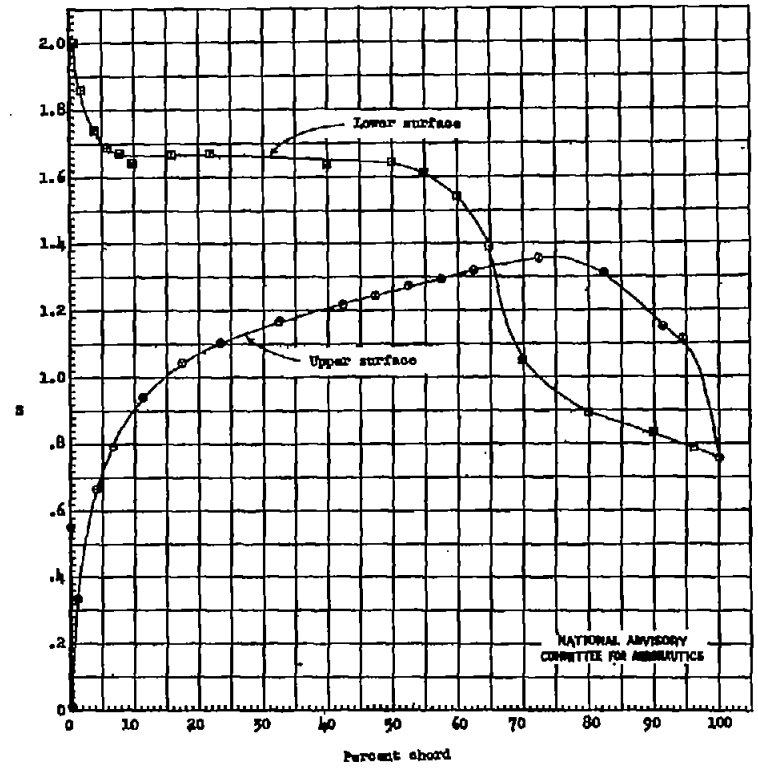

(f) $\alpha_0 = -4.1°$.

Figure 4.- Continued.

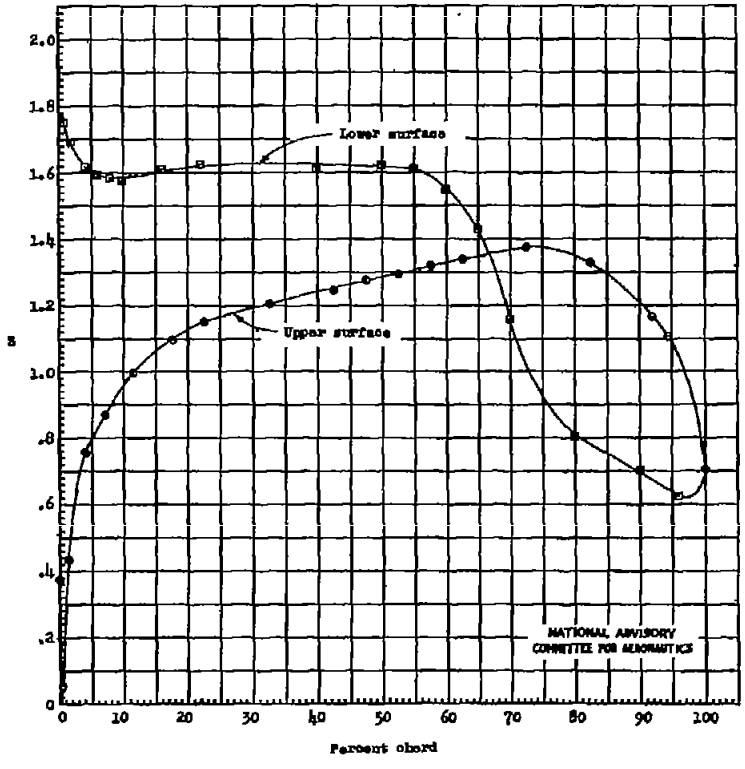

(g) $\alpha_0 = -3.6°$.

Figure 4.- Continued.

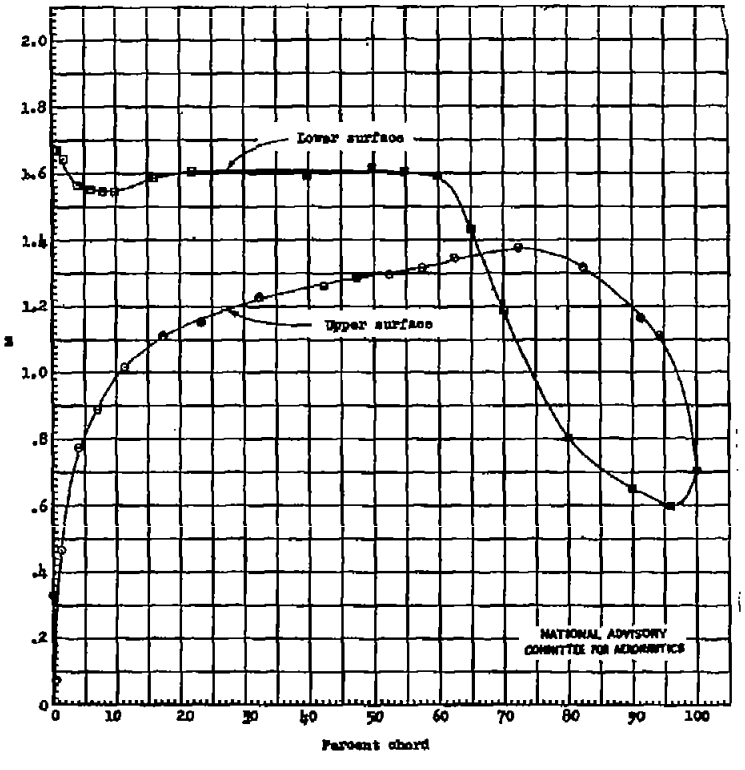

(h) $\alpha_0 = -3.4°$.

Figure 4.- Continued.

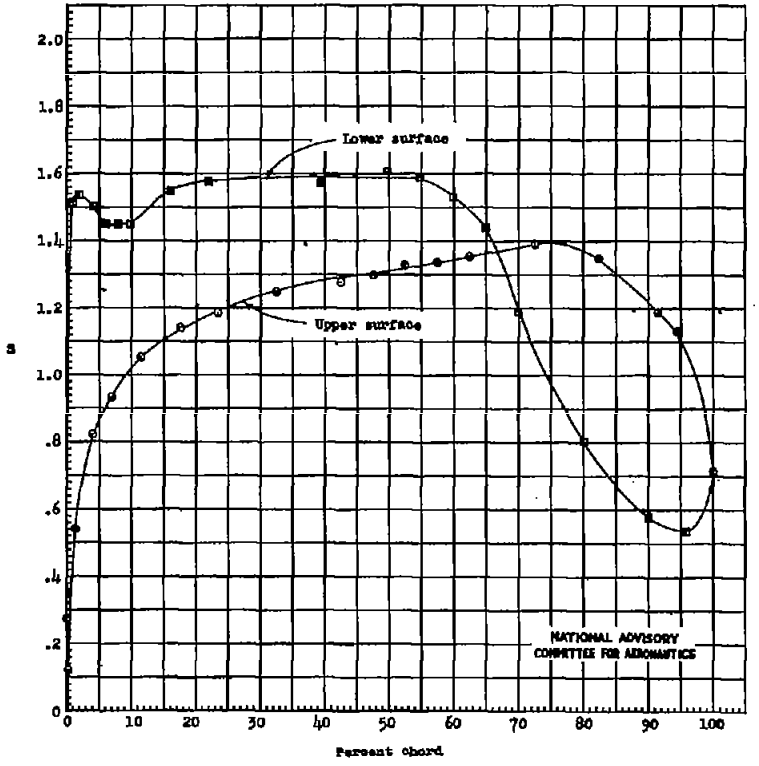

(i) $\alpha_0 = -3.1°$.

Figure 4.- Continued.

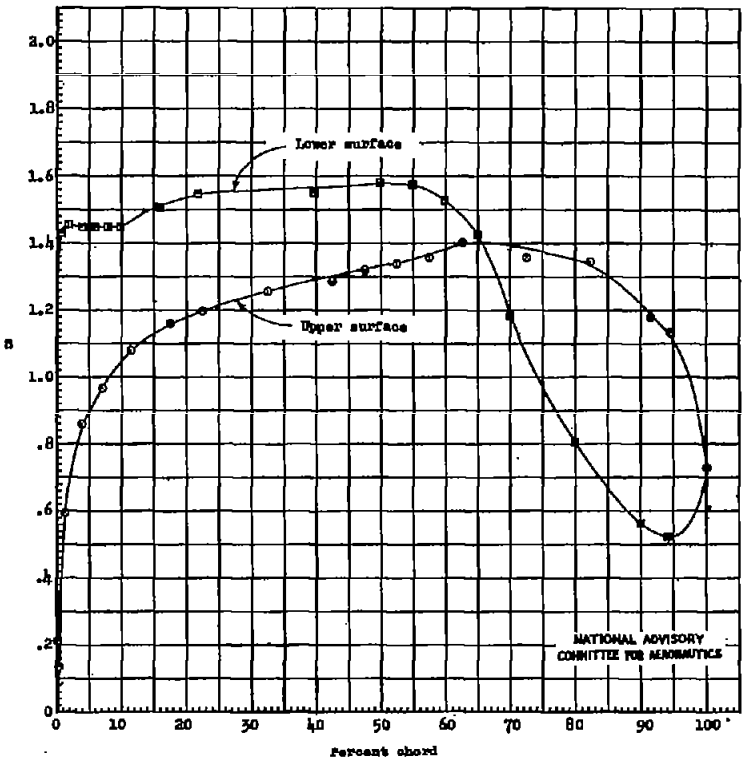

(j) $\alpha_0 = -2.8°$.

Figure 4.- Continued.

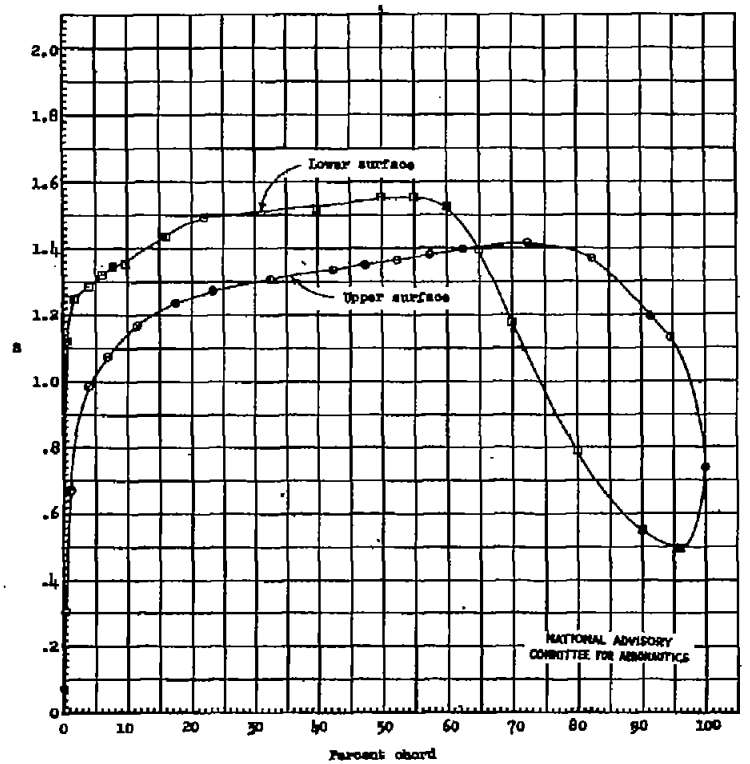

(k) $\alpha_0 = -2.0°$.

Figure 4.- Continued.

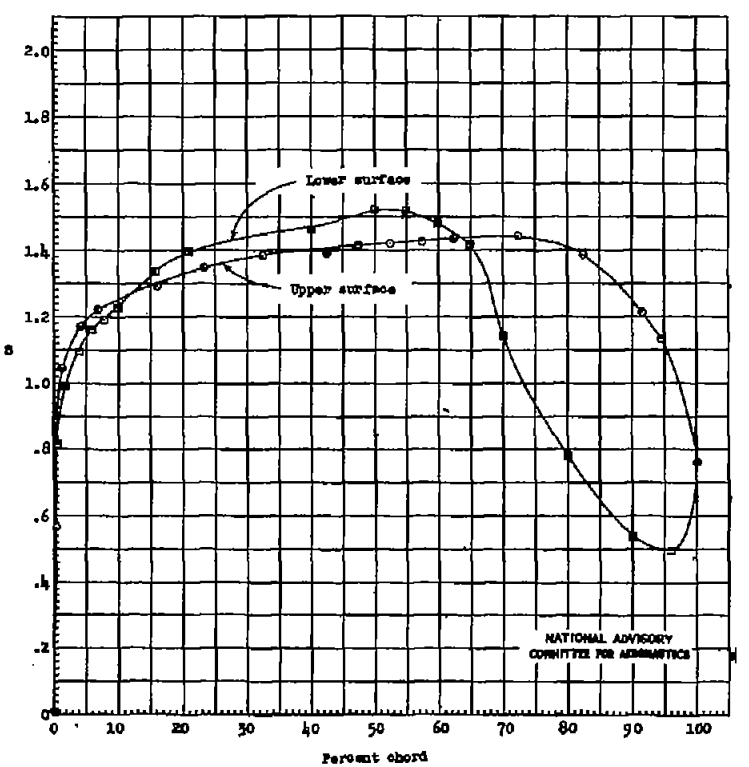

(l) $\alpha_0 = -1.0°$.

Figure 4.- Continued.

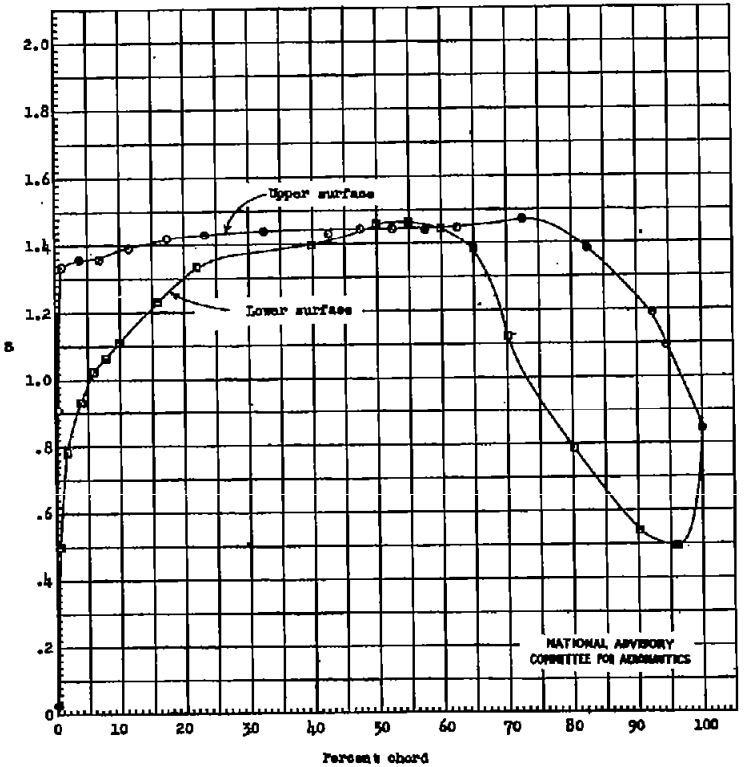

(m) $\alpha_0 = 0°$.

Figure 4.- Continued.

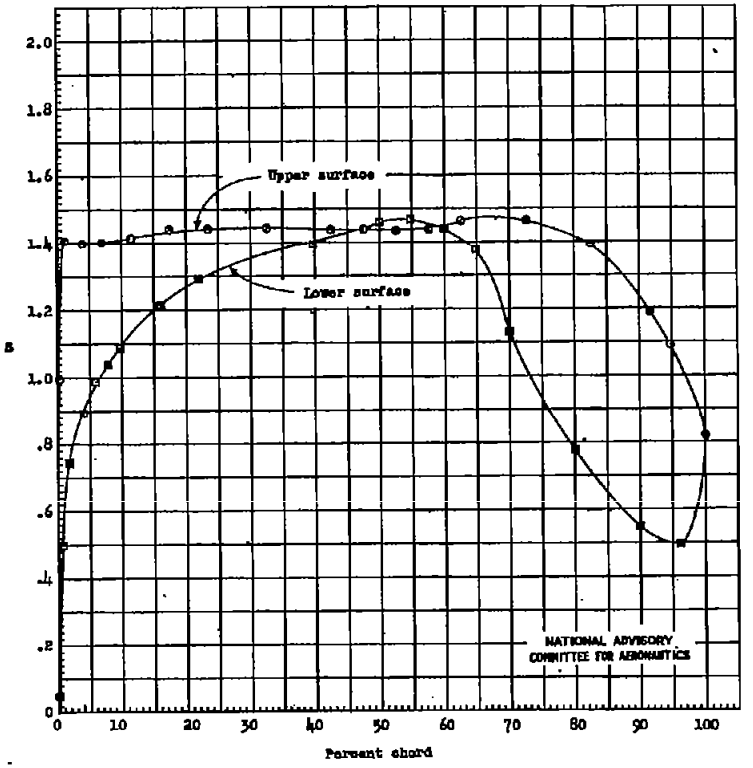

(n) $\alpha_0 = 0.3°$.

Figure 4.- Continued.

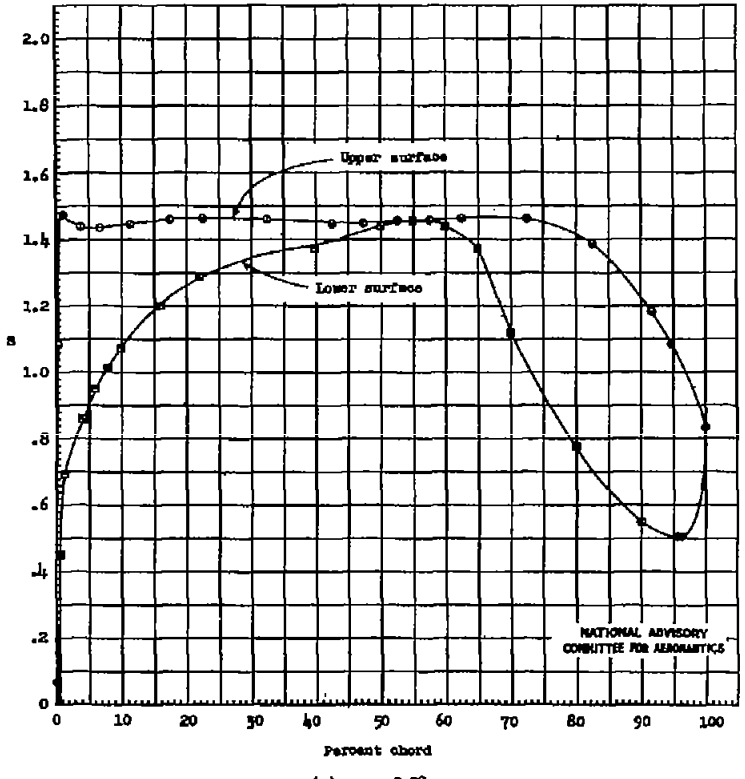

(c) $\alpha_0 = 0.5°$.

Figure 4.- Continued.

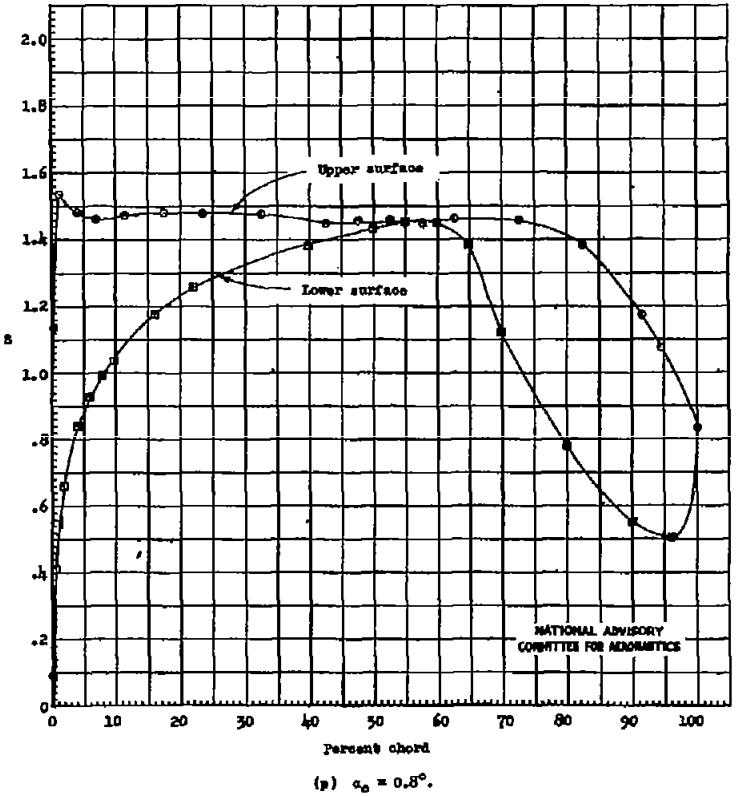

(p) $\alpha_0 = 0.8°$.

Figure 4.- Continued.

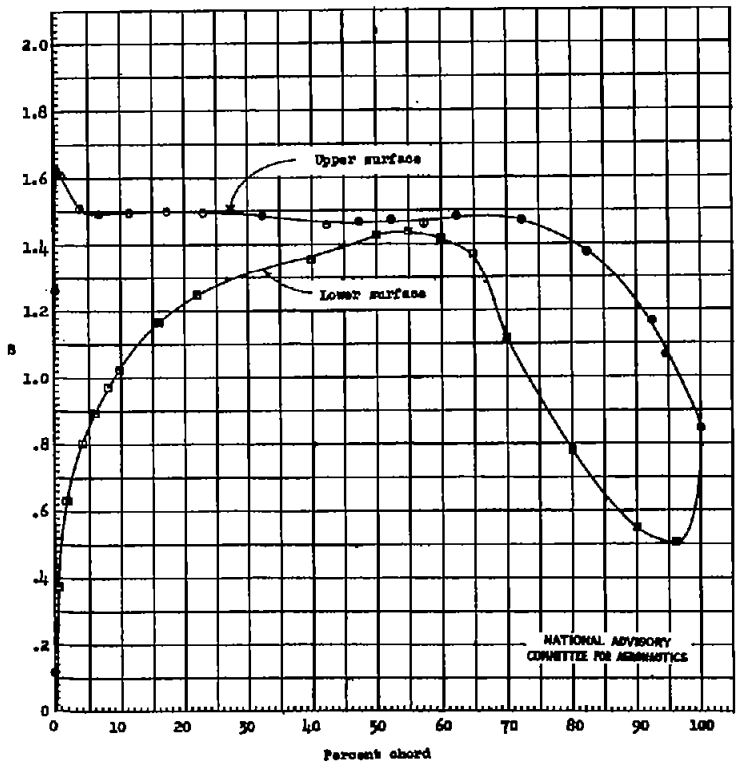

(q) $\alpha_0 = 1.0°$.

Figure 4.- Continued.

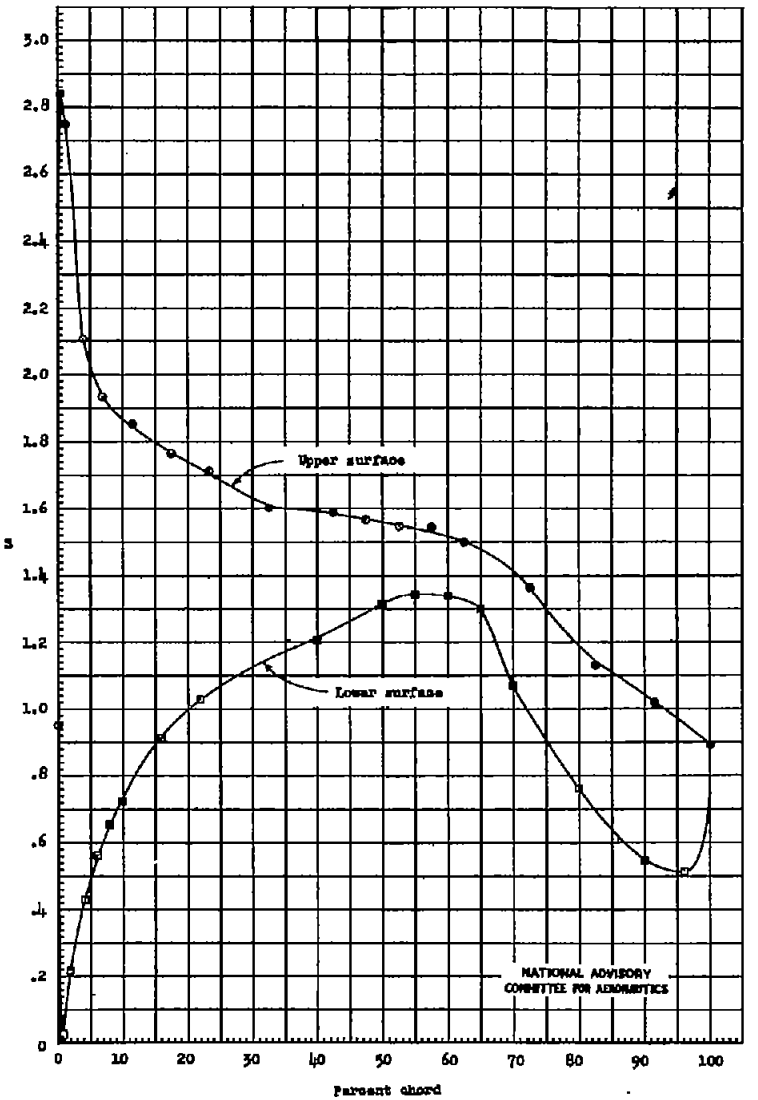

(r) $\alpha_0 = 4.1°$.

Figure 4.- Continued.

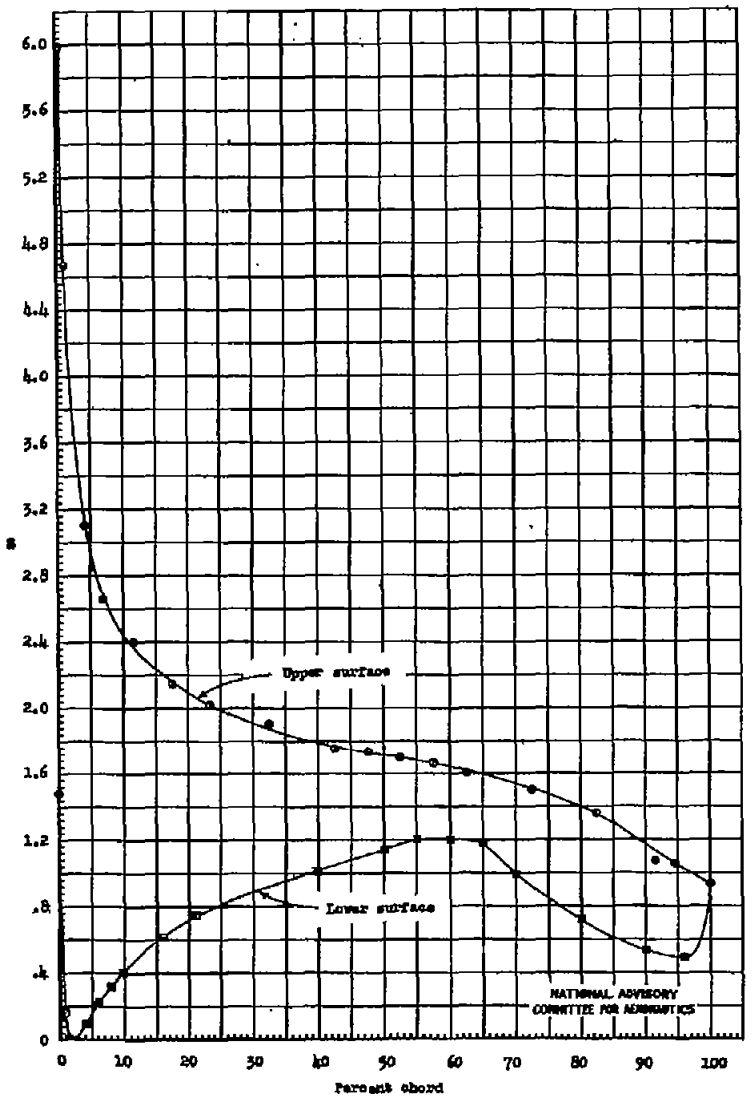

(s) $\alpha_0 = 8.1°$.

Figure 4.- Continued.

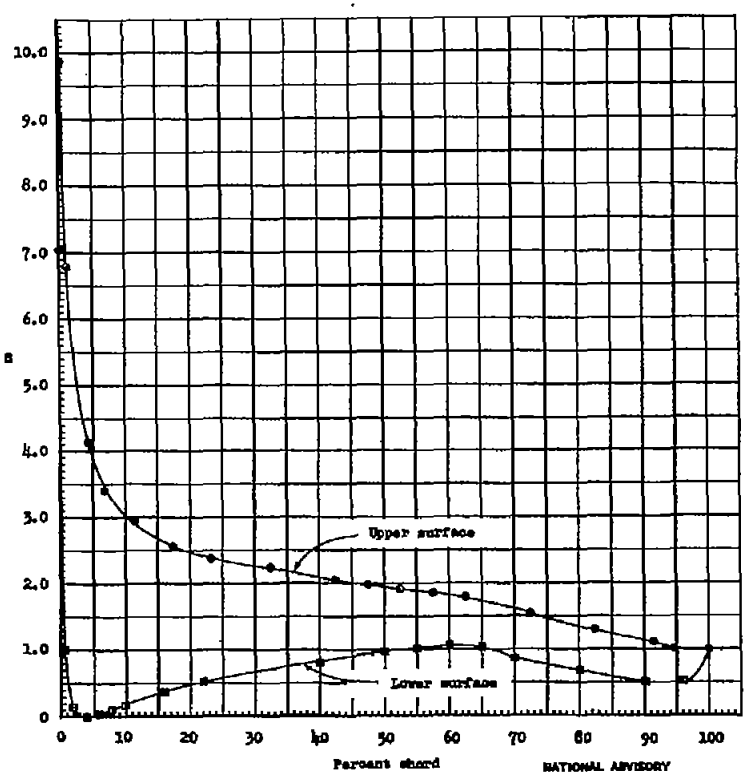

(t) $\alpha_0 = 12.2°$.

Figure 4.- Continued.

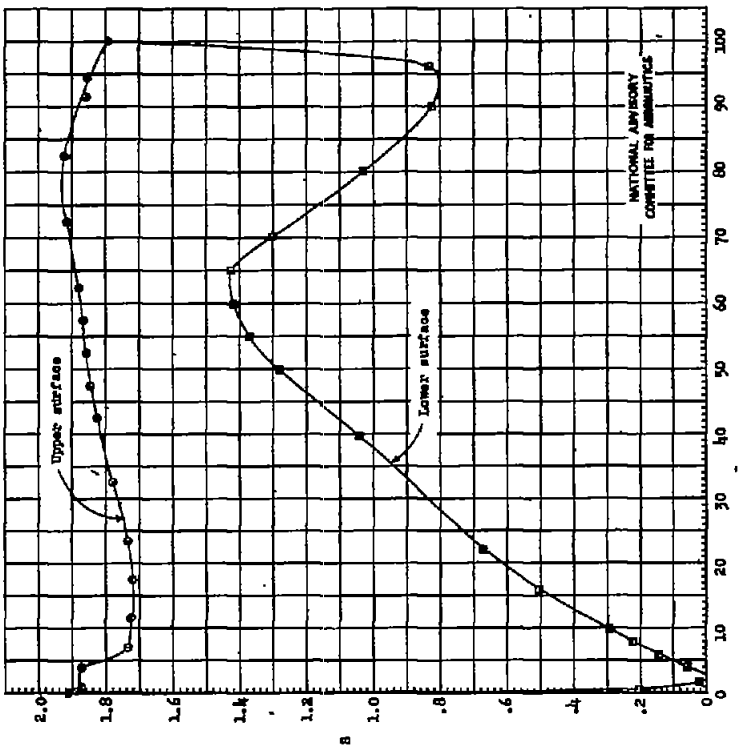

(v) $\alpha_0 = 19.3°$.

Figure 4.- Concluded.

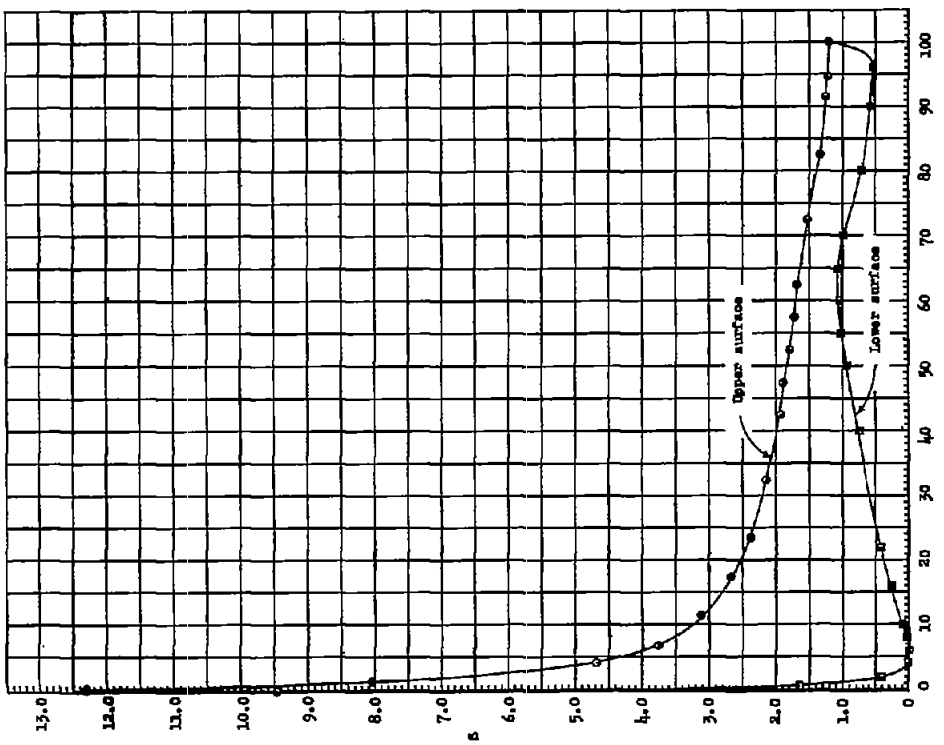

(u) $\alpha_0 = 16.2°$.

Figure 4.- Continued.

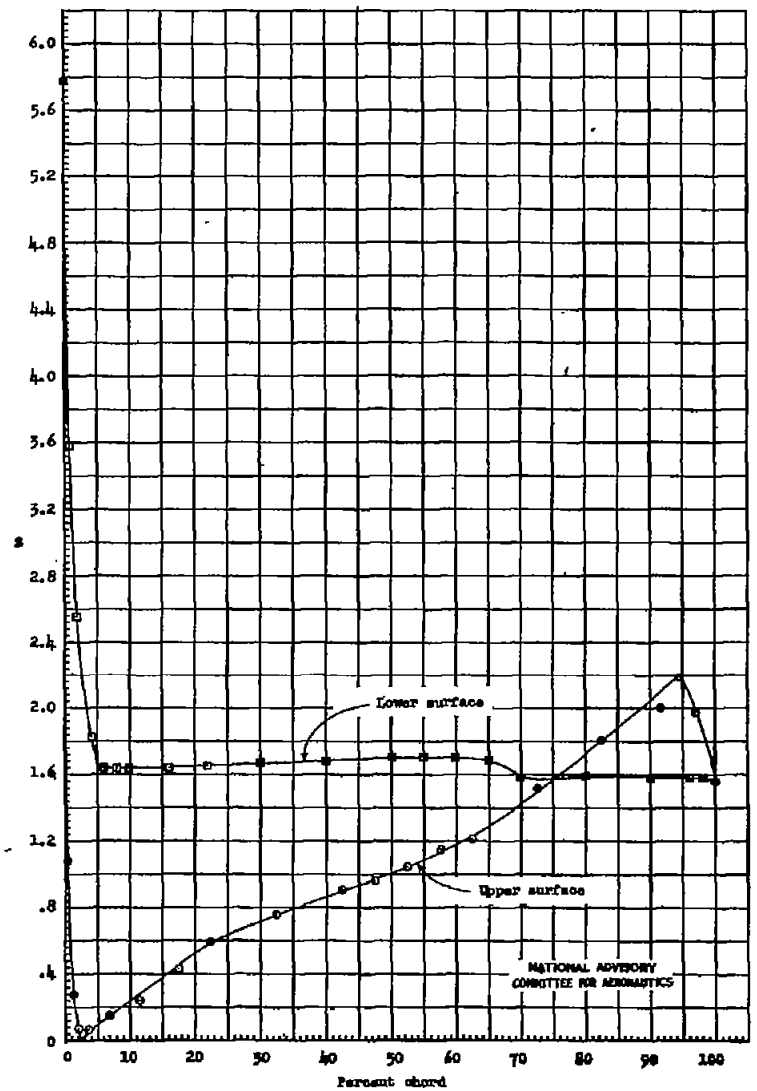

(a) $\alpha_0 = -22.3°$.

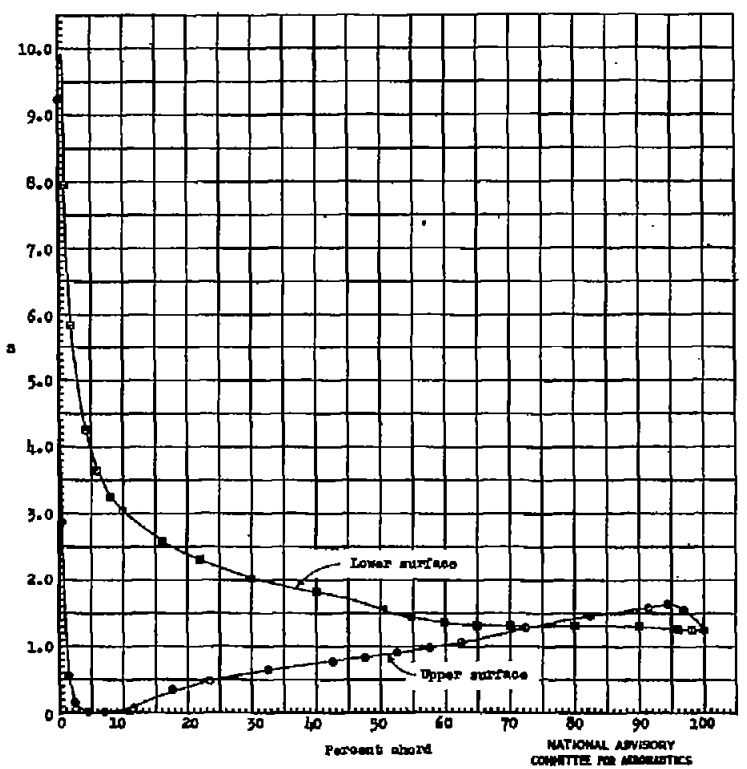

(b) $\alpha_0 = -18.5°$.

Figure 5.- Experimental pressure distribution of the NACA 66(215)-416 $\begin{bmatrix} a = 0.6, & \alpha_{l_i} = -1.6 \\ a = 1.0, & \alpha_{l_i} = 2.0 \end{bmatrix}$ airfoil section. $R = 6 \times 10^6$; EDT test 632.

Figure 5.- Continued.

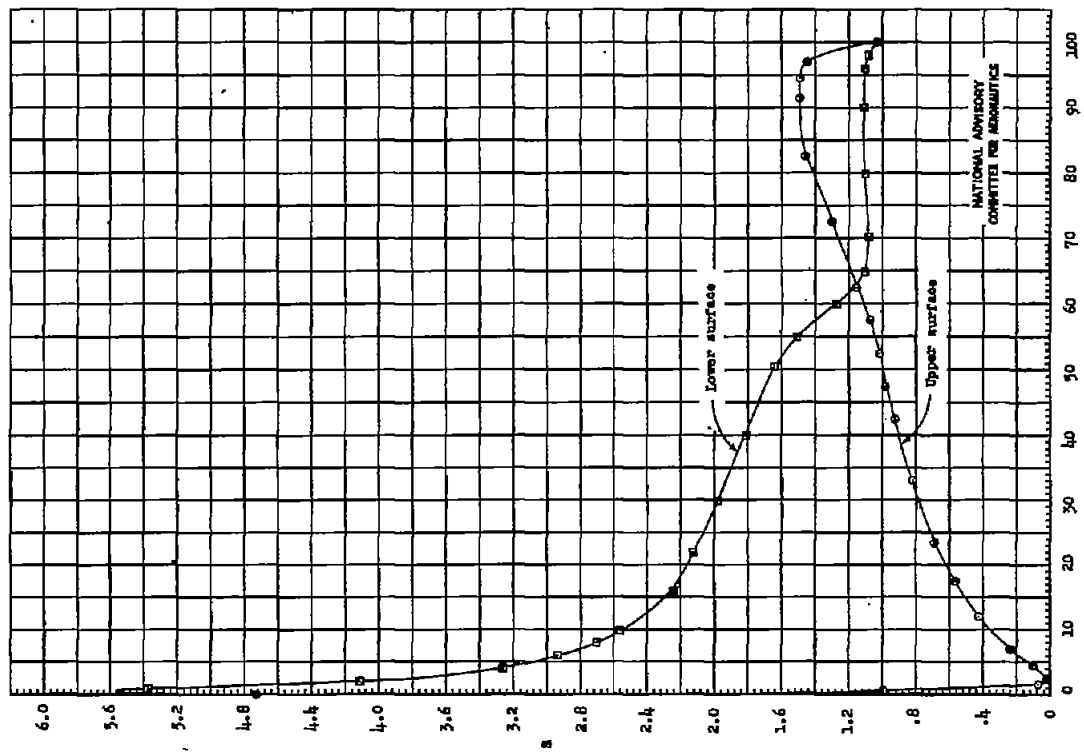

(d) $\alpha_0 = -12.2°$.

Figure 5.- Continued.

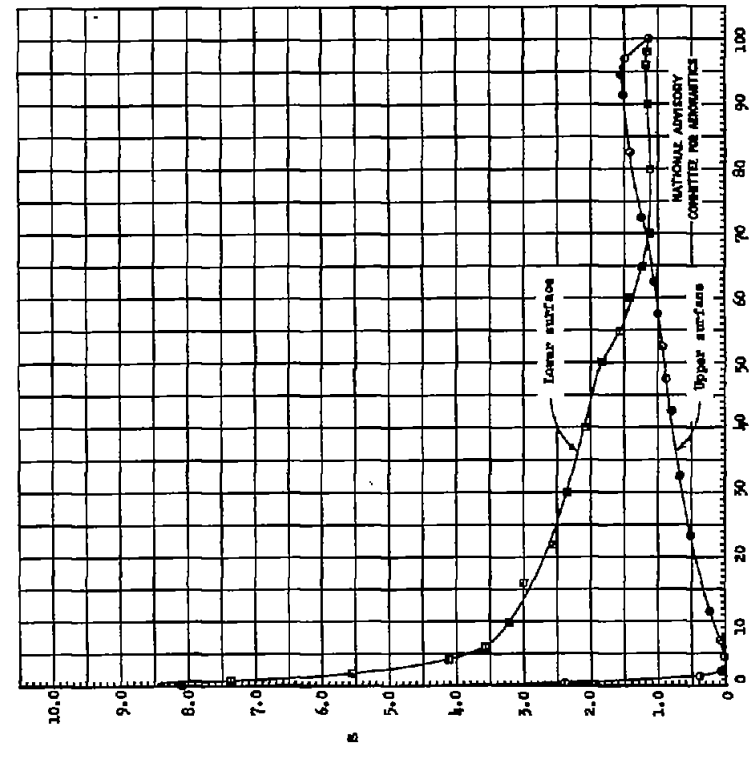

(e) $\alpha_0 = -16.2°$.

Figure 5.- Continued.

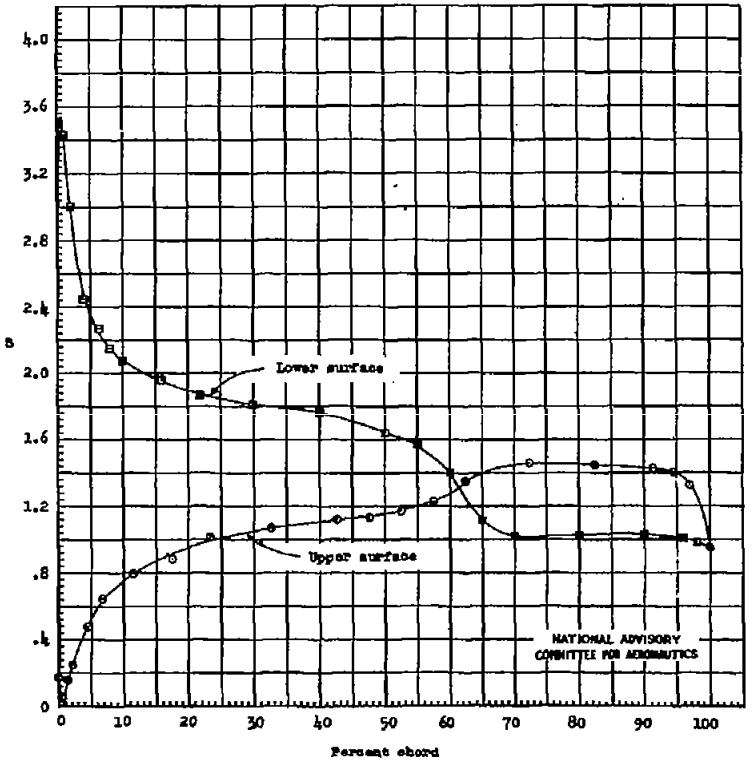

(e) $\alpha_0 = -8.1°$.

Figure 5.- Continued.

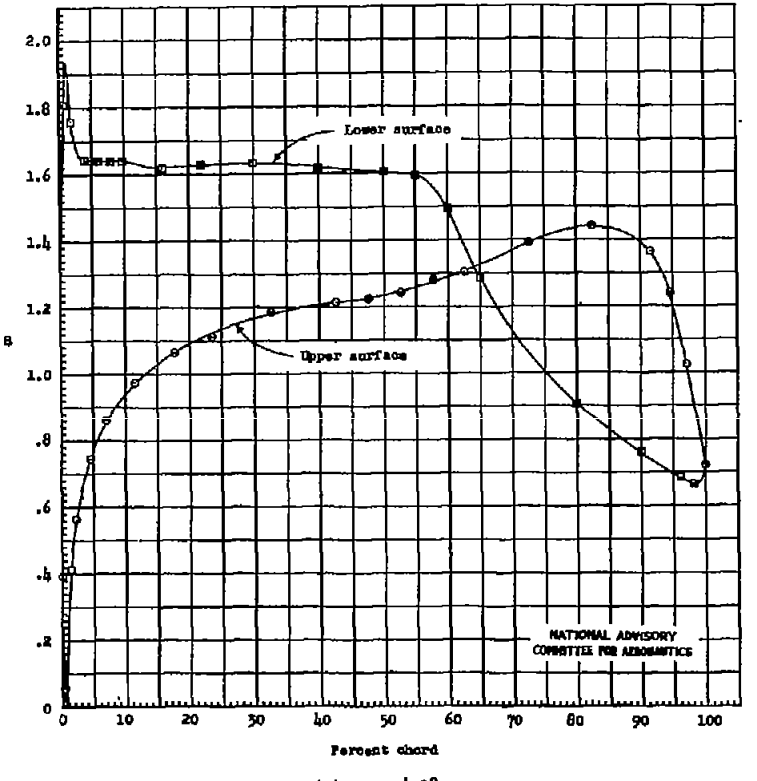

(f) $\alpha_0 = -4.1°$.

Figure 5.- Continued.

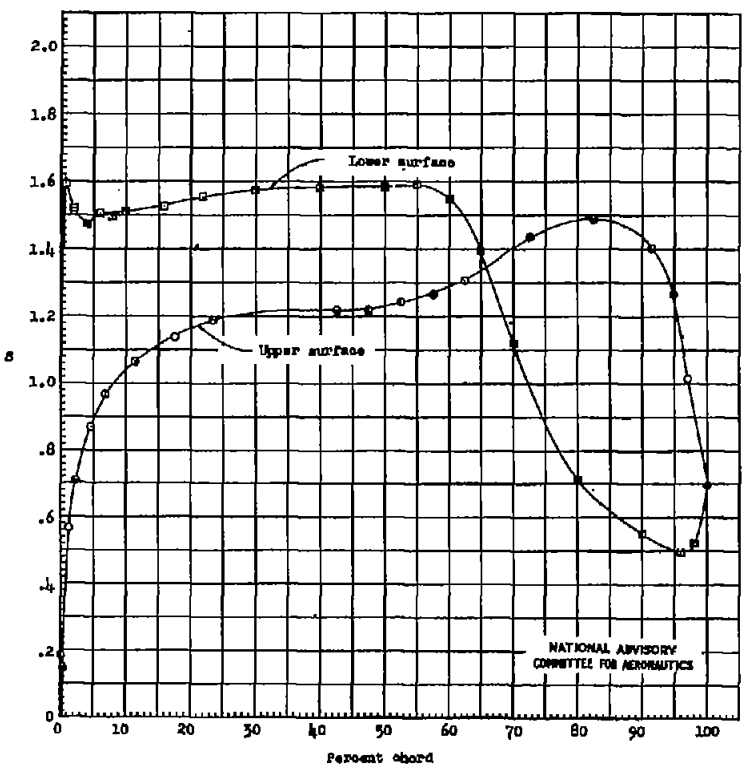

(g) $\alpha_o = -3.4°$.

Figure 5.- Continued.

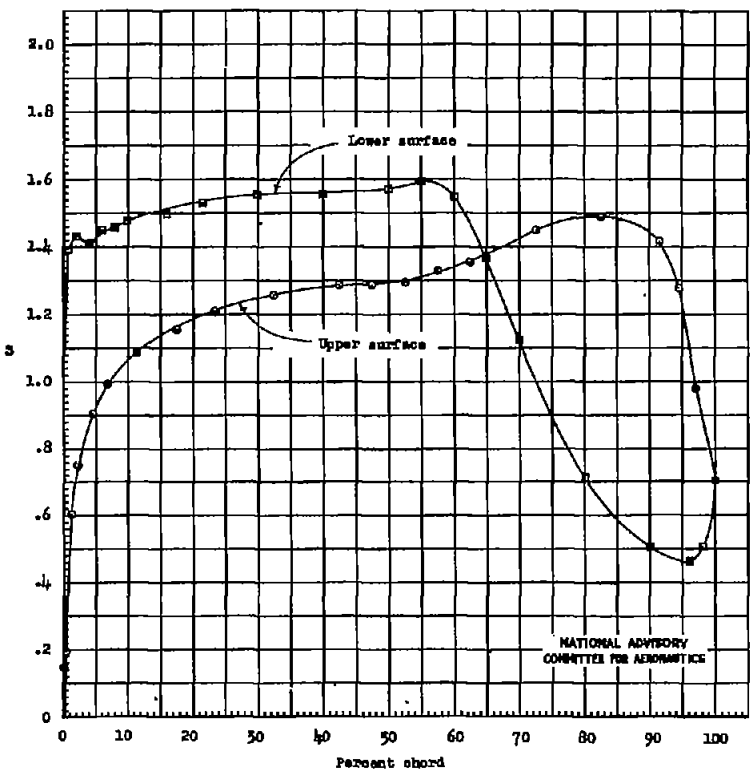

(h) $\alpha_o = -3.1°$.

Figure 5.- Continued.

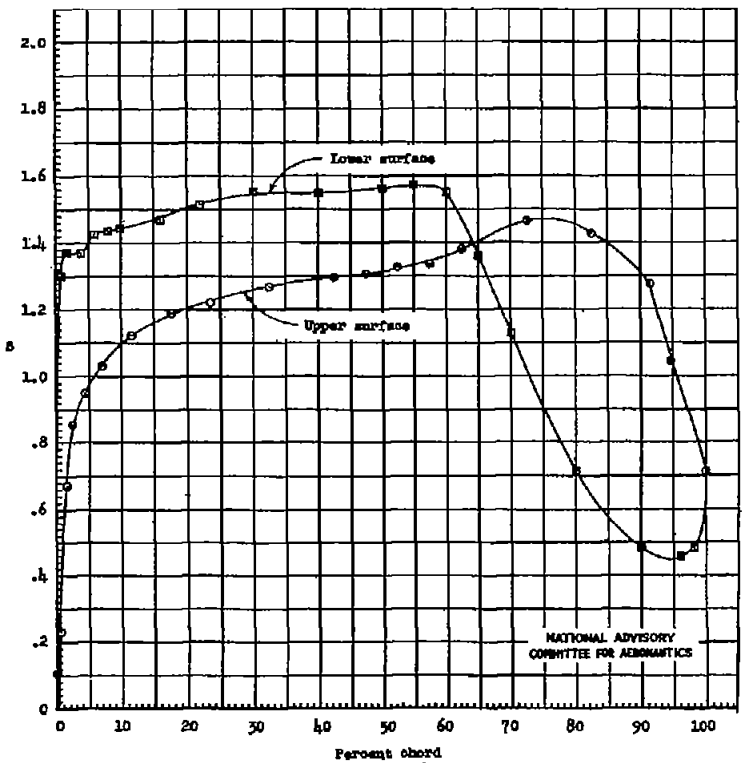

(i) $\alpha_o = -2.8°$.

Figure 5.- Continued.

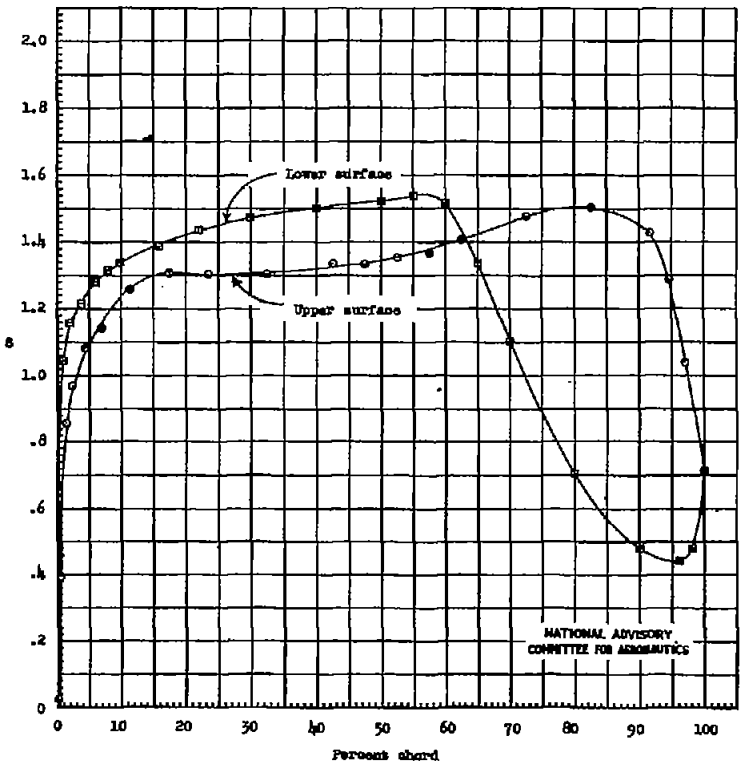

(j) $\alpha_o = -2.0°$.

Figure 5.- Continued.

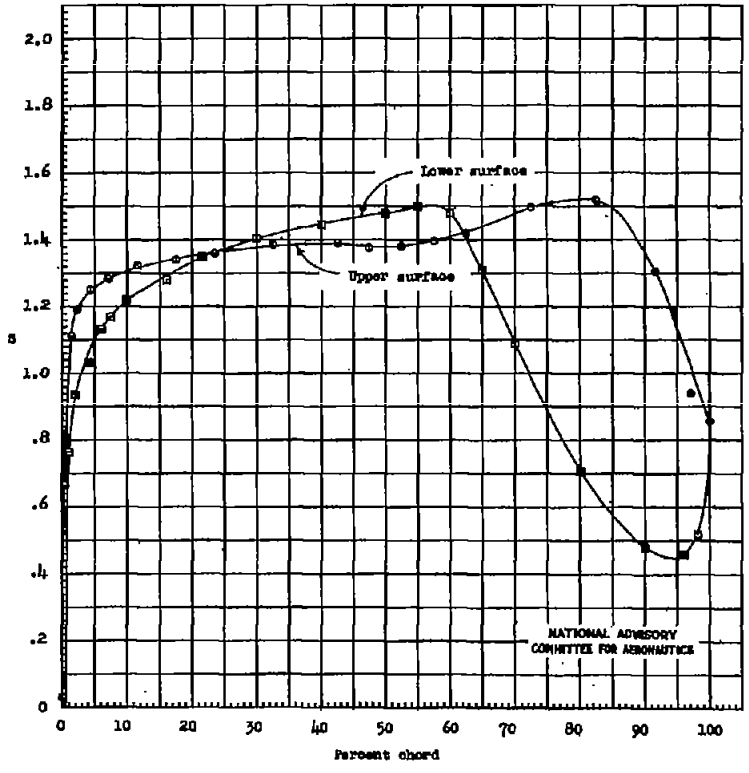

(k) $\alpha_0 = -1.0^\circ$.

Figure 5.- Continued.

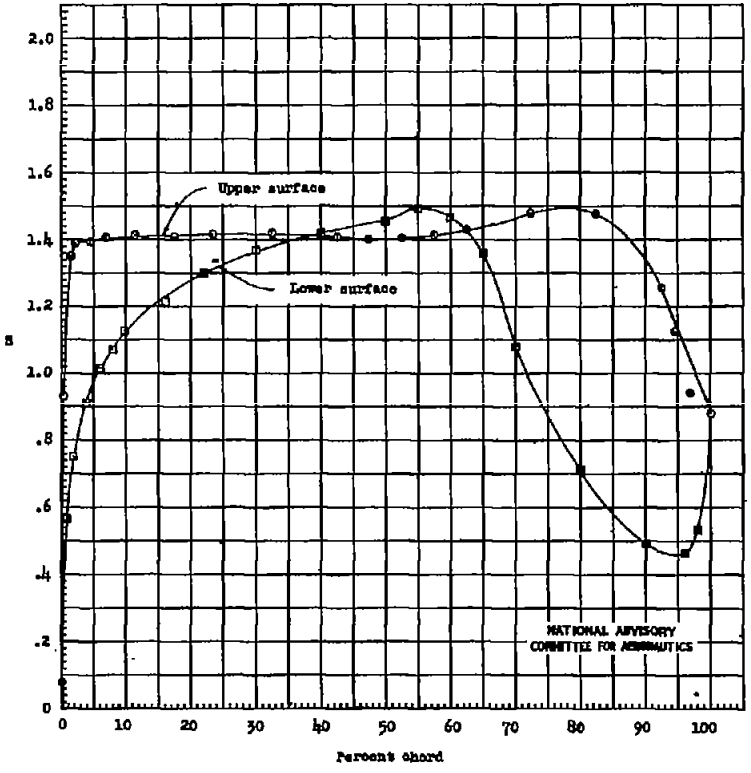

(l) $\alpha_0 = 0^\circ$.

Figure 5.- Continued.

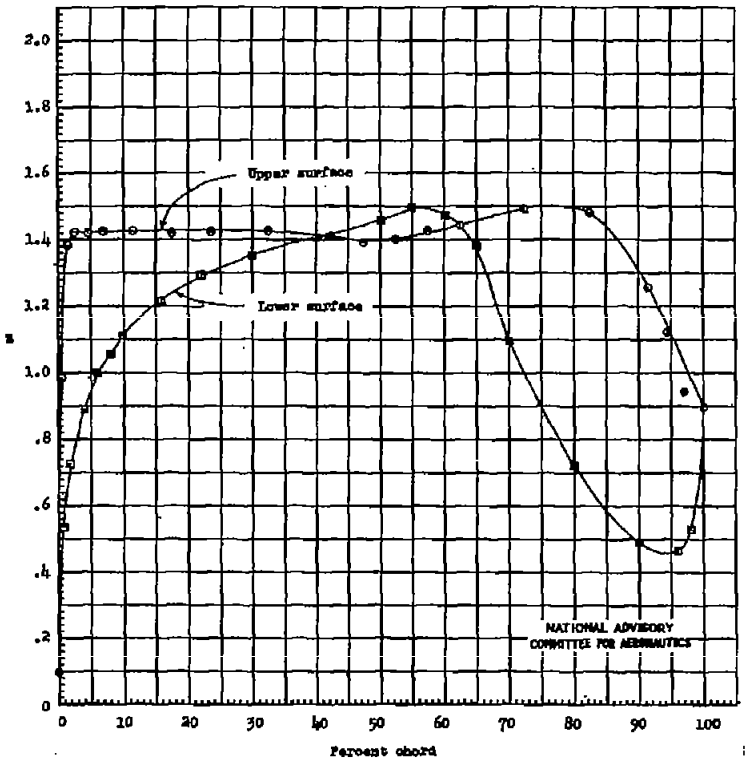

(m) $\alpha_0 = 0.3°$.

Figure 5.- Continued.

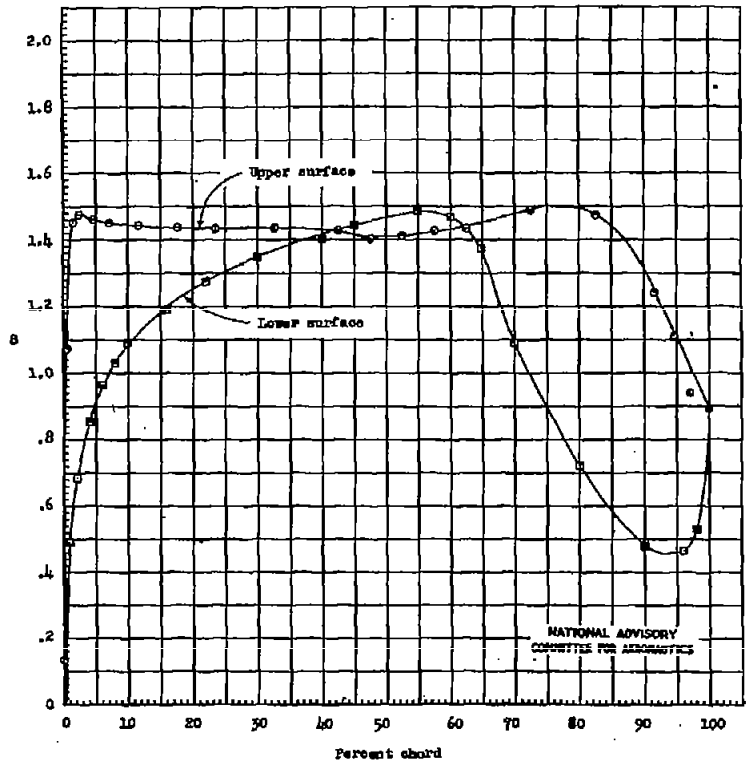

(n) $\alpha_0 = 0.5°$.

Figure 5.- Continued.

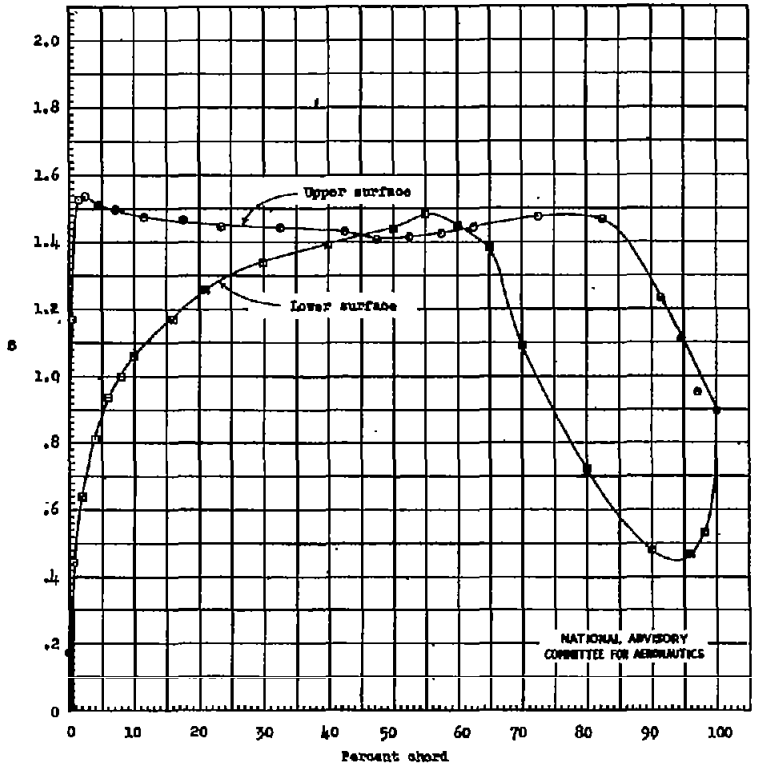

(o) $\alpha_0 = 0.8°$.

Figure 5.- Continued.

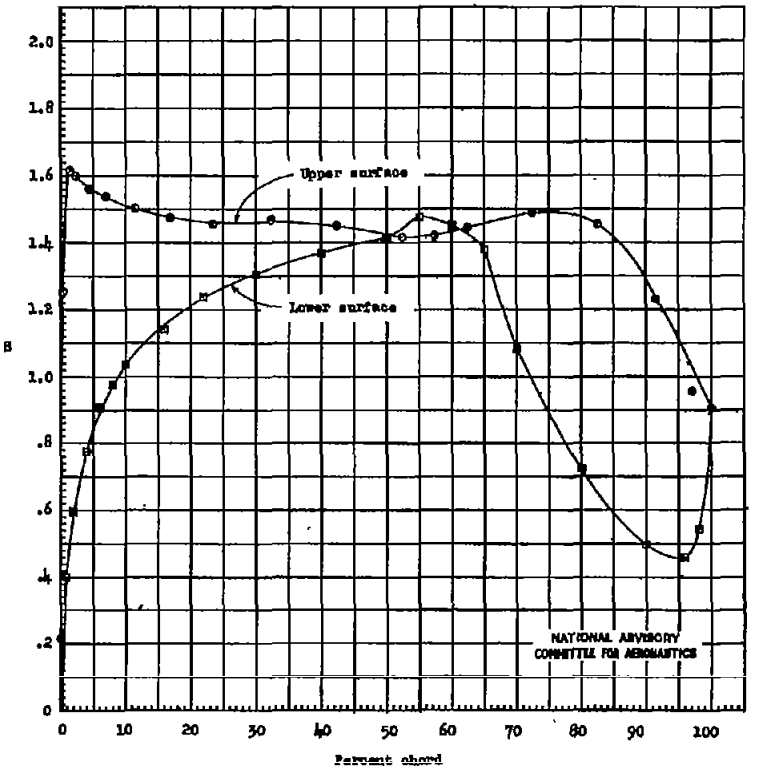

(p) $\alpha_0 = 1.0°$.

Figure 5.- Continued.

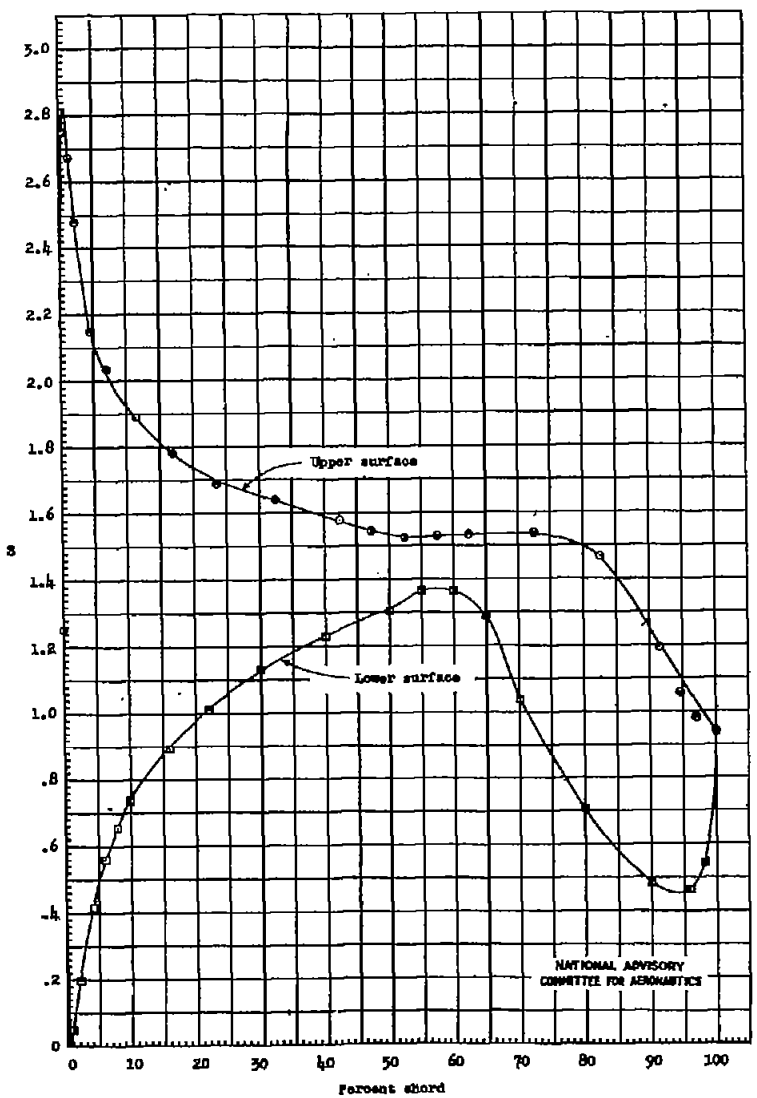

(q) $\alpha_o = 4.1°$.

Figure 5.- Continued.

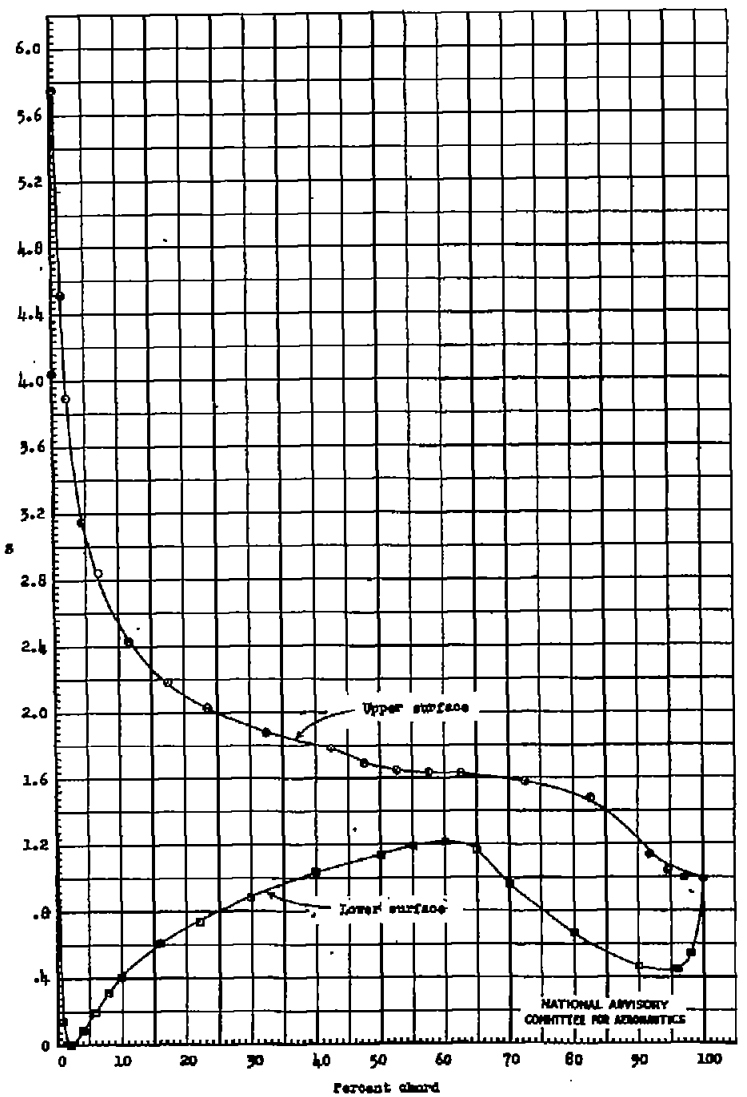

(r) $\alpha_o = 8.2°$.

Figure 5.- Continued.

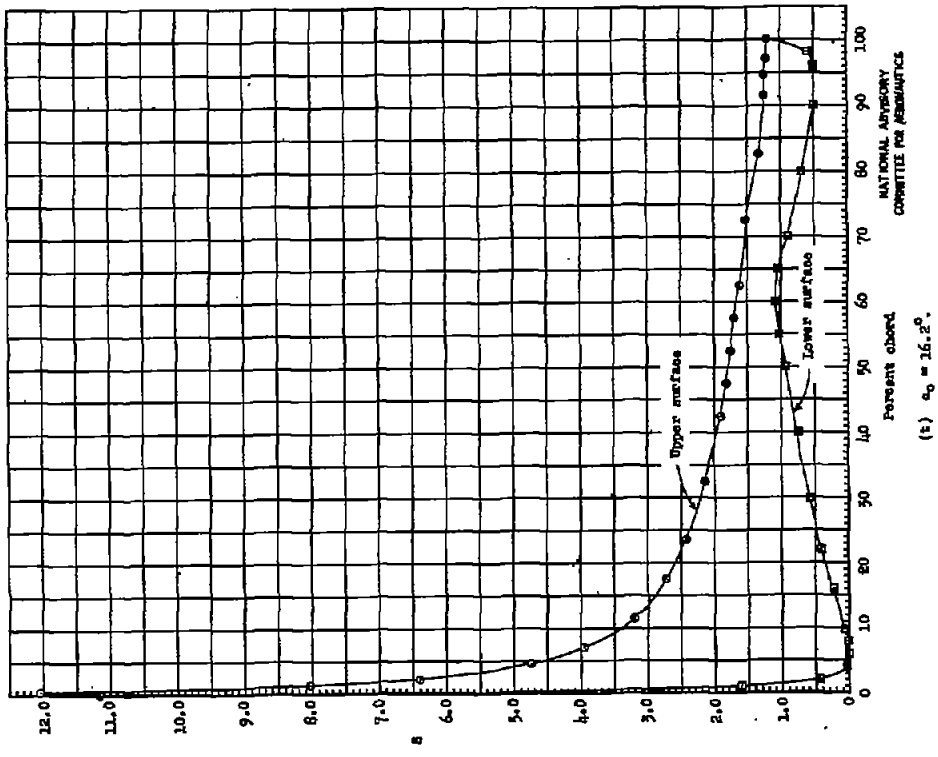

(t) $\alpha_0 = 16.2°$.

Figure 5.- Continued.

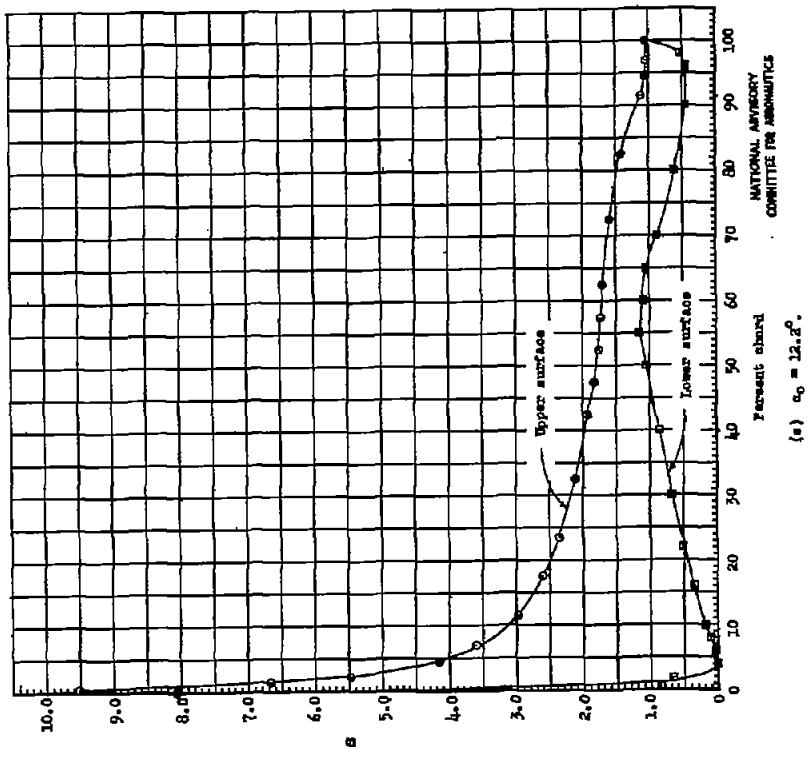

(s) $\alpha_0 = 12.2°$.

Figure 5.- Continued.

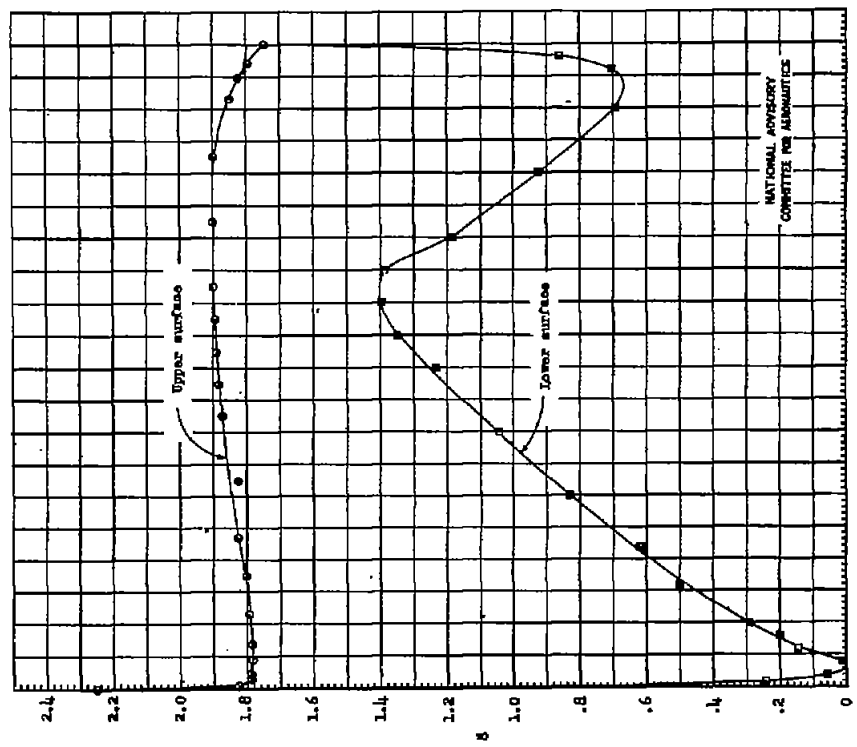

(u) $c_l = 19.5°$.

Figure 5.- Concluded.

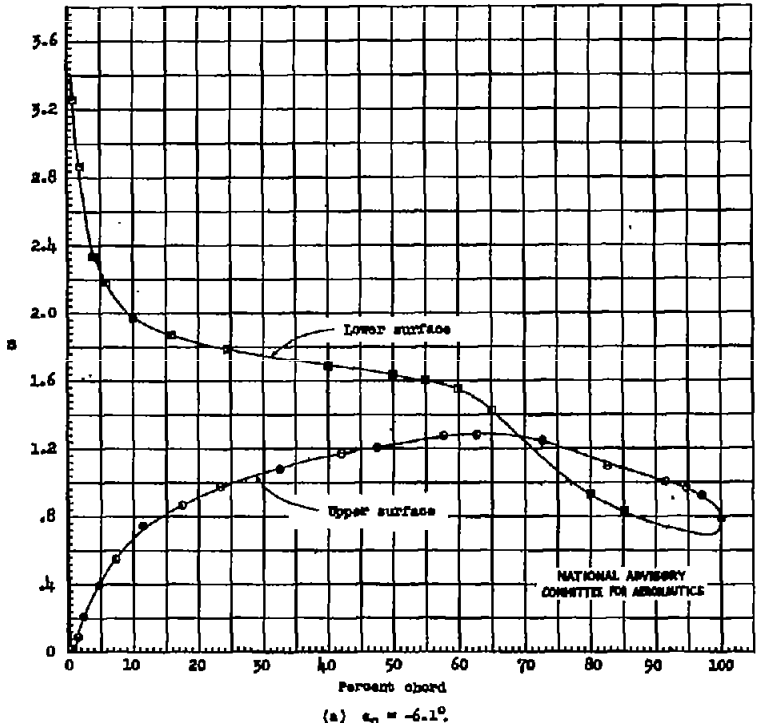

(a) $\alpha_0 = -6.1°$.

Figure 6.- Experimental pressure distribution of the NACA 66(215)-216 $\begin{bmatrix} a = 0.6, & \delta_{t_1} = -0.5 \\ a = 1.0, & \delta_{t_1} = 0.7 \end{bmatrix}$ airfoil section. $R = 6 \times 10^6$; TDT tests 543 and 551.

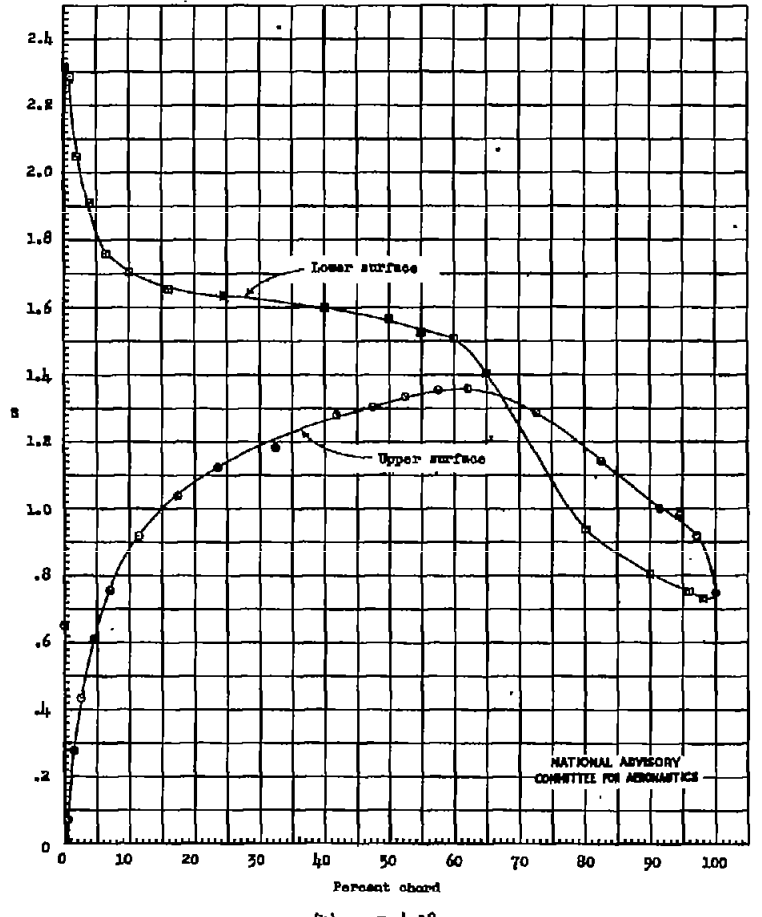

(b) $\alpha_0 = -4.1°$.

Figure 6.- Continued.

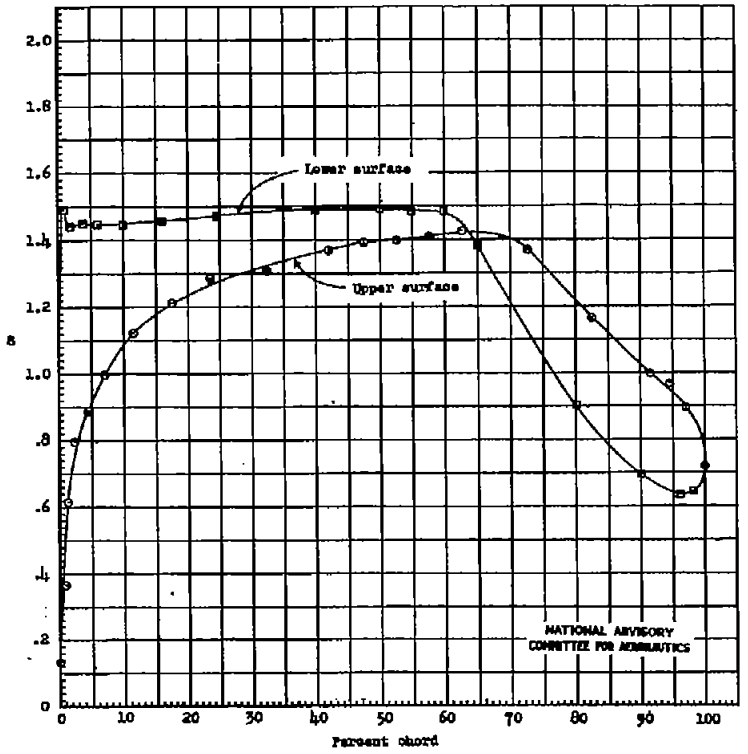

(a) $\alpha_0 = -2.0^\circ$.

Figure 6.- Continued.

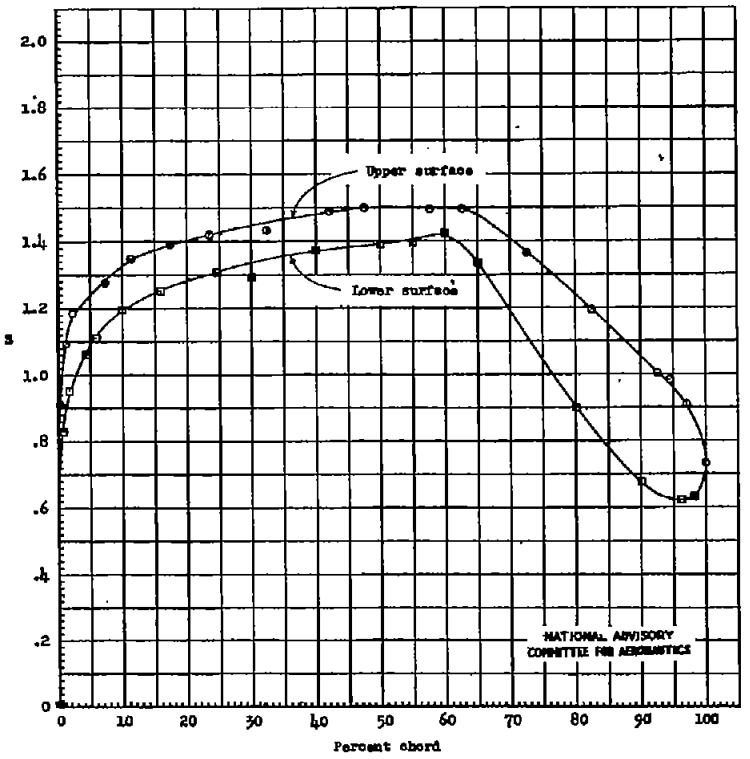

(d) $\alpha_0 = 0^\circ$.

Figure 6.- Continued.

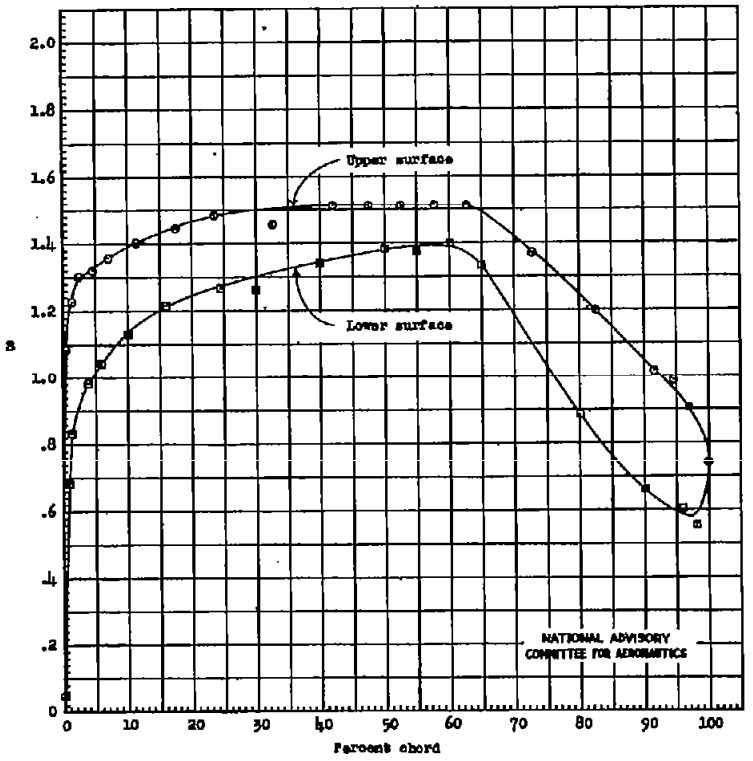

(e) $\alpha_0 = 0.5°$.

Figure 6.- Continued.

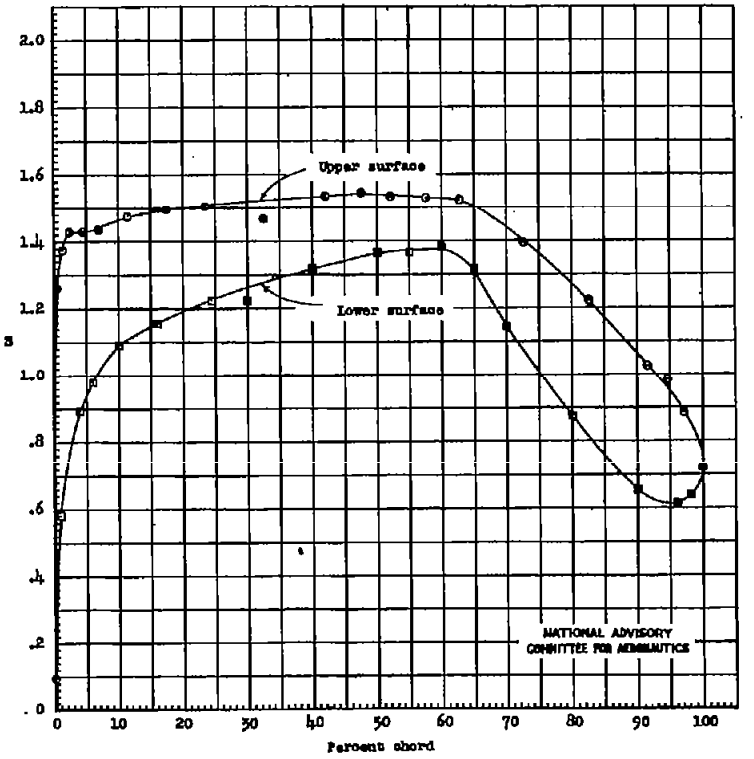

(f) $\alpha_0 = 1.0°$.

Figure 6.- Continued.

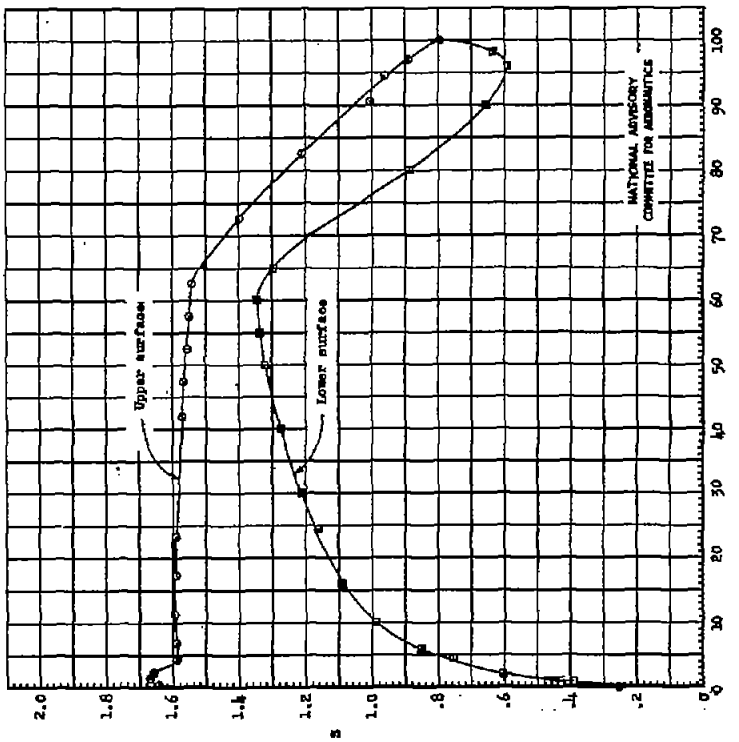

(h) $\alpha_0 = 2.0°$.

Figure 6.- Continued.

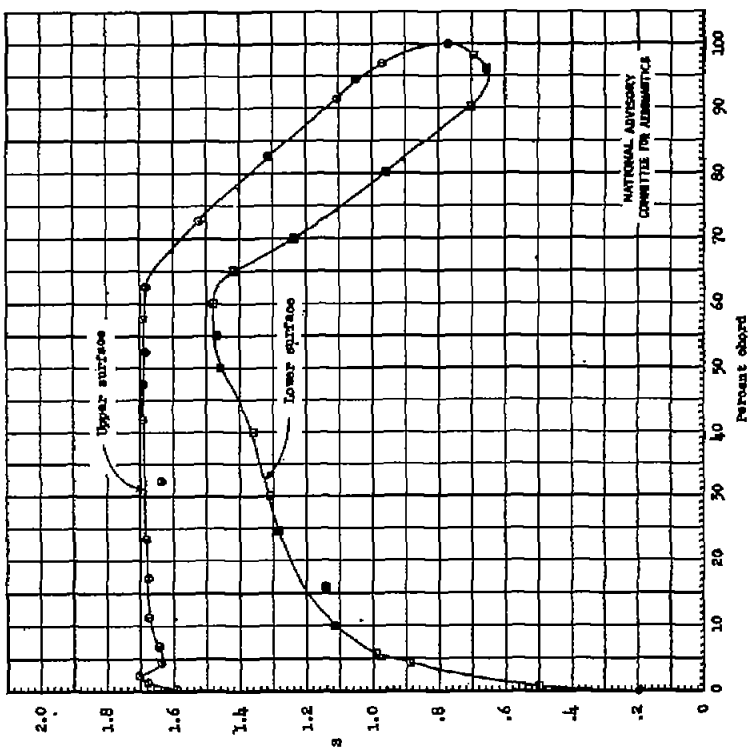

(i) $\alpha_0 = 1.5°$.

Figure 6.- Continued.

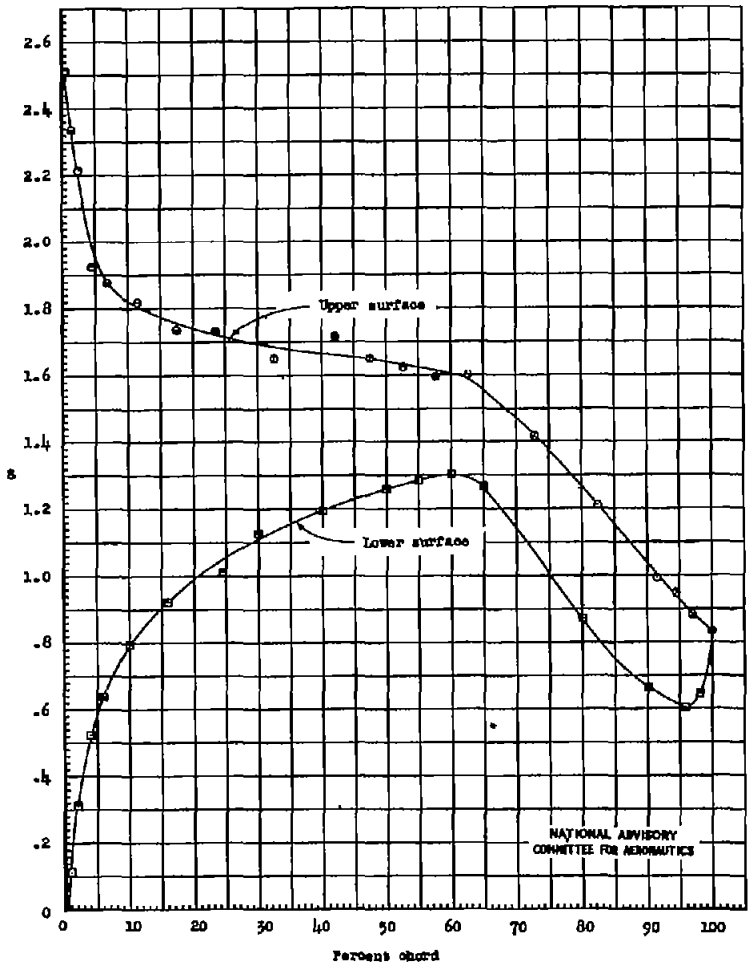

(i) $\alpha_0 = 4.1°$.

Figure 6.- Continued.

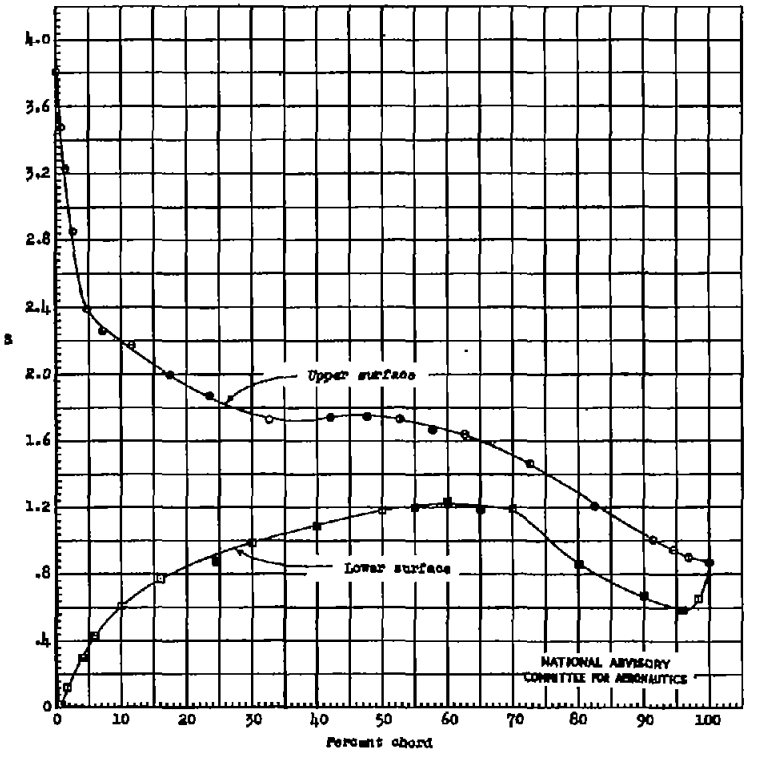

(j) $\alpha_0 = 6.1°$.

Figure 6.- Continued.

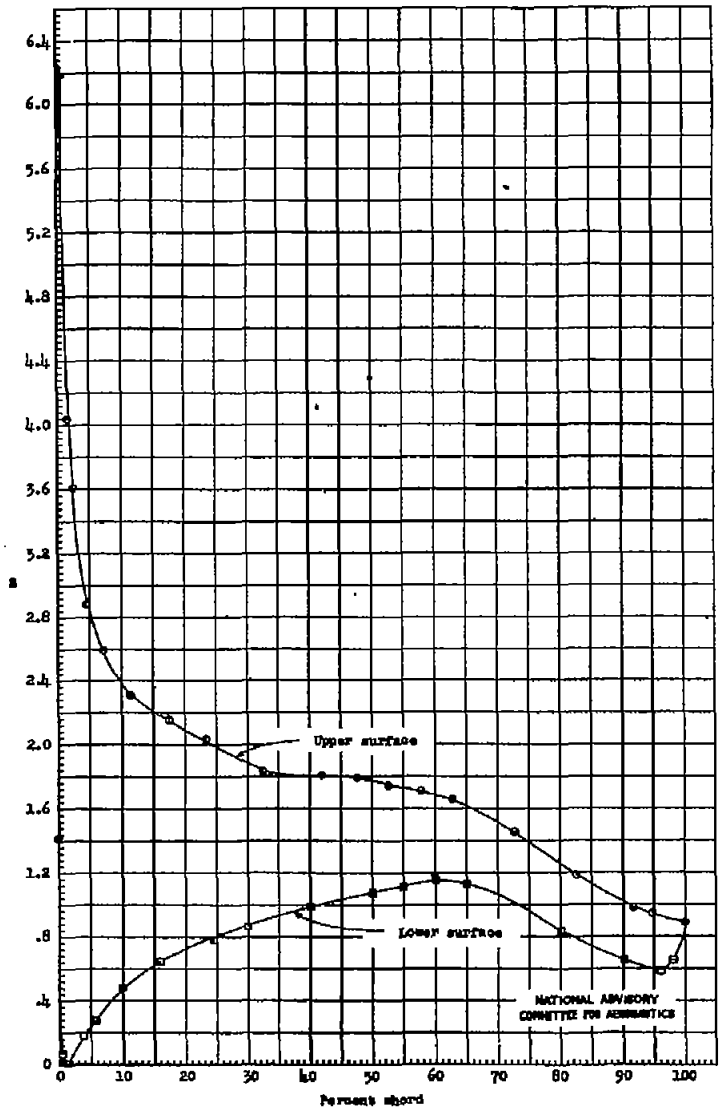

(k) $\alpha_0 = 8.1°$.

Figure 6.- Continued.

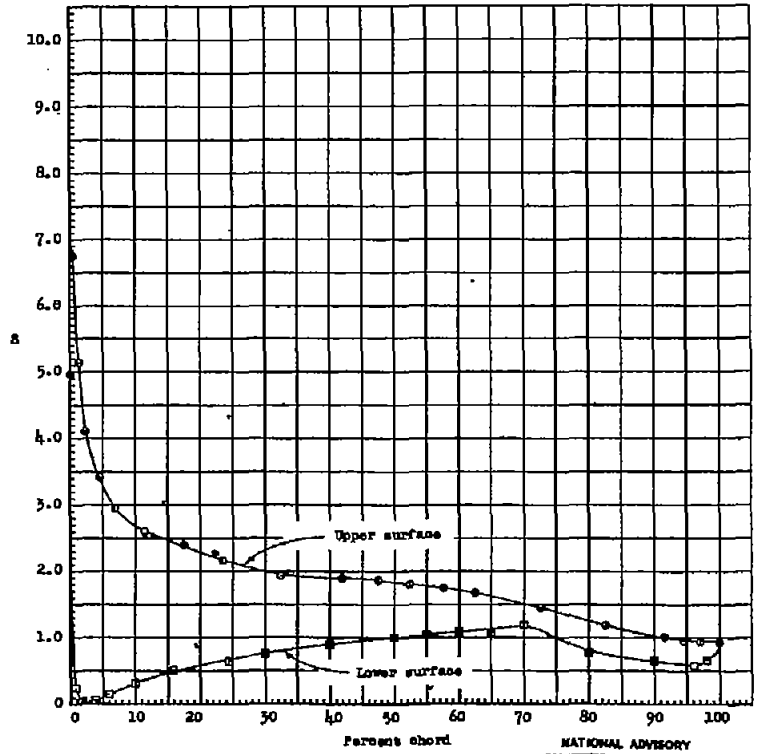

(l) $\alpha_0 = 10.2°$.

Figure 6.- Continued.

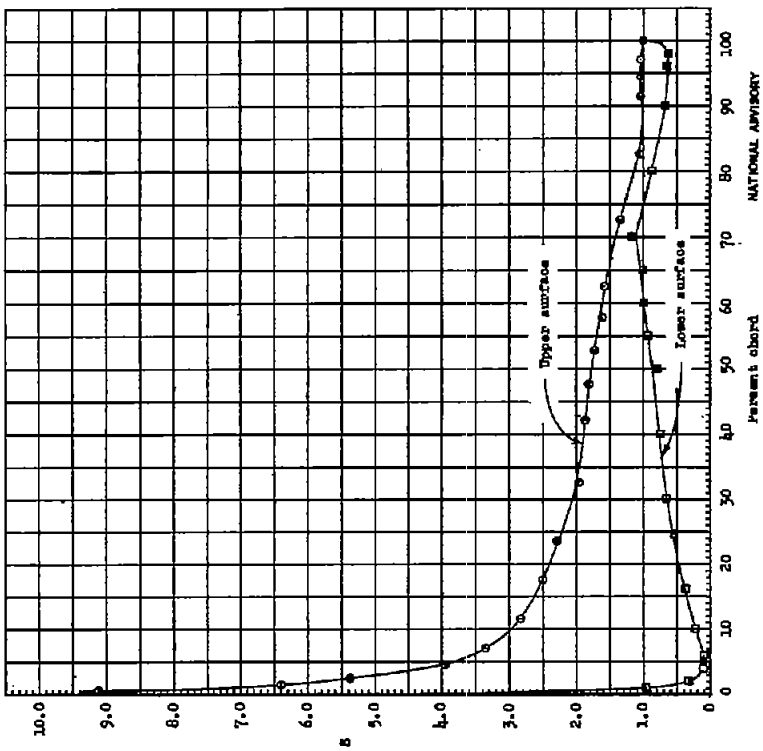

(n) $\alpha_0 = 14.2°$.

Figure 6.- Continued.

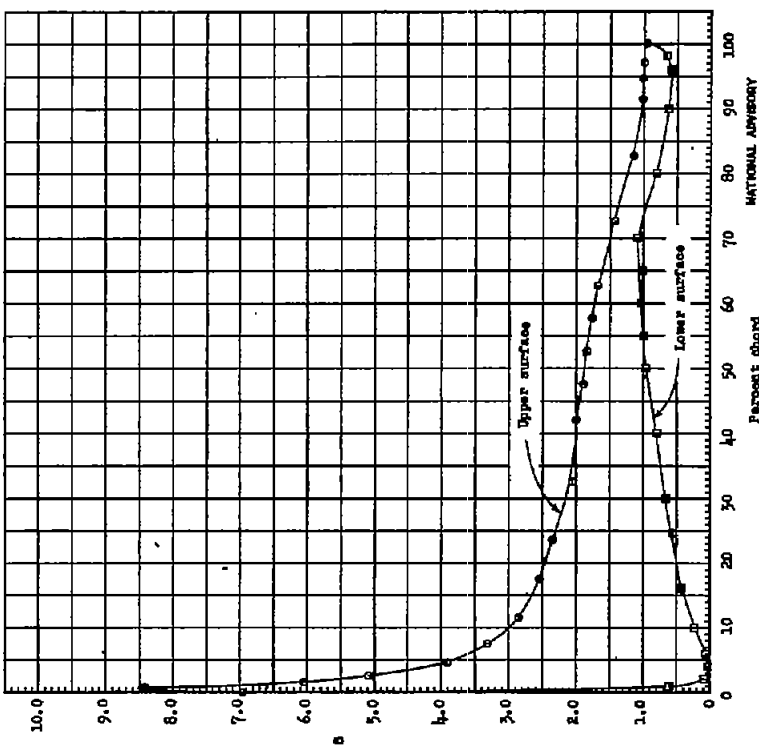

(m) $\alpha_0 = 12.2°$.

Figure 6.- Continued.

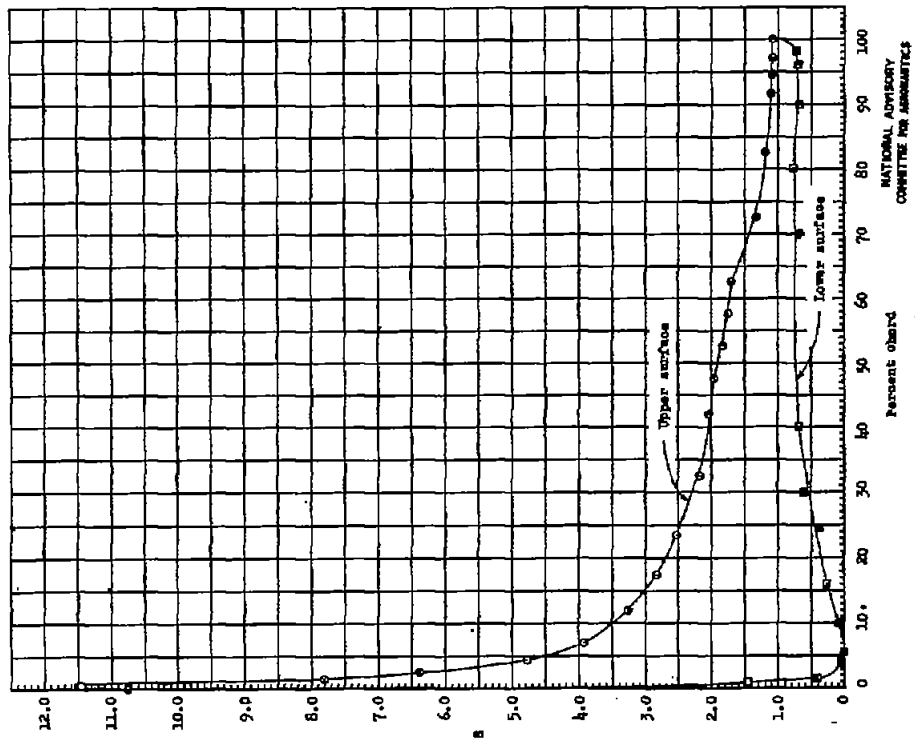

(c) $c_l = 16.2°$.

Figure 6.- Concluded.

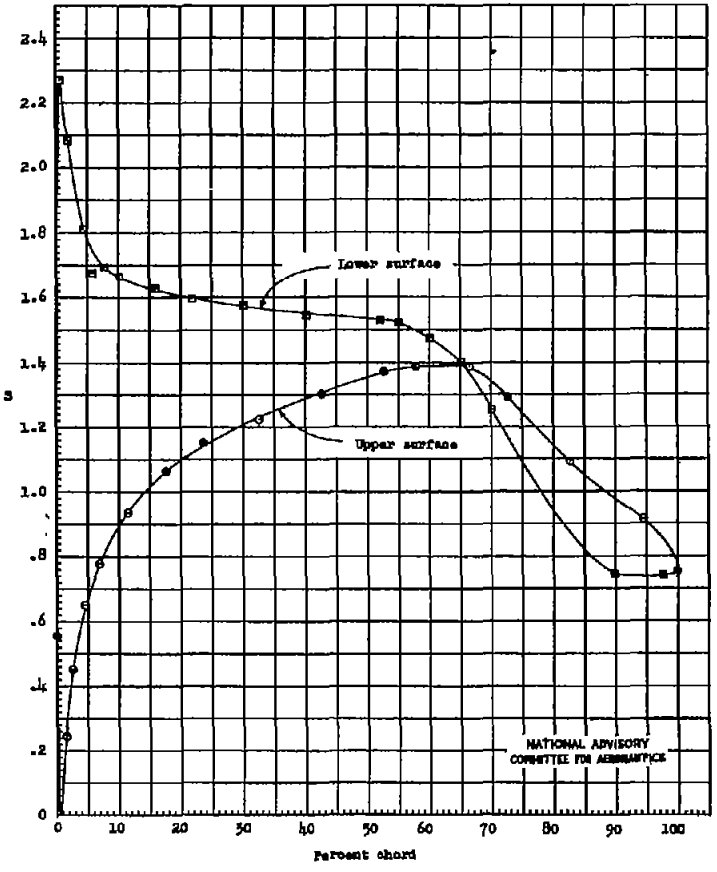

(a) $\alpha_0 = -4.1°$.

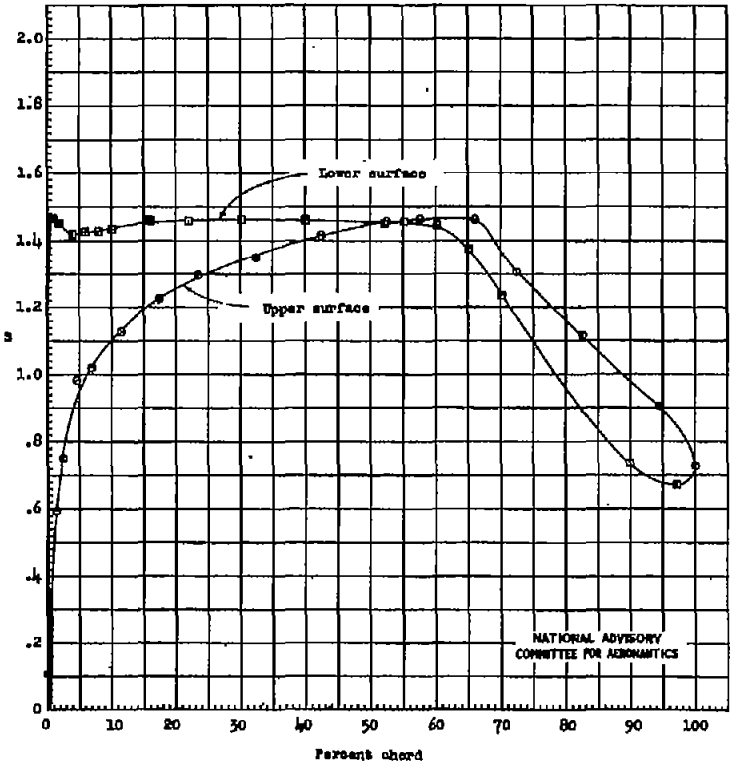

(b) $\alpha_0 = -2.0°$.

Figure 7.- Continued.

Figure 7.- Experimental pressure distribution of the NACA 66(215)-216 $\begin{cases} a = 0.6, & \alpha_{i_1} = -0.3 \\ a = 1.0, & \alpha_{i_1} = 0.5 \end{cases}$ airfoil section. $R = 6 \times 10^6$; TDT tests 539 and 572.

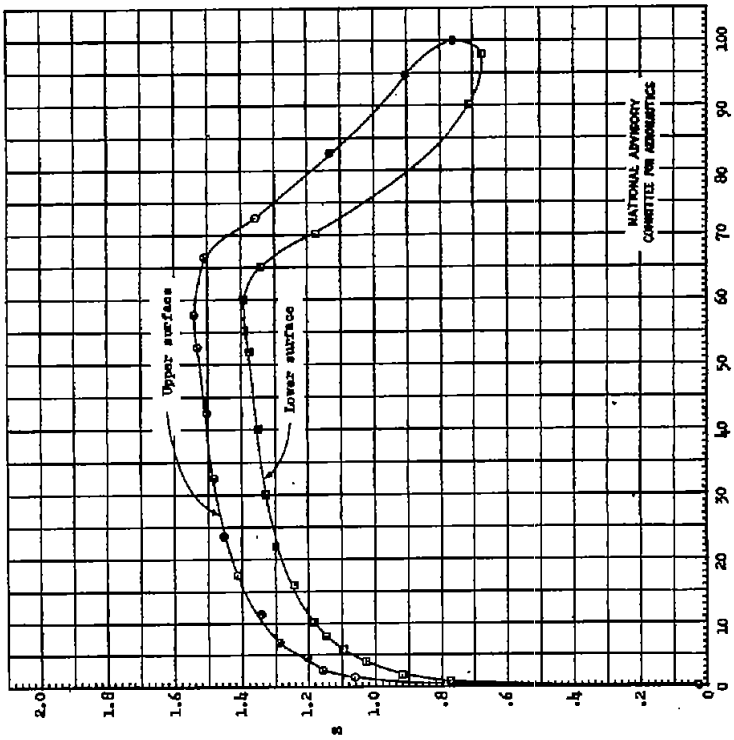

(c) $\alpha_0 = 0°$.

Figure 7.- Continued.

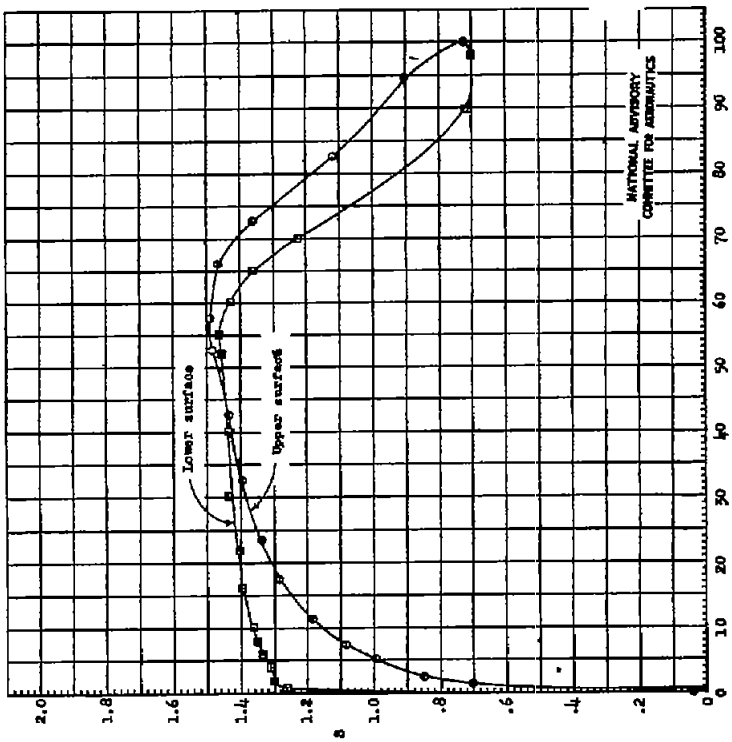

(d) $\alpha_0 = -1.5°$.

Figure 7.- Continued.

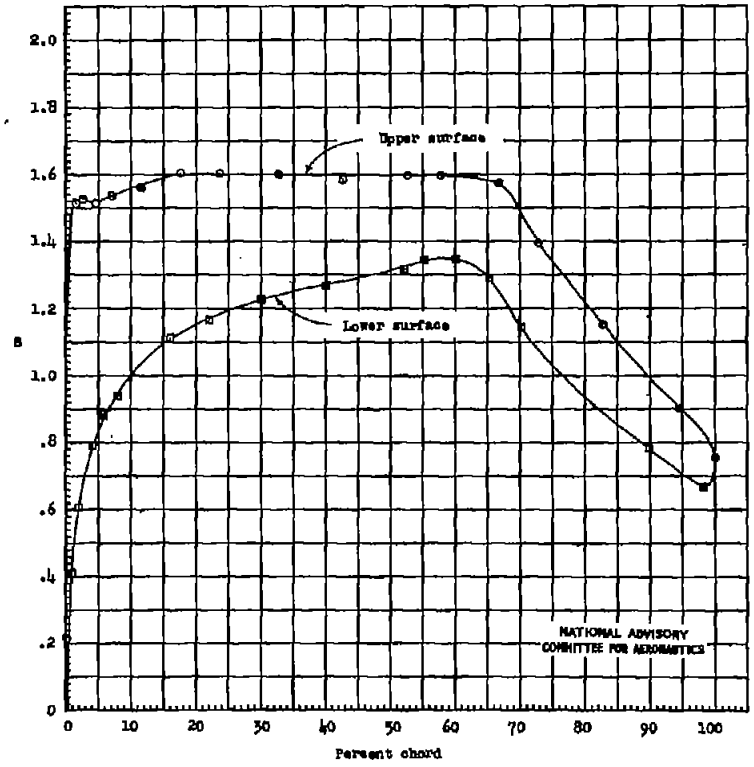

(e) $\alpha_0 = 1.5°$.

Figure 7.- Continued.

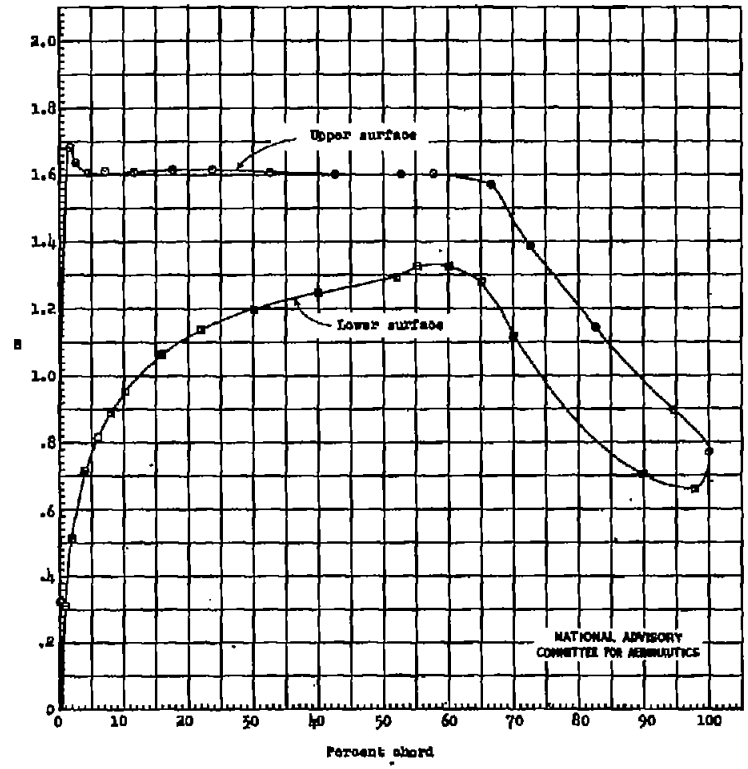

(f) $\alpha_0 = 2.0°$.

Figure 7.- Continued.

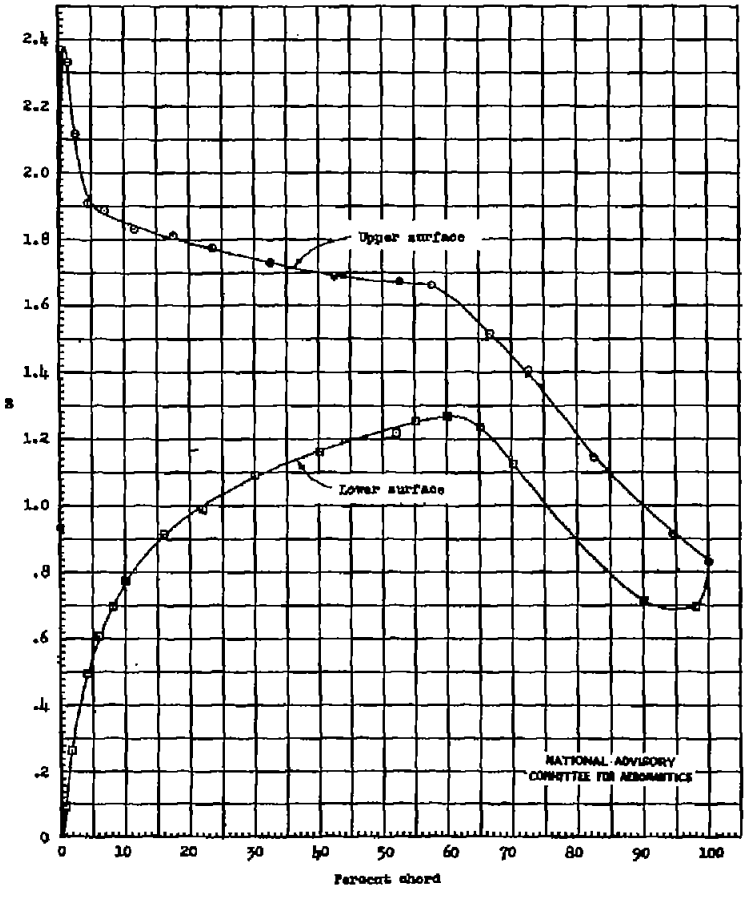

(g) $\alpha_0 = 4.1°$.

Figure 7.- Continued.

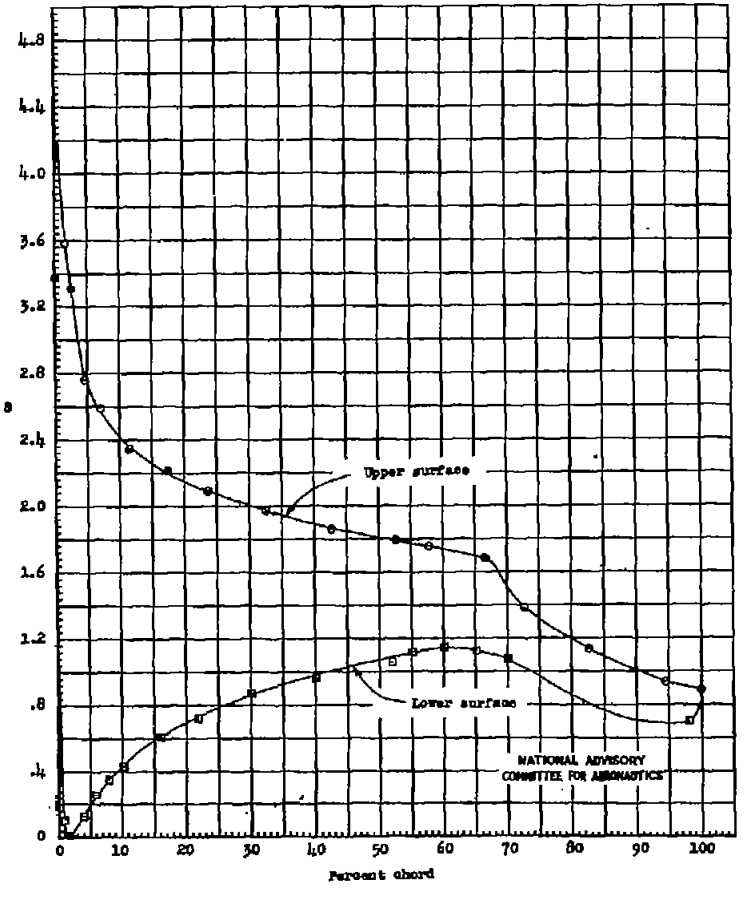

(h) $\alpha_0 = 8.1°$.

Figure 7.- Continued.

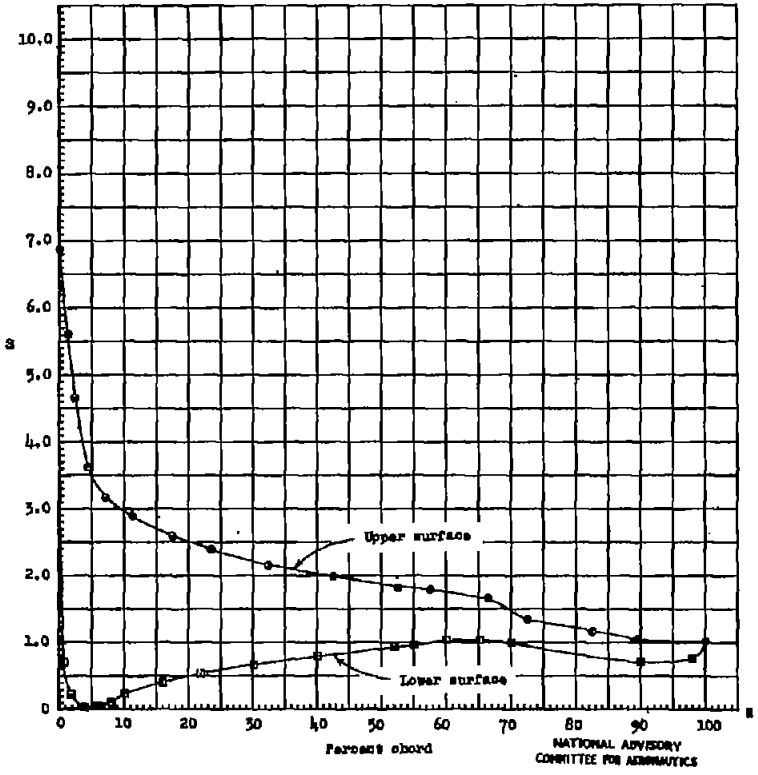

(i) $\alpha_0 = 12.2°$.

Figure 7.- Continued.

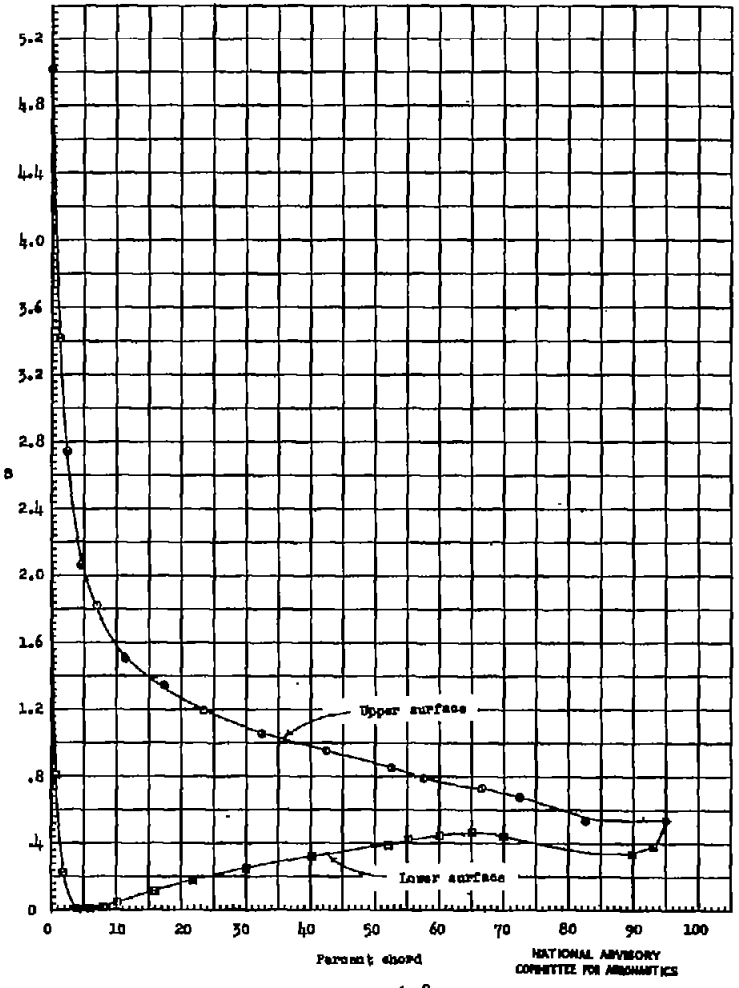

(j) $\alpha_0 = 16.2°$.

Figure 7.- Concluded.

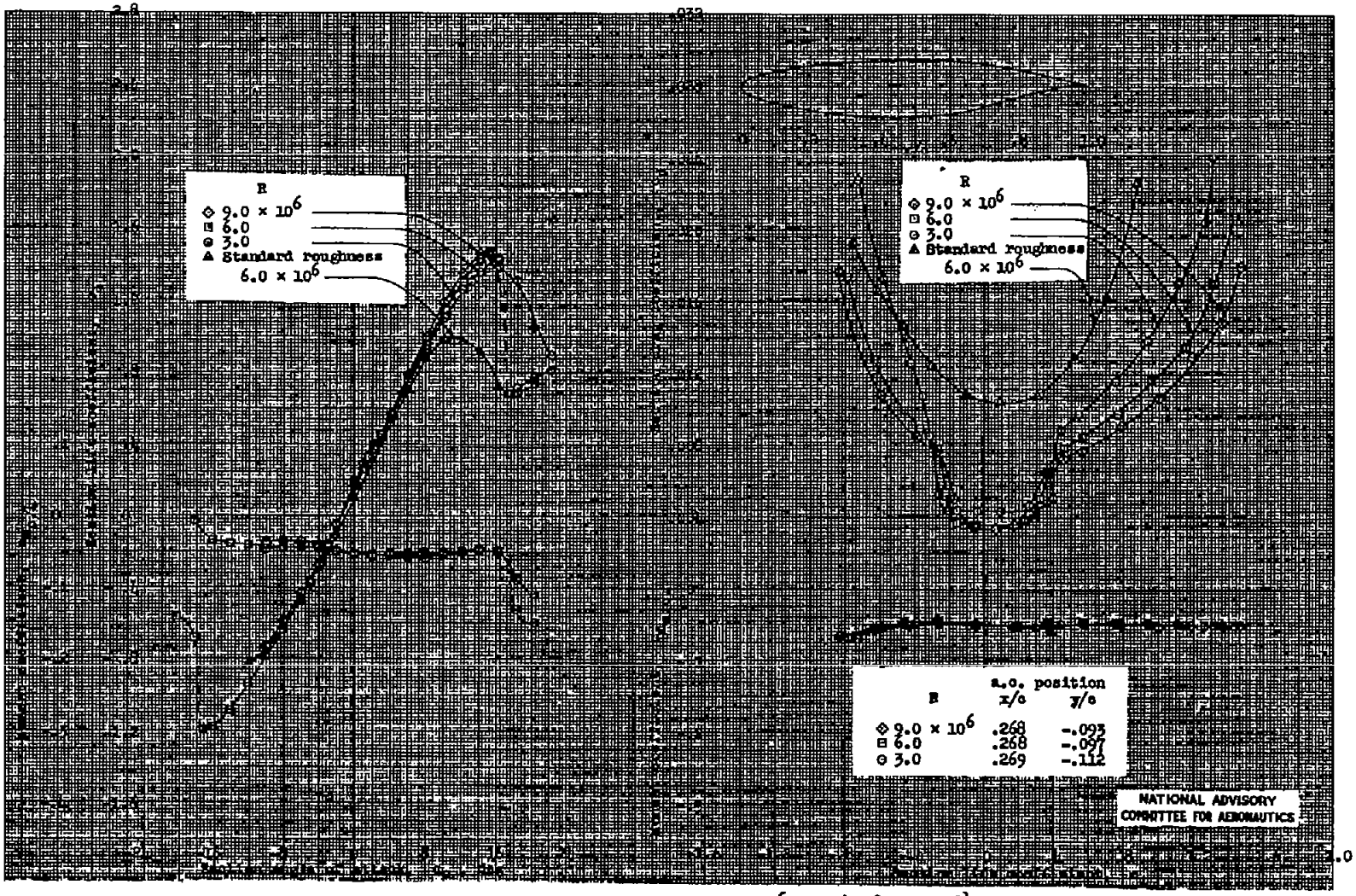

Figure 8.- Aerodynamic characteristics of the NACA 66(215)-216 $\begin{cases} a = 0.6, & c_{l_1} = -0.8 \\ a = 1.0, & c_{l_1} = 1.0 \end{cases}$ airfoil section, 24-inch chord. TDT tests 455, 458, 459, 518.

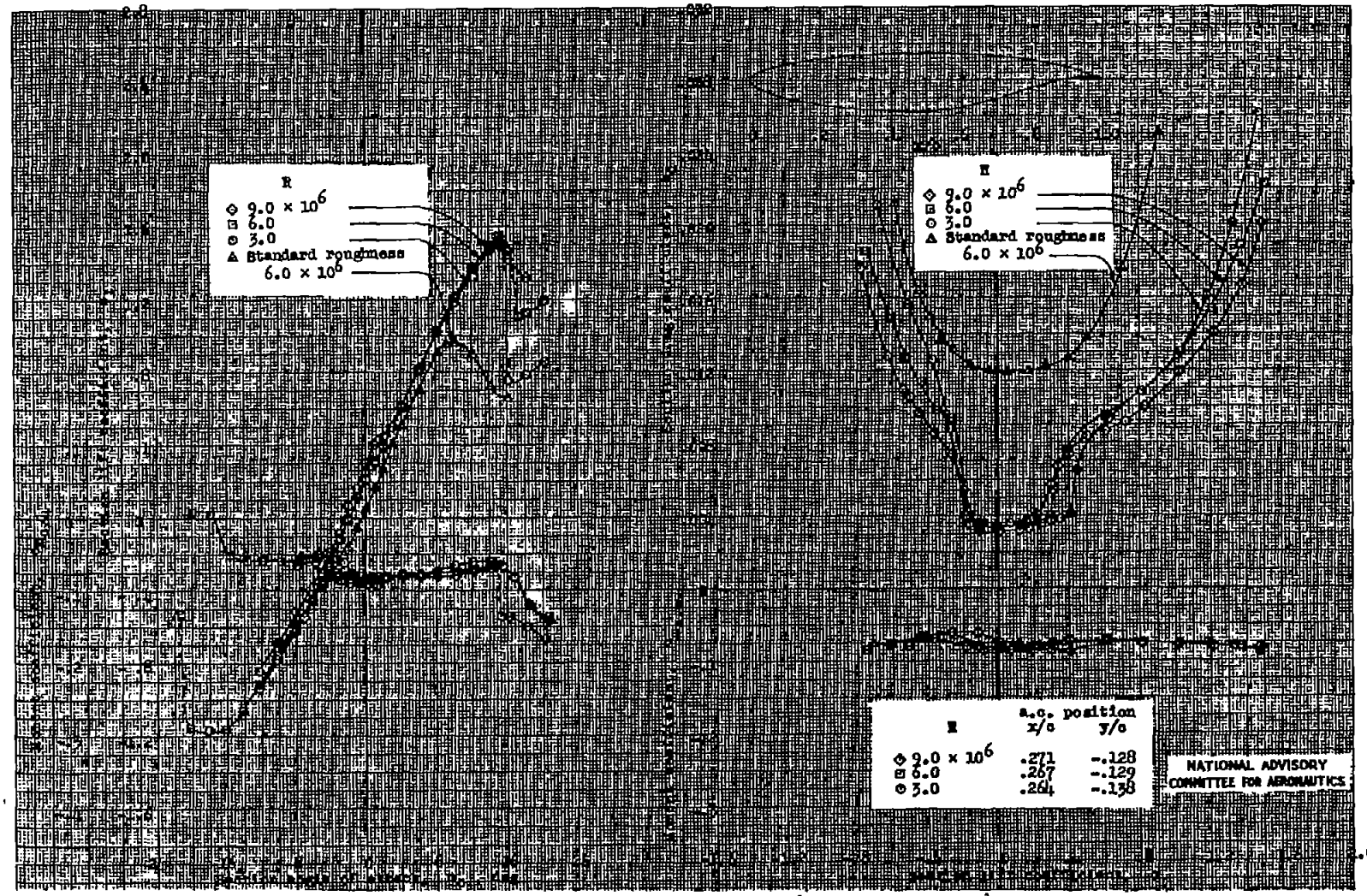

Figure 9.- Aerodynamic characteristics of the NACA 66(215)-316 $\begin{cases} a = 0.6, & c_{l_i} = -1.2 \\ a = 1.0, & c_{l_i} = 1.5 \end{cases}$ airfoil section, 24-inch chord. TDT tests 616 and 622.

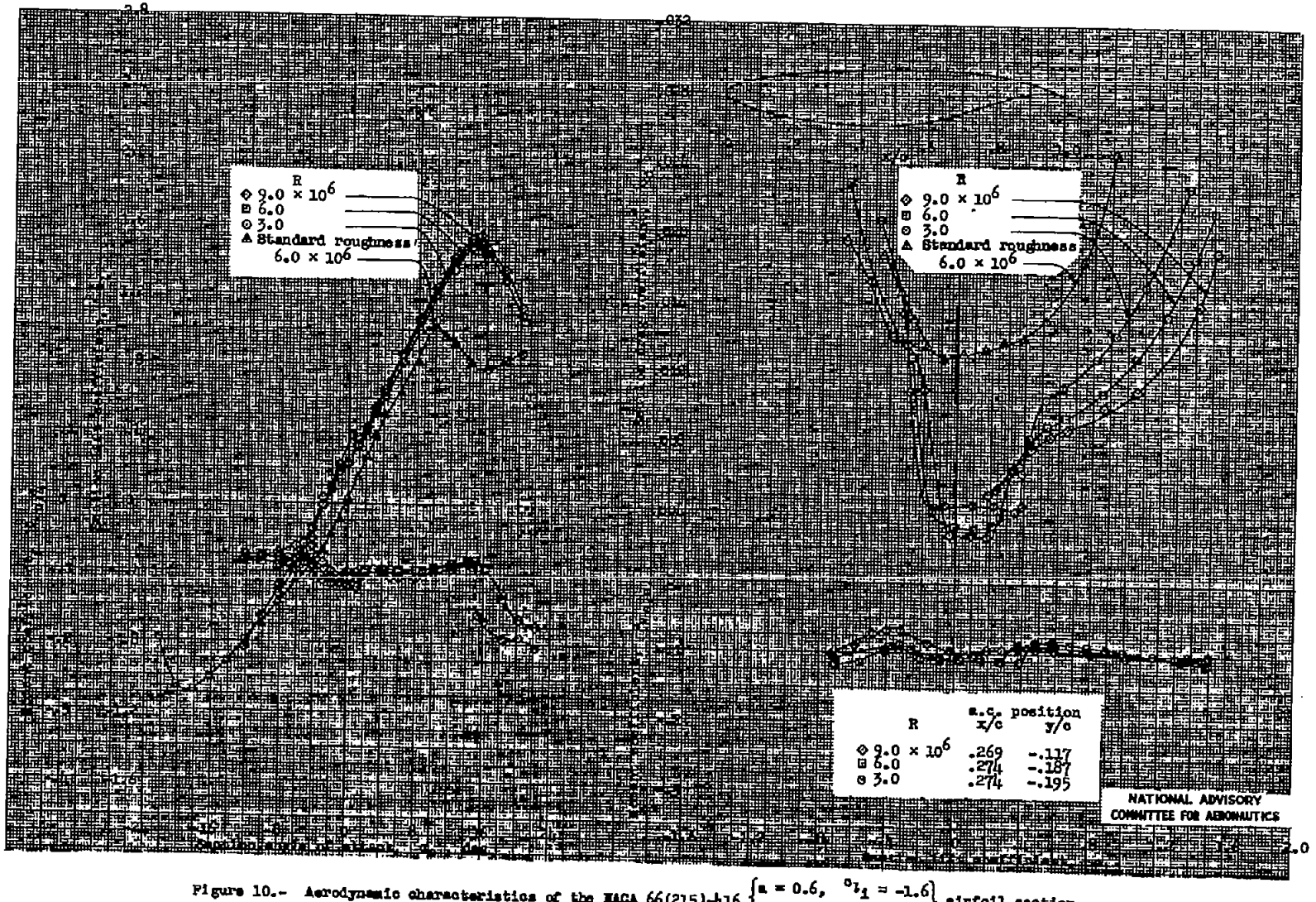

Figure 10.- Aerodynamic characteristics of the NACA 66(215)-416 $\begin{cases} a = 0.6, & {}^{o}i_1 = -1.6 \\ a = 1.0, & {}^{o}i_1 = 2.0 \end{cases}$ airfoil section, 24-inch chord. TDT tests 620, 621, and 632.

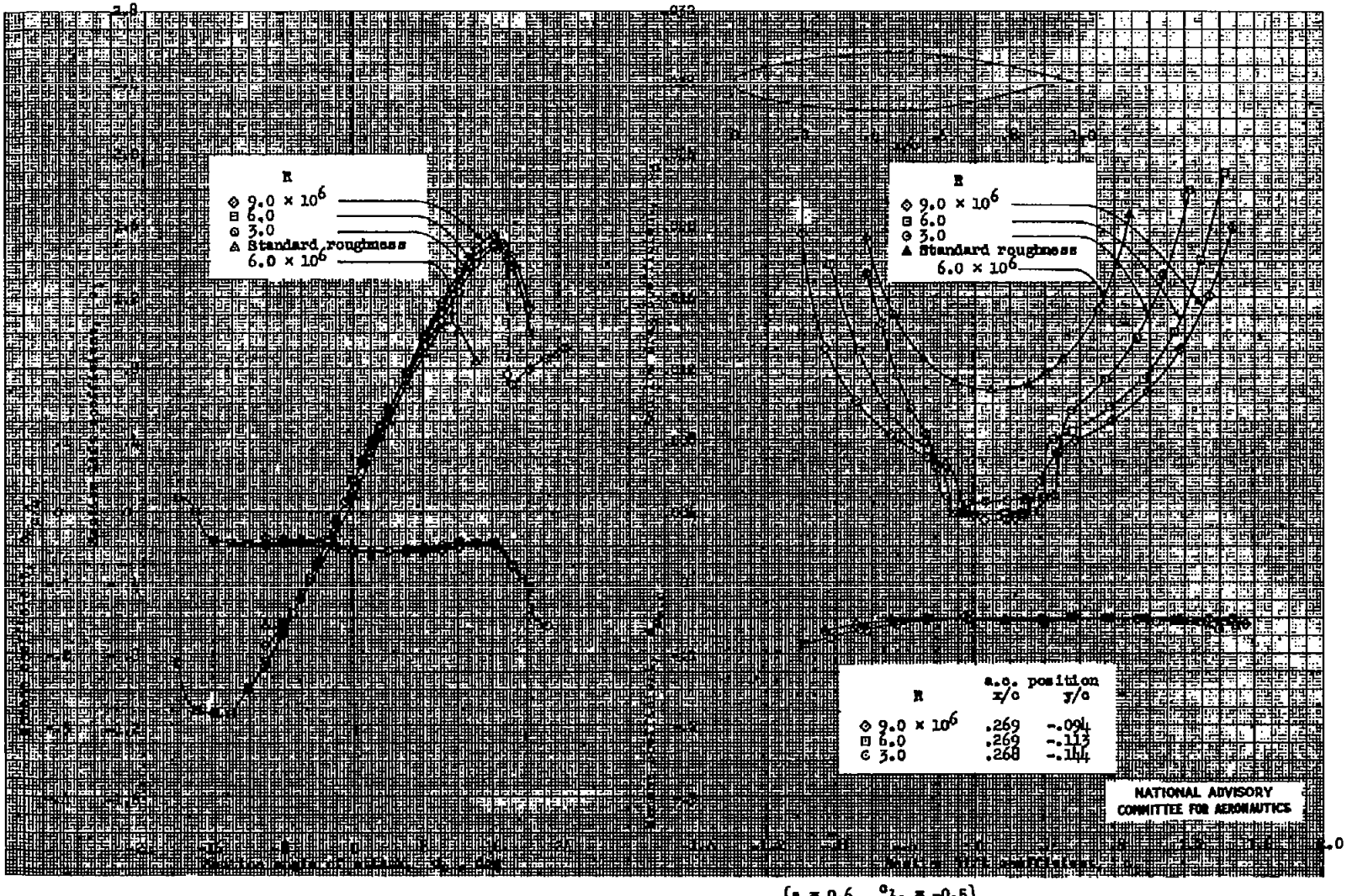

Figure 11.- Aerodynamic characteristics of the NACA 66(215)-216 $\begin{cases} a = 0.6, & i_t = -0.5 \\ a = 1.0, & i_t = 0.7 \end{cases}$ airfoil section, 24-inch chord. TDT tests 540 and 555.

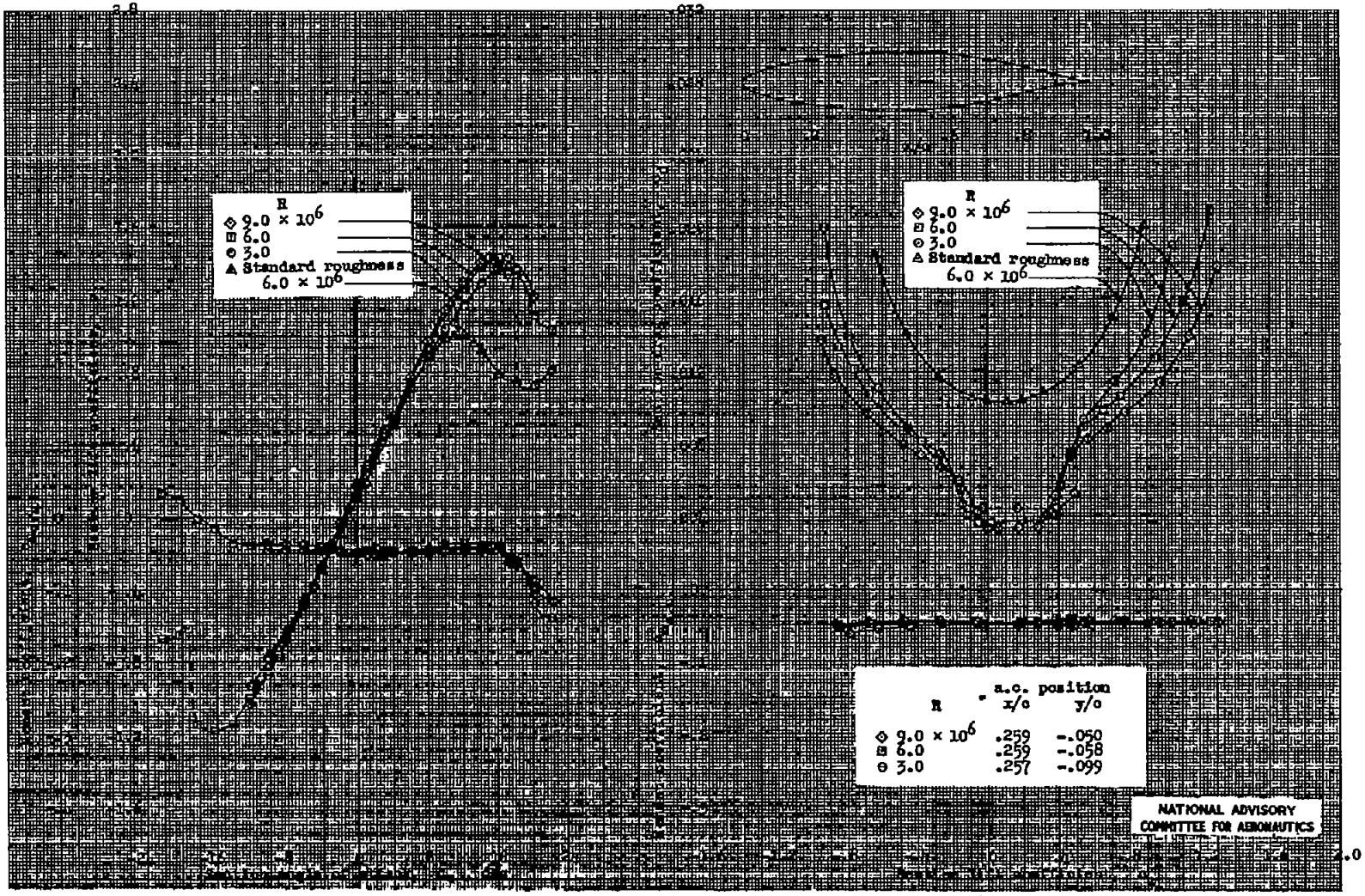

Figure 12.- Aerodynamic characteristics of the NACA 66(215)-216 $\begin{cases} a = 0.6, & c_{l_i} = -0.3 \\ a = 1.0, & c_{l_i} = 0.5 \end{cases}$ airfoil section, 24-inch chord. TDT tests 556, 560, and 567.

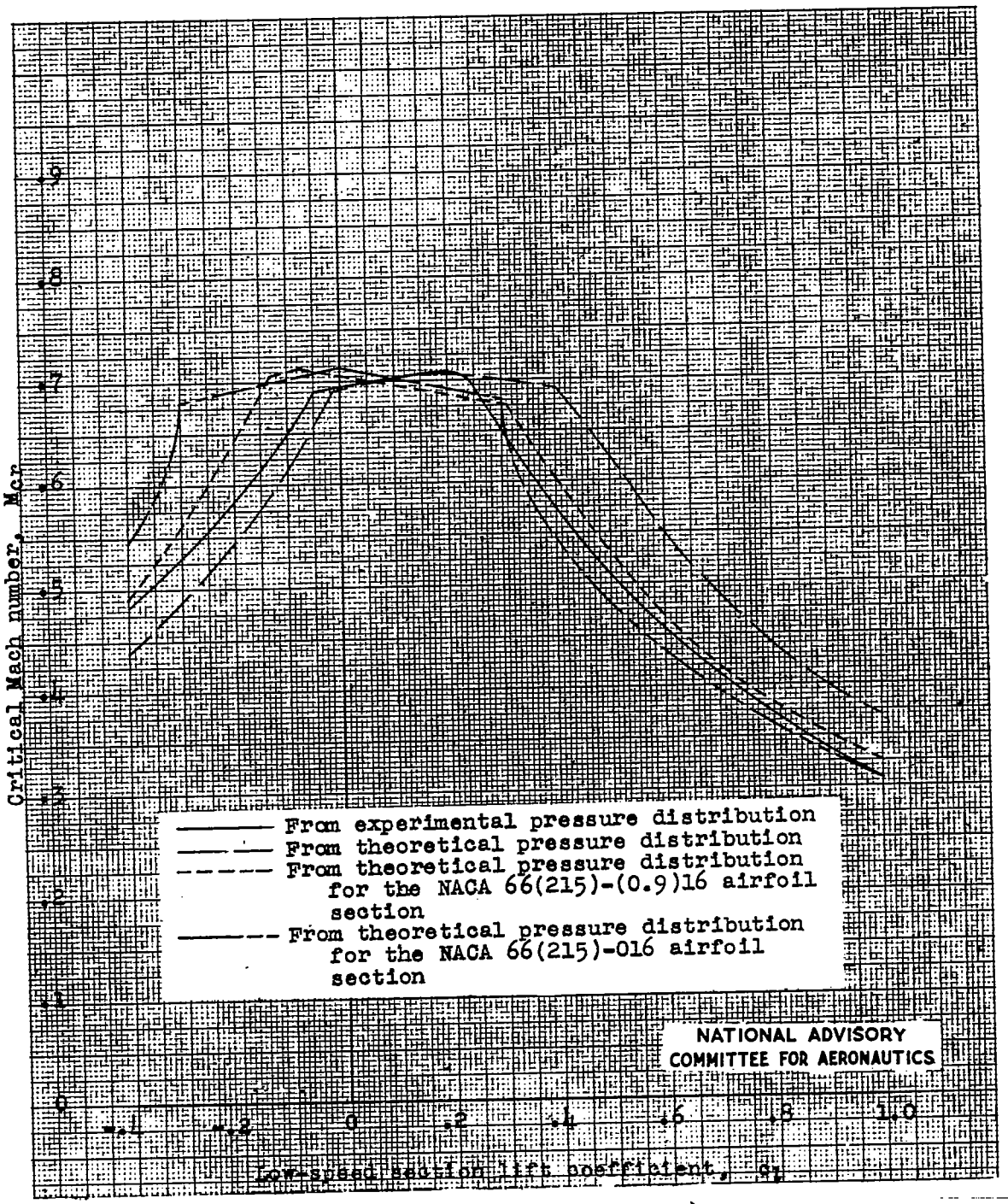

(a) NACA 66(215)-216 $\begin{cases} a = 0.6, & c_{l_i} = -0.8 \\ a = 1.0, & c_{l_i} = 1.0 \end{cases}$ airfoil section.

Figure 13 .- Comparison of the predicted critical Mach numbers obtained from the theoretical and experimental low-speed pressure distributions.

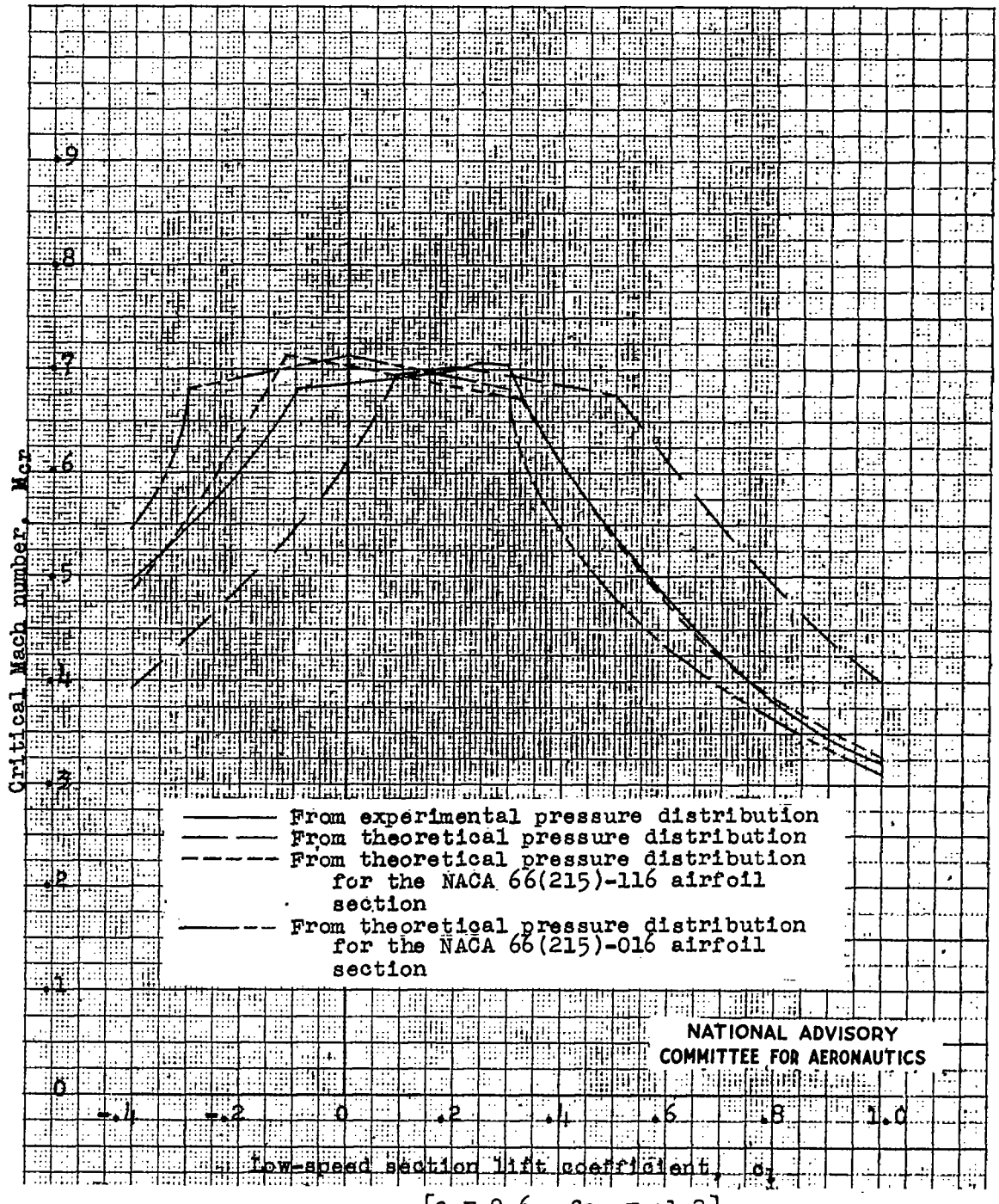

(b) NACA 66(215)-316 $\begin{cases} a = 0.6, & c_{l_i} = -1.2 \\ a = 1.0, & c_{l_i} = 1.5 \end{cases}$ airfoil section.

Figure 13.- Continued.

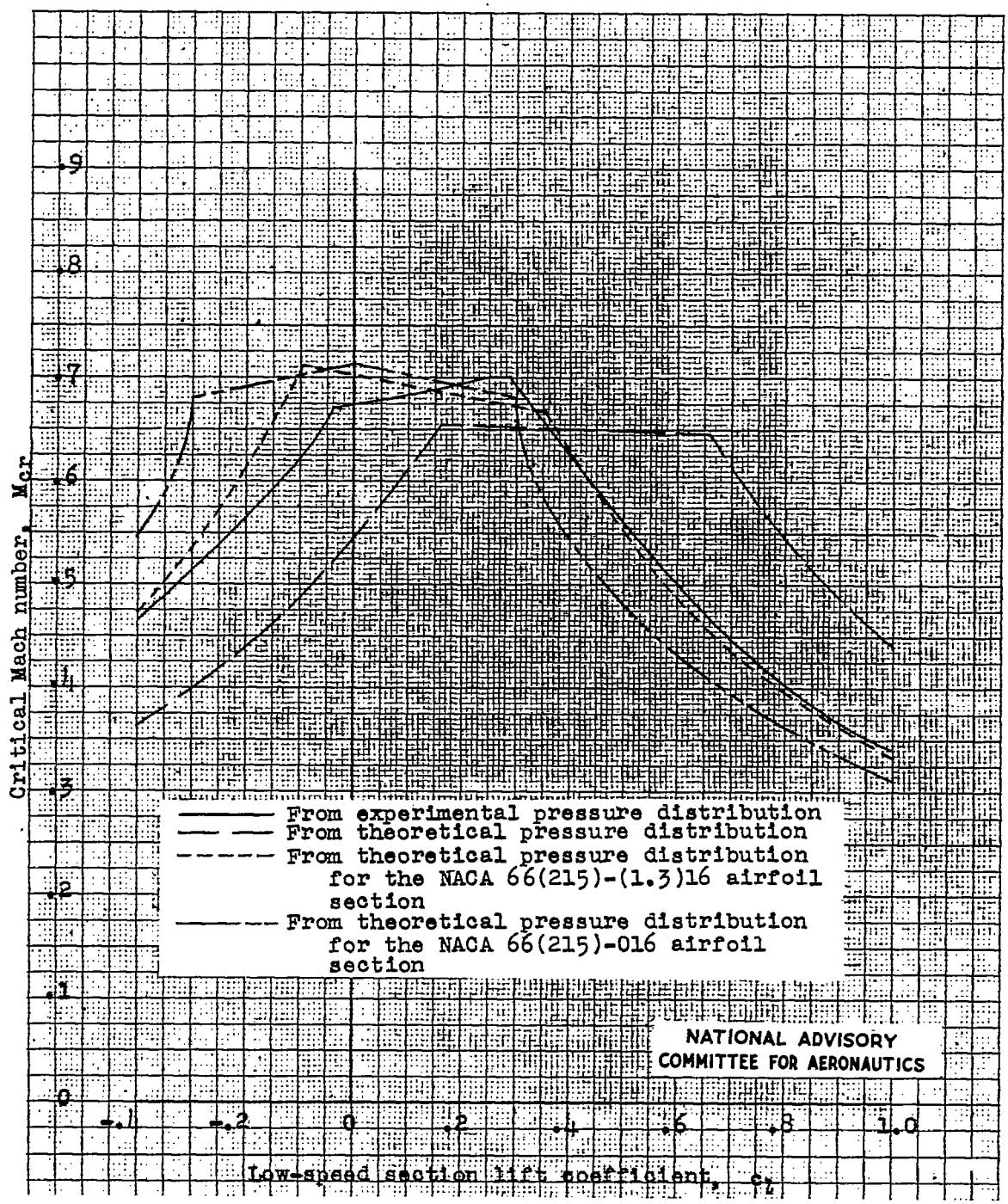

(c) NACA 66(215)-416 $\begin{cases} a = 0.6, & c_{l_i} = -1.6 \\ a = 1.0, & c_{l_i} = 2.0 \end{cases}$ airfoil section.

Figure 13.- Continued.

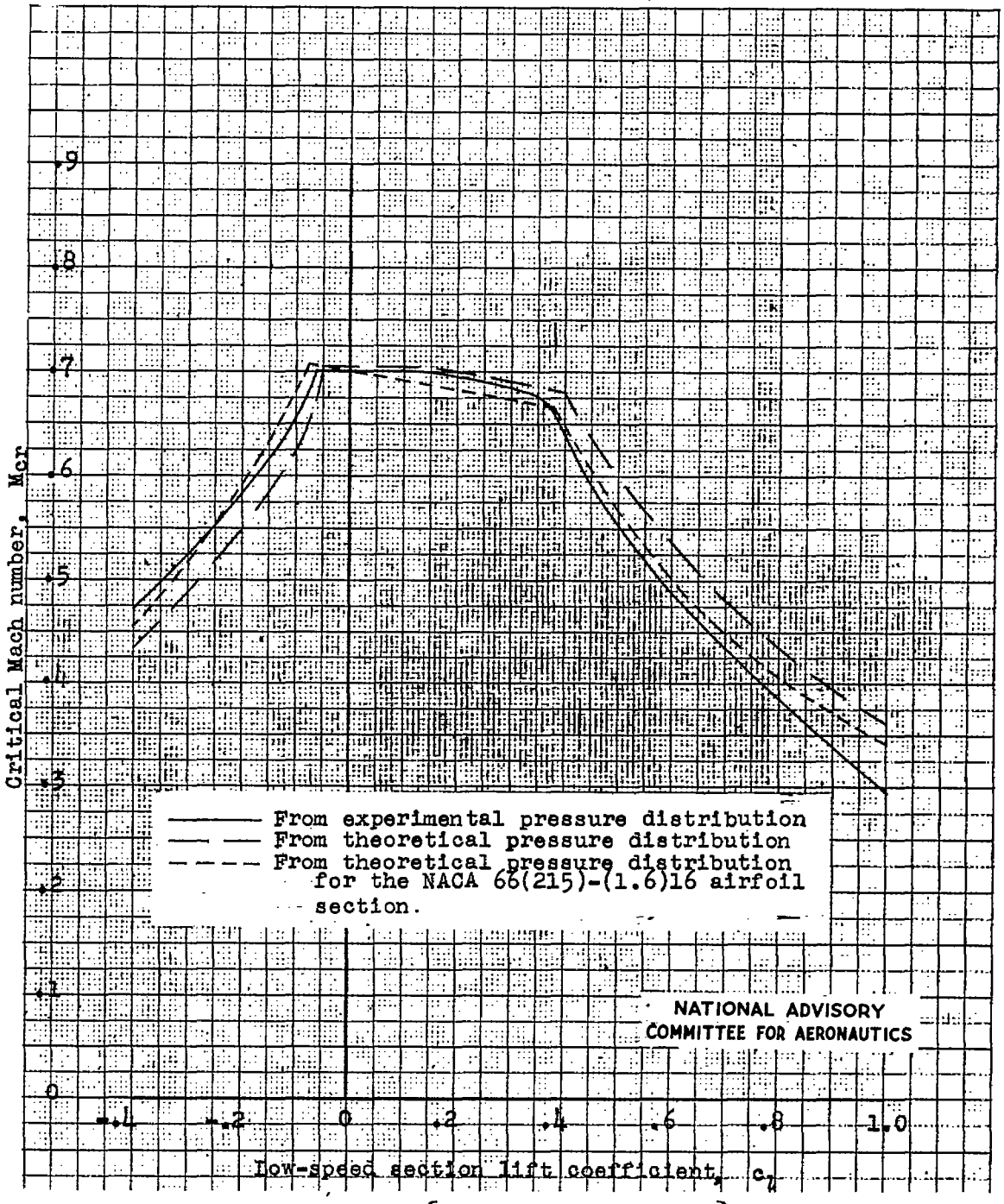

(d) NACA 66(215)-216 $\begin{cases} a = 0.6, & c_{l_i} = -0.5 \\ a = 1.0, & c_{l_i} = 0.7 \end{cases}$ airfoil section.

Figure 13.- Continued.

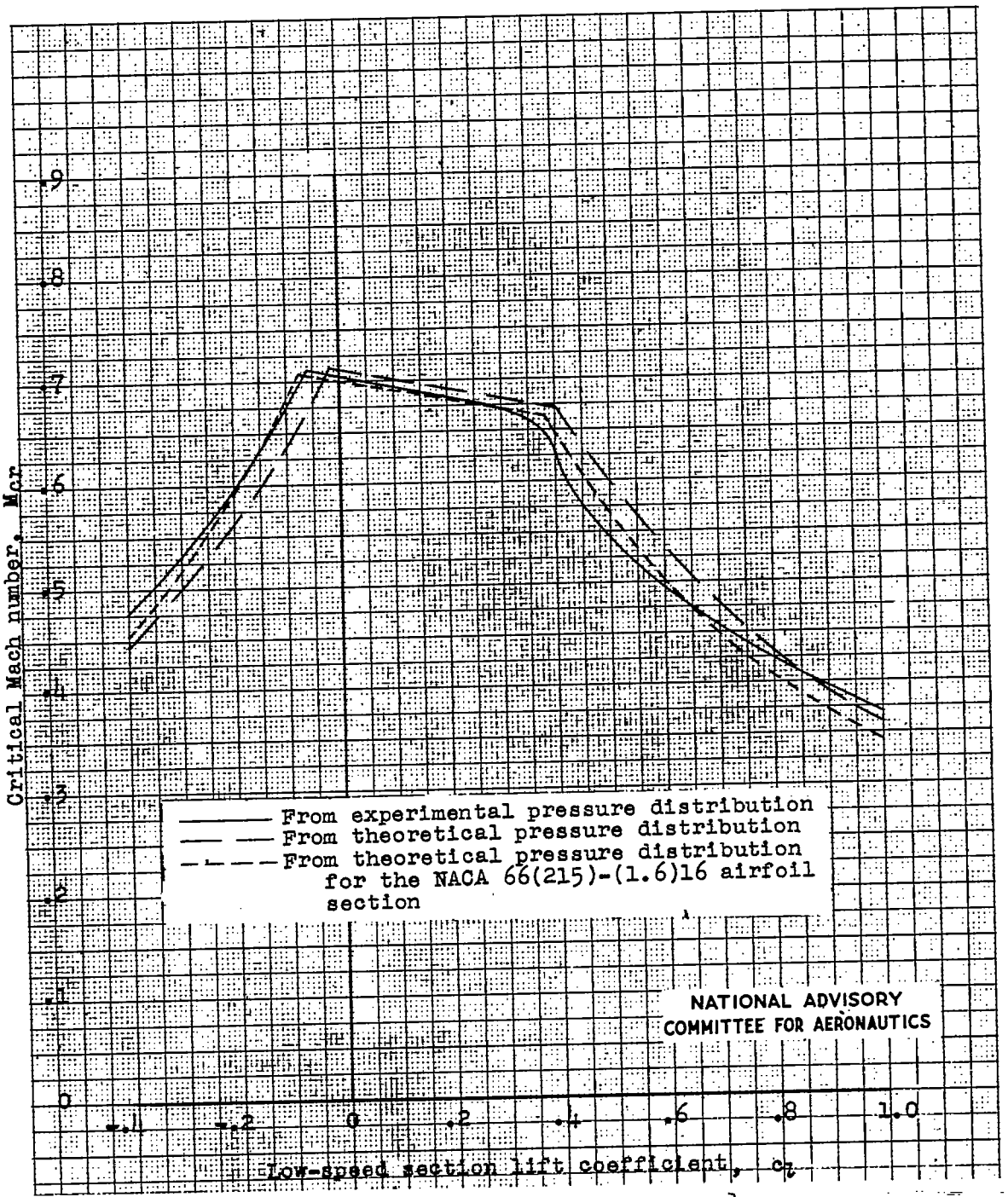

(e) NACA 66(215)-216 $\begin{cases} a = 0.6, & c_{l_i} = -0.3 \\ a = 1.0, & c_{l_i} = 0.5 \end{cases}$ airfoil section.

Figure 13.- Concluded.

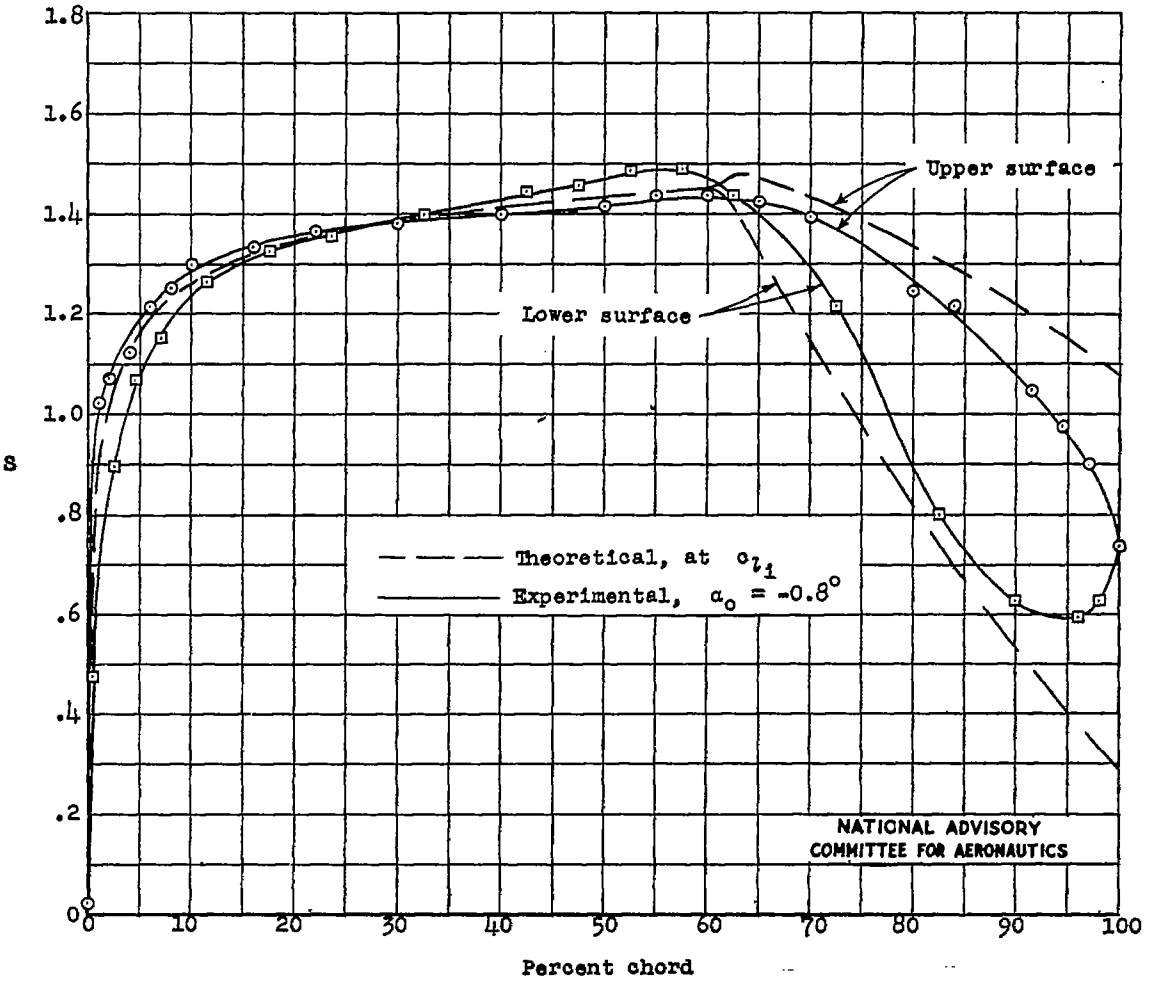

(a) NACA 66(215)-216 $\left\{\begin{matrix} a = 0.6, & c_{l_i} = -0.8 \\ a = 1.0, & c_{l_i} = 1.0 \end{matrix}\right\}$ airfoil section.

Figure 14.- Comparison of the experimental pressure distribution at the effective design lift coefficient with the theoretical pressure distribution at the design lift coefficient.

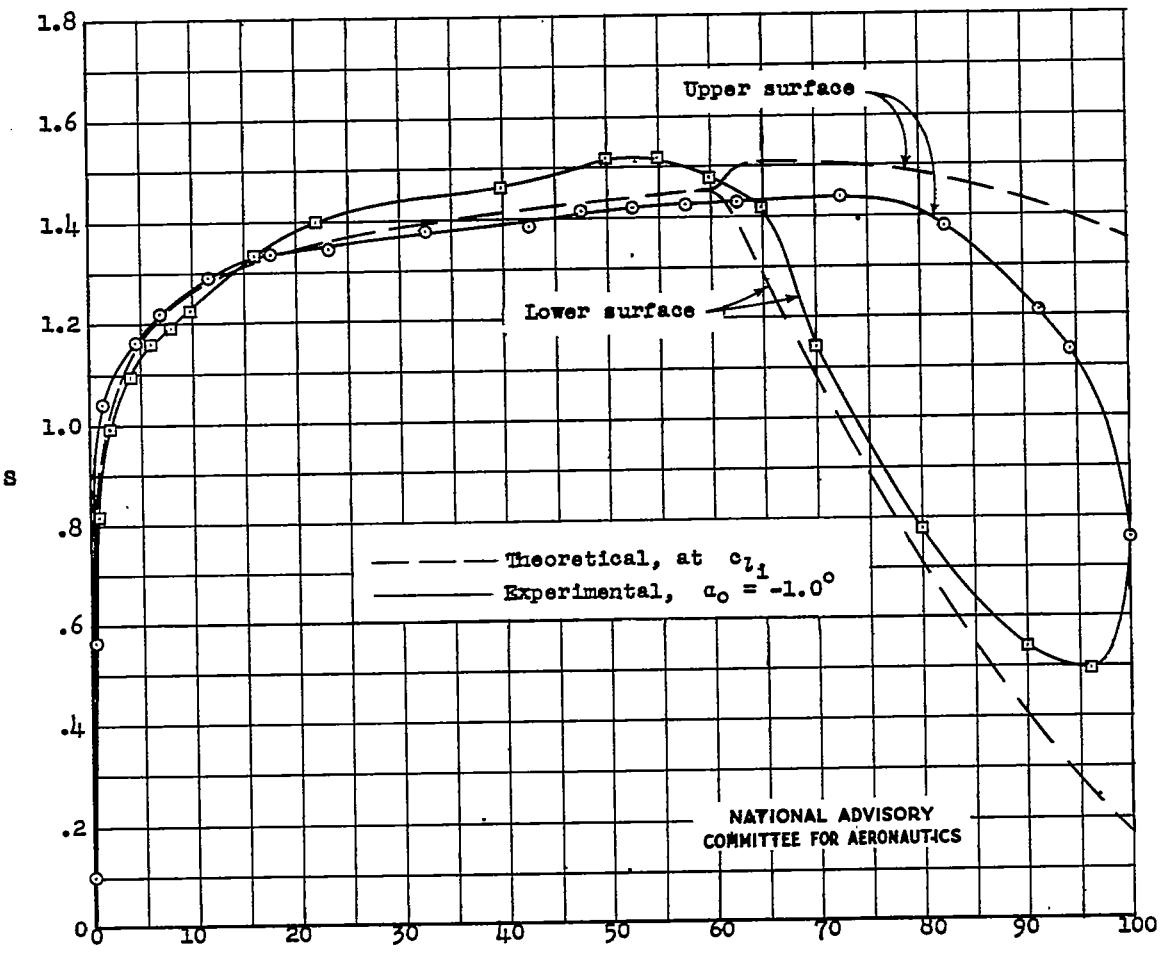

(b) NACA 66(215)-316 $\left\{\begin{matrix} a = 0.6, & c_{l_i} = -1.2 \\ a = 1.0, & c_{l_i} = 1.5 \end{matrix}\right\}$ airfoil section.

Figure 14.- Continued.

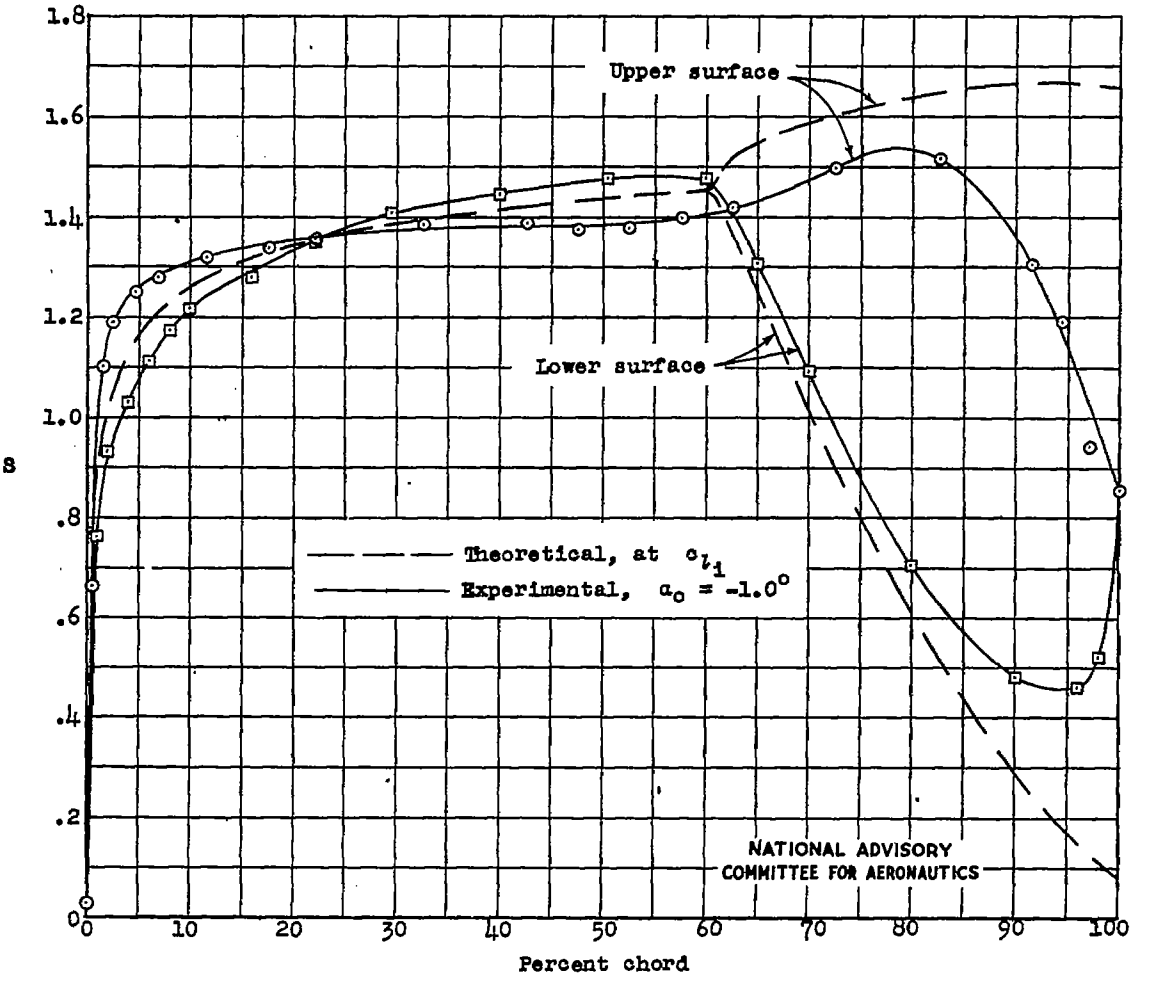

(c) NACA 66(215)-416 $\begin{cases} a = 0.6, & c_{l_i} = -1.6 \\ a = 1.0, & c_{l_i} = 2.0 \end{cases}$ airfoil section.

Figure 14.- Continued.

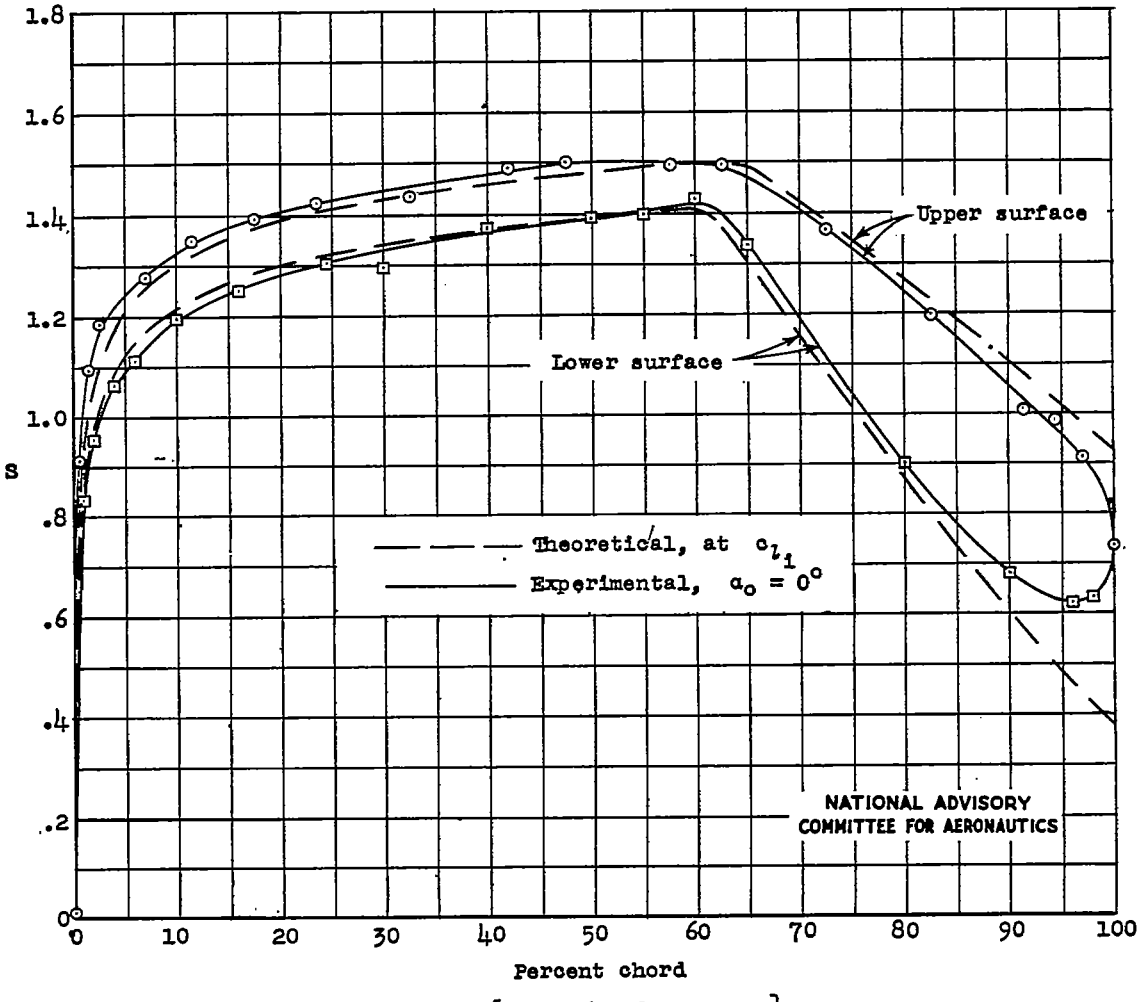

(d) NACA 66(215)-216 $\begin{cases} a = 0.6, & c_{l_i} = -0.5 \\ a = 1.0, & c_{l_i} = 0.7 \end{cases}$ airfoil section.

Figure 14.- Continued.

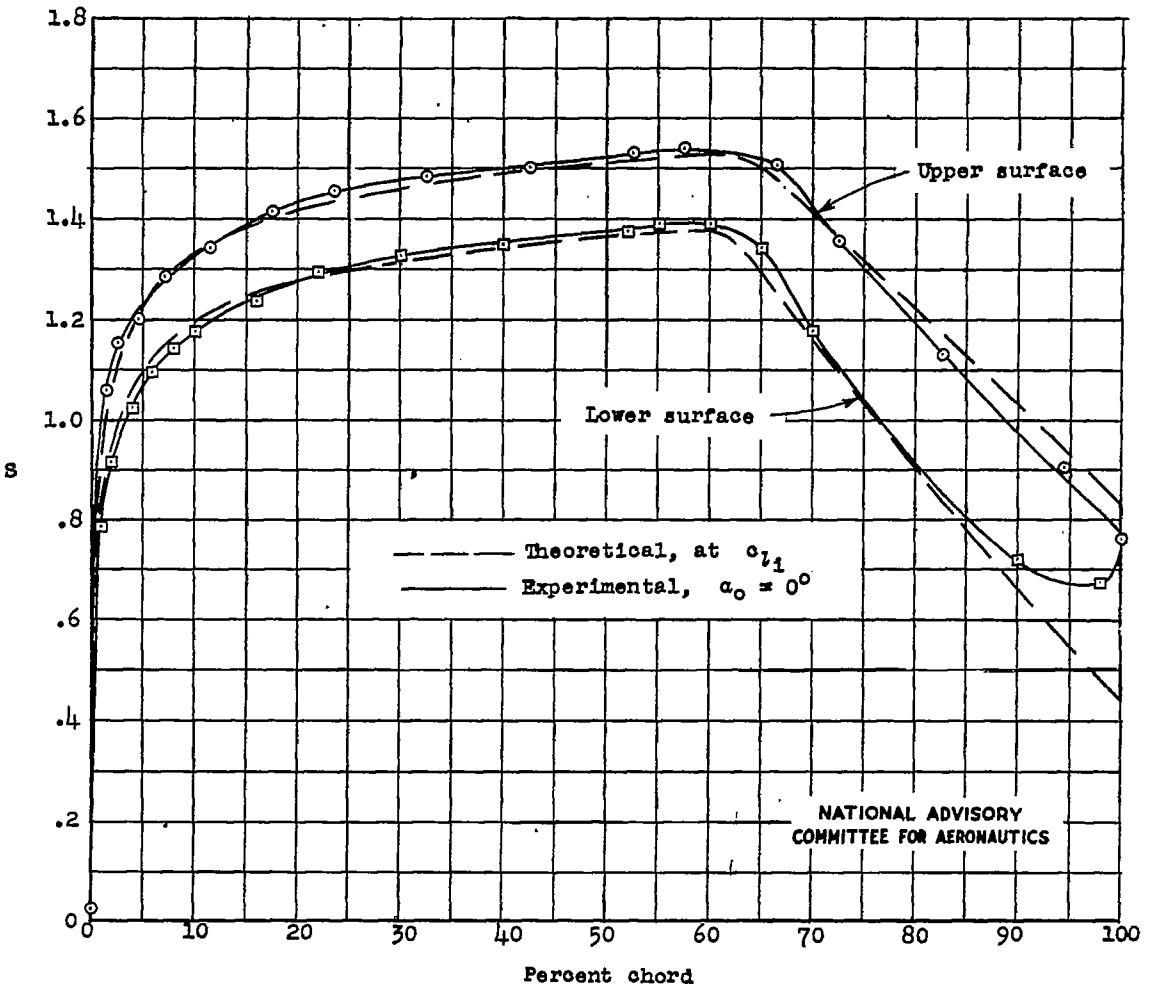

(e) NACA 66(215)-216 $\begin{cases} a = 0.6, & c_{l_i} = -0.3 \\ a = 1.0, & c_{l_i} = 0.5 \end{cases}$ airfoil section.

Figure 14.- Concluded.